Guidance-Based On-Line Motion Planning for Autonomous Highway Overtaking

by

Usman Shaukat Ghumman

A thesis submitted in conformity with the requirements
for the Degree of Master of Applied Sciences
Mechanical and Industrial Engineering
University of Toronto

Your file Votre référence
ISBN: 978-0-494-45129-8
Our file Notre référence
ISBN: 978-0-494-45129-8

Guidance-Based On-Line Motion Planning for Autonomous Highway Overtaking

Master of Applied Science

Ghumman Usman, 2008

Graduate Department of Mechanical and Industrial Engineering

University of Toronto

Abstract

In the context of intelligent transportation, this Thesis presents a novel on-line trajectory-generation method for autonomous highway overtaking. The focus of this Thesis has been on two autonomy aspects of overtaking manoeuvre: (*i*) time optimal overtaking in the possible presence of obstacle vehicles in the passing lane, while ensuring passenger comfort, and (*ii*) ensuring that a safety distance is always maintained between vehicles in order to avoid any collision. The proposed scheme is guidance based, real-time applicable, and ensures safety and passenger ride comfort.

The propose methodology is based on the principles of *Rendezvous Guidance*, the passing vehicle is guided in real-time to match the position and velocity of a *shadow* target (i.e., rendezvous with) during the overtaking manoeuvre. The shadow target's position and velocity are generated based on real-time sensory information gathered about the slower vehicle ahead of the passing vehicle as well as other vehicles which may be travelling in the passing lane.

The guidance principle is also used to prevent any potential collision with these *obstacle* vehicles. The proposed method can be used as a fully autonomous system or simply as a driver-assistance tool. The proposed method was implemented in both computer simulations and experiments. The results clearly demonstrate the tangible efficiency of the proposed method.

To my Parents and my Wife.

Acknowledgments

Working as an M.A.Sc. student, at University of Toronto, was a magnificent and challenging experience for a person like me who had arrived in a completely new country. During the time devoted to the completion of my studies, many people were instrumental, directly or indirectly, in shaping the course of my academic career. It was hardly possible for me to thrive in my masters' work without the support of these great personalities. Here is a small tribute to all the individuals from whose help I have greatly benefitted.

First of all, I would like to thank my supervisor Professor Beno Benhabib, for the inspiring and encouraging way in which he guided me toward a deeper understanding of the knowledge necessary to perform the work carried out in this thesis. I am indebted to his invaluable comments and suggestions and also to his great patience with my work that allowed me to thrive in my studies.

I would also like to thank Faraz Ahmed for his great support and inspiration during my stay at the University. I am greatly thankful for his guidance and support during my research work and for his invaluable comments and suggestions to improve this thesis.

I was also privileged to enjoy the company of my colleagues in the CIMLab, Hans deRuiter, Matthew Mackay and Ashish Macwan who provided all the help that I asked for and have made my studies at the University of Toronto all the more enjoyable.

I am eternally grateful for the support and encouragement of my parents, family and friends, both here and afar, without whom life would be meaningless. A special thanks for my wife for

her tireless and dedicated support to me in pursuing my dreams. I would like to especially thank Imran and Amina, who made sure that my stay in Canada was as comfortable as possible.

Finally, I gratefully acknowledge the financial support of National University of Science and Technology(NUST).

LIST OF PUBLICATIONS GENERATED FROM THIS THESIS

This thesis work has so far resulted in two publications: one journal and one conference paper.

The list of papers is given below.

Journal Paper:

[1] U. Ghumman, F. Kunwar and B. Benhabib, "Guidance-Based On-Line Motion Planning for Autonomous Highway Overtaking," *International Journal for Smart Sensing and Intelligent Systems*, Vol. 1, No.2, June 2008, pp. 549-571.

Conference Paper:

[1] U. Ghumman, F. Kunwar and B. Benhabib, "Real-Time Motion Planning for Overtaking A Slower-Moving Vehicle," (Accepted for presenting in 15th World Congress on ITS, New York, 2008).

Table of Contents

List of Tables

List of Figures

Nomenclature and Acronyms

Latin Letters

A	Acceleration limit
$a_{Y\,max}$	Maximum value of lateral acceleration
a_{RG}	Acceleration command
Cb	Chrominance-blue intensity
Cr	Chrominance-red intensity
n	Navigational Constant
O_D	Obstacle in the driving lane
O_P	Obstacle in the passing lane
P	Pursuer
r	Distance between the pursuer and the shadow target
$\dot{r}$	Relative velocity vector between pursuer and shadow target
$\dot{r}_{max}^{rend}$	Maximum allowable closing/rendezvous velocity
$\dot{r}_{max}^{cr}$	Maximum closing velocity
RGB	Red Green Blue color space
S	Shadow target
s	second
t_i	Time at instance i
v_{max}^{rel}	Maximum relative velocity
v_{Ave}	Average Velocity
v_{OD}	Velocity of obstacle in driving lane
v_{OP}	Velocity of obstacle in passing lane
v_P	Pursuer velocity
v_S	Velocity of shadow target
v_{RG}	Desired velocity vector
v_{st}	Starting Velocity of pursuer
v_{max}	Speed Limit

Y	Luminance

Greek Letters

a	Closing velocity component
λ	Angle between LOS and reference line
φ	Maximum angle pursuer can turn

Acronyms

AHS	Automated Highway Systems
ALVINN	Autonomous Land Vehicle In a Neural Network
APNG	Augmented Proportional Navigation Guidance
CCD	Charge-Coupled Device
CLOS	Command to Line-OF-Sight
DGPS	Digital Global Positioning System
EKF	Extended Kalman Filter
FOV	Field-of-View
fps	Frames per second
FVR	Feasible Velocity Region
FVS	Feasible Velocity Set
HSI	Hue-Saturation Intensity
KF	Kalman Filter
LIDAR	Light Detection And Ranging
LOS	Line Of Sight
MSSLC	Minimum Safety Spacing for Lane Changing
NN	Neural Networking
PATH	Partners for Advanced Transit and Highway
PN	Proportional Navigation
PNG	Proportional Navigation Guidance
PP	Pure Pursuit
RG	Rendezvous Guidance

RL	Rendezvous Line
ROI	Region of Interest
TPNG	True Proportional Navigation Guidance
RS	Rendezvous Set
VCPNG	Velocity Compensated Proportional Navigation Guidance
VL	Velocity Line

1 INTRODUCTION

1.1 Motivation

Intelligent vehicles are defined as vehicles that can move autonomously and navigate in everyday traffic, in highway, and in urban environments. Such vehicles could offer the advantages of increased road safety and better quality and efficiency of people and goods movements. Integration of intelligent features and autonomous functionalities on to vehicles would also lead to major economic benefits ranging from reduced fuel consumption, efficient exploitation of the road network, and reduced personnel.

Intelligent transportation systems have been widely researched in the past two decades by the academic community as well as automotive manufacturers for increased safety, passenger comfort, traffic congestion, etc. [1]. Although manufacturers have concentrated their efforts on developing technologies to help drivers, academic interest on the subject matter has primarily been on the autonomy of driving. Driving has often been characterized as comprising of three distinct levels of activities: strategic, tactical, and operational [2]. At the highest (strategic) level, a route is planned and goals are set; at the intermediate (tactical) level, manoeuvres are selected to achieve short-term objectives—such as deciding whether to pass a (slow-moving or stopped)

blocking vehicle; and, at the lowest level, the tactical manoeuvres are translated into control commands.

The overtaking manoeuvre is one of the critical actions that a driver performs while travelling on a highway. Errors in this decision-making process, typically caused by driver failure to accurately and timely interpret information about other vehicles in close proximity, have often resulted in catastrophic accidents [2]. In order to eliminate such errors, or at least minimize their impact, and increase the level of safety, the vehicles of the future would have to incorporate intelligent algorithms that will allow them to accurately consider all aspects of a lane-changing/overtaking manoeuvre. A number of real-time issues would need to be addressed; (*i*) calculating proximities to other vehicles, (*ii*) determining when the lane-change manoeuvre should start, and (*iii*) developing optimal and safe trajectories.

Majority of autonomous-driving research has been on *lane following*, as part of promoting driver-assistance systems (e.g., [3-44]). Limited research, however, has been carried out on *lane-changing*, though, primarily proposing non-real-time solutions that are commonly based on lane-following approaches (e.g., [45-59]). Since, these systems have not been primarily designed for lane-changing, or vehicle overtaking, they usually yield non-smooth lane transitions. Some of the studies have addressed the *smoothness* issue but have paid little attention to collision avoidance [60-73].

A vehicle's acceleration (lateral, longitudinal, and vertical) and angular motion (roll, pitch and yaw) contribute to ride comfort (or ride discomfort), which are often evaluated in comparison to set standards. In this context, comfort disturbances have been classified as: (*i*) *direct* comfort disturbance caused by a sudden motion of the vehicle, and (*ii*) *indirect* comfort disturbance commonly caused by high lateral accelerations and/or lateral jerks while negotiating transition curves [37]. The limits for lateral and axial acceleration, while negotiating a transition curve, have typically been set to 1.25 m/s^2 and 5 m/s^2, respectively, with a mean comfort rating of 2.5 [74,75].

Another important factor in lane changing is the maintenance of a safe distance during the manoeuvre. Although studies on the calculation of a minimum safe distance, for a collision-free overtaking manoeuvre, have differed on their recommendations, they commonly assumed worst-

case assumptions scenarios (e.g., [61, 76, and 77]). In the absence of information on the passing vehicle's performance ability (including braking capability) and road conditions, most studies recommend a (worst-case scenario) minimum safe (closing) distance based on 2 s of driving separation as an *ideal* value for preventing most accidents under emergency conditions.

Thus, the focus of this Thesis is on two autonomy aspects of overtaking manoeuvre: (*i*) time-optimal overtaking in the potential presence of obstacle vehicles in the passing lane while ensuring passenger comfort, and (*ii*) ensuring that a safety distance is always maintained between vehicles in order to avoid any collision. The main contribution of this Thesis is, thus, a novel time-optimal guidance based on-line trajectory (i.e., time-phased path) planning methodology for the guidance of a pursuer vehicle overtaking a slower (obstacle) vehicle on a highway setting in the presence of other vehicles travelling in the passing lane.

1.2 Literature Review

Recent research on motion planning for autonomous vehicles has benefited from the results of extensive past work on lane keeping, vehicle grouping/convoy following, lane changing, etc. Only most pertinent literature in this regard is reviewed below.

1.2.1 Lane Keeping

The problem of lane keeping is important in relation to Automated Highway Systems (AHS). Therefore, a wide section of pertinent literature has addressed the issue of lane keeping [3-44]. Four main methods of dealing with this issue have been proposed: (*i*) image processing, (*ii*) neural networks, (*iii*) on-board sensors, and (*iv*) global positioning [78].

Image-processing based techniques for lane keeping are typically based on the use of captured images of lane markers or detection of road boundaries. Once identified, the next step would be to find a polynomial curve that can represent the center-line of the lane. Based on this curve fit, one can assess the lateral distance between the center of the lane and the longitudinal axis of the vehicle [78]. The aim of detecting the lane markers or road boundaries is to provide on-board intelligent computing devices with information about the driving environment. The knowledge would help autonomous vehicles effectively perform road following and lane keeping.

For detection of lane marking, [3] proposes a method which detects lane marking by color analysis of road-scene images using Hue-Saturation-Intensity (HIS) color model. In this method, full color images are converted into HSI color representation, within the Region Of Interest (ROI), aiming to detect road-surface conditions. With simple thresholding operations, lane markings on various road-scene images are detected. In [4], a method based on history of located markers has been proposed. In this method, the algorithm adjusts the black and white color levels found in the images in order to maximize the induced contrast. Then, by using the "history of located lane markers in previous image frames, information about lane markers that have already been located in this frame, and geometric properties of the ground to image plane projection" areas that were expected to contain lane markers, images are extracted. The algorithm, then, proceeds to apply a matched filter to the pixel brightness of the images and statistically tests the areas suspected of containing lane markings. Based on the areas of the image that qualified as lane-marking, a low-order polynomial curve that could represent the road lane's center is fitted. This line is the reference point for estimating the lateral offset of the vehicle from the middle of the lane. One of the strengths of this algorithm is that it could be adapted to either dashed-lane or solid-lane markers if images were to be captured far enough ahead of the vehicle.

The work on the accuracy of detecting lane markings was further improved in [5] by expanding the dynamic range of a typical camera by developing a visual sensor which has a dynamic range of about 30 times that of a normal CCD camera. This set-up improved lane-marker detection accuracy by about 6%. The use of a stochastic method for estimating road shape ahead of a vehicle was proposed in [6]. This method utilises a single on-board colour camera, together with inertial and velocity information, to estimate both the position of the host car with respect to the lane it is following and also the width and curvature of the lane ahead at distances of up to 80 m.

A real-time color-learning algorithm was proposed in [7]. The algorithm is capable of dealing with unstructured, non-homogeneous, complex road shapes with varying lighting conditions. The system makes use of color classification and learning to create road and background color models. In [8], road curvature and orientation are estimated by isolated edge points. A watershed technique for road segmentation and obstacle detection was used in [9,10]. This techniques consist of applying a temporal filter for noise reduction (and connection of

ground markings), followed by edge detection and watershed segmentation. Another class of lane detection methods rely on top-view (birds eye) images computed from images acquired by the camera [11-13]. These methods are reliable in obtaining lane orientation in world coordinates, but, require on-line computation of the top-view images.

A lane-tracking system based on particle filtering and multiple cues was proposed in [14]. This method does not track the lanes explicitly, but computes parameters such as lateral offset and yaw of the vehicle with respect to the center of the road. Deformable road models have also been widely used for lane detection [15-22]. A method for curve detection based on the combination of perceptual grouping and a filter similar to Kalman's [79], with applications in autonomous driving, was proposed in [23]. In [24], a linear/parabolic model for lane tracking was presented. In this method, the linear part was used to fit lane borders in the near vision field, while the parabolic part fits the far field.

Various Neural Networking (NN) approaches have also been proposed for lane-following problems. "Autonomous Land Vehicle In a Neural Network" (ALVINN) is a NN-based algorithm that takes a video image as input and outputs a steering direction [25]. Trained properly, the system can handle non-homogeneous roads in various lighting conditions. However, the approach only works on straight roads. Another NN-based system [26] makes use of a dynamically trained NN to distinguish between areas of road and non-road. This approach is capable of dealing with non-homogeneous road appearance if the non-homogeneity is accurately represented in the training data. In order to generate training data, assumptions on the shape and location of the road are made.

The California Partners for Advanced Transit and Highways (PATH) has adopted a magnetic road reference system [27-30]. In this system, equally-spaced magnets are buried in the center of each automated lane, and magnetometers on-board a vehicle sense the magnetic field generated by each magnet. The lateral controller calculates the lateral deviation from the outputs of the magnetometers and uses the information to determine the steering command that will keep the vehicle in the lane. However, a problem concerning magnetic systems involves contradicting background magnetic fields. In [31], an algorithm for eliminating the background magnetic field was proposed. In order to accomplish this task, they made use of two sensors – a compass sensor

and a measuring sensor. The measuring sensor finds the overall magnetic field, while the compass sensor locates only the background magnetic field. Therefore, the difference between the two represents the magnetic field due purely to the road magnets. Based on this pure magnetic signal (only road magnets), it is possible to determine the relative location of the magnetic sensor that is aboard the vehicle in relation to the road-imbedded magnets.

The use of magnetic sensors was also proposed in [32]. In this study, a magnetic sensing system is used for lateral vehicle control. However, in reaching this goal, the study proposes that acquiring the appropriate magnetic material and sensing system could alleviate part of the background interference (earth magnetic field, AC-generated noise, electrical fields, and external magnetically permeable objects). [33] proposes an Extended Kalman Filter (EKF) based magnetic guidance for the lane-following problem.

[34] dealt with the development of the backup systems for magnetometer-based vehicle lateral control during magnetometer failure. It proposes the use of Light Detecting and Ranging (LIDAR) as a backup system in case of failure of magnetometer. In the case of total failure of the magnetometers, the control algorithm would work on the measurement of the relative position of the leading vehicle with respect to its preceding vehicle by an on-board LIDAR. A LIDAR based approach was also proposed in [35]. This method is dependent on the presence of retroreflective road markers, as such, in terms of installation costs, it is very similar to the magnetic-marker solution. The difference is that many jurisdictions already have retroreflective road markers installed on their main highways. The problem arises when background light could interfere with the reception of light. In response, [35] devised a method of rejecting background light from the signal by using the time-of-flight concept to calculate the relative distance to the retroreflective marker.

In contrast to handling the costly infrastructure expense of installing magnetic sensors on roadways, another method to handle lane keeping would be to implement the use of Digital Global Positioning (DGPS) [36]. The main issue with DGPS usage for lane keeping is that it requires to receive positioning signals in real-time. Namely, acquisition and processing times need to be realistic.

1.2.2 Grouping/Convoy Following

Another area of interest in the field of autonomous vehicles is grouping of vehicles together and moving them in the form of a convoy. By grouping them and optimizing the relationship within a group of vehicles, it is possible to produce AHS that can incorporate a higher density of vehicles as well as reduce traffic congestion. The main idea is that vehicles will be able to travel at relatively closer distances and with increased velocities.

In [80], a NN approach for vehicle-following scenarios was implemented. Based on the control data extracted from a human driver, two NNs are programmed to operate in a similar fashion. One NN is designated for steering, while the other one for speed considerations. The main benefit of the research presented in this paper is that the NN controller can be incorporated with any vehicle independent of the systems' dynamics. In [36], an analytic method was presented for finding the relative distance, direction angle, and pose angle. It uses lamps that are mounted on the back of the leader vehicle in order to extract the necessary information even when obstacles hindered the Line Of Sight (LOS). When the following vehicle loses sight of the leader vehicle due to an obstacle it is still able to follow its intended trajectory. The paper focuses around the use of a monocular vision based position sensor with a CCD camera while implementing a NN with back propagation for measuring purposes.

A trajectory-based lateral-control system was developed in [81]. This method evolves around the idea of tracking the overall path of the leader vehicle rather than its instantaneous relative position. It focuses on the fact that if the 3D points of the leader-vehicle path with time markers are given, the overall trajectory can be constructed. In addition, they incorporated the fact that the velocity and steering position of the following vehicle needed to be recorded as well. It uses this information to compare the displacement error between the two vehicles at a given time as lateral control input to ensure that the following vehicle moves on the same trajectory as the leader vehicle. Another approach could be the use of "contact convoy". This type of platoon configuration refers to a string of vehicles that are actually in physical contact with one another. A contact convoy would virtually eliminate relative navigational problems [82]. In this case, the system would need to invoke a "non-coupling intelligent inter-vehicle device." The apparatus

would theoretically be able to normalize the vehicle's position as well as reduce the required energy.

A vehicle-following system based on the combination of laser radar, the inter-platoon navigational infrastructure, and an inter-vehicle communication system was proposed in [83]. In this system, the main process consisted of the position and direction of the leader vehicle being measured by the navigation system and communicated to the remainder of the platoon. From this information, the following vehicles would produce a "trace line" that mapped out the leader vehicle's path. Deviation from this targeted path was measured by the navigation system aboard each individual vehicle.

In [84], research results concerning the necessary braking actuation requirements for automated highway platooning are examined for the braking dynamics within a multiple surface-sliding control strategy. The main proposal concerns the transition from brake to throttle and vice versa. In other related research [85, 86], the switching control (between throttle and brake) was based upon the throttle angle, α: If α is larger than or equal to zero, then, the actuator invokes the throttle commands. On the other hand, when α is less than zero, braking is initiated.

Another issue of importance for intelligent vehicles, especially in the case of platoons, is merging. Merging refers to when a vehicle wants to join an already existing platoon of vehicles. This issue was addressed in [87] under two different road layouts. In the first layout, the merging point is instantaneous, i.e., the vehicles are forced to merge together at a fixed point, e.g., where two converging roads unite. The other layout is flexible, i.e., the merging vehicle has some time to adjust its reference speed and to assimilate within the platoon.

1.2.3 Existing Lane Changing/Overtaking Strategies

Limited research has been carried out on *lane changing/overtaking* (e.g., [45-73]), and primarily proposing non-real-time solutions. The proposed strategies are commonly based on (*i*) lane-following approaches, (ii) geometric-shape approaches, and (iii) acceleration-profile approaches. The strategies that are based on lane-following approaches are not been primarily designed for lane changing, or vehicle overtaking, hence, they could yield non-smooth lane transitions resulting in discomfort to the passengers. Geometric-shape approaches also do not pay much

attention to passenger comfort. The acceleration-profile approaches do consider passenger comfort as an input parameter but assume constant velocities during the lane-change/overtaking manoeuvre. Also, both geometric-shape and acceleration-profile approaches are primarily off-line solutions to the problem and cannot react to changing velocities of vehicles or emergency situations.

The concept of lane changing for an autonomous vehicle was addressed by [45] by using the ALVINN (lane-keeping network) system [25]. The solutions presented for this approach involves lane transition through network switching. They propose the use of the ALVINN system to help realign the vehicle in a parallel lane. The ALVINN system corrects the lateral displacement of the vehicle when it deviates from the center line of the lane. By switching to an opposing ALVINN network that represents the transition lane, the vehicle would automatically switch lanes. The method was further improved in [46] by using incremental view lane-transition. This technique depends upon the use of two virtual viewing cameras and the ALVINN system. The views created by these cameras make it seem as if the vehicle is misaligned from the center of the lane. This is done by offsetting the test view from the driving view, therefore, the ALVINN system automatically tries to correct the lateral displacement error. After the realignment is complete, the virtual cameras once again act as if the car is off-center and the ALVINN system repeats the entire process. The full lane transition is just a series of small corrections performed by the ALVINN system. The main benefit of this procedure is that the system can determine whether or not transferring to the new lane is advisable before performing the manoeuvre.

In [47], an algorithm for path generation for the lane changing manoeuvre was presented based on the use of a vision system. The vision system detects reference lines (lane markings or road edges). The line, captured with the on-board vision, is approximated with a cubic polynomial curve for ensuring that vehicle moves within the lane. However, when the vehicle changes lanes, the path generated with the sampled points is gradually transferred over the lane markings from the right lane to the left lane to generate a path for lane changing.

In [48], the problem of lane changing was addressed through the means of lateral control based on vision-navigational principles. The main idea is that the vehicle would use a simple

vision system for basic lane keeping. However, if the system detects an obstacle in the vehicle's path, then, it should have the capability to autonomously navigate itself laterally to avoid any collision. The specific system in this research was based on the use of two stereo cameras. Any disparity between the left and right cameras represents an area that needs to be avoided through lateral navigation. In terms of lateral control, it uses a cubic polynomial curve to approximate the path that should be taken to promote lane changing.

In [49,50], a lane-changing system based on magnetic markers was proposed. The magnetic markers are embedded along the road center-line every 1.2 m and two sets of magnetometers are installed under the front and rear bumpers of the vehicle. The input for lane following and lane changing is taken from these magnetic markers. On-board longitudinal and lateral control systems deal with both the lane-keeping and lane-changing tasks.

For geometric-shaped approaches, [60] made an analytical study of geometric shapes that can be used for high-speed, single lane-change manoeuvres. The study recommended that ramp sinusoidal, spline, and polynomials can be used for generating a lane-changing path. The use of a ramp sinusoidal function to describe the ideal lane-change path was proposed in [61] because it provides a continuous function of continuous curvature and it accommodates changing velocity. [62] presented a method which interpolates cubic splines to generate a smooth path. This method represents the vehicle's path of travel by five parabolic curves (segments) that are linked together. While increasing the number of segments, improves the generated vehicle path smoothness.

In order to overcome the problem of discontinuity between concatenated paths, [63] presented a solution based on clothoids. Clothoidal curves have a linear relationship between curvature and arc length. This fundamental feature guarantees the comfort of the passengers because it maintains a constant variation of the centrifugal acceleration. This method is based on a general off-line approximation of the Fresnel integrals into Rational Bezier Curves (RBC), which are later used in the generation of on-line clothoidal paths. The major drawback in this technique is that it requires complicated computation of Fresnel integrals.

[64] uses a quintic polynomial equation for trajectory generation for the overtaking manoeuvre. The equation is used to find the next point on the trajectory in both x and y

directions. A disadvantage of this approach is the lack of control on the lateral acceleration, and also the total time to complete the manoeuvre needs to be known *a priori*. In this method, the time to complete the manoeuvre is calculated before the start of the manoeuvre depending upon the velocity of both the pursuer vehicle and the obstacle vehicle to be overtaken. Since it is an off-line method, it cannot compensate for changing velocities. A quintic polynomial method was also used in [65], but, in this case it is assumed that the end point of the lane-changing manoeuvre is known and the instantaneous points in lateral direction are calculated for every instance. This method is also an off-line method and cannot work with changing conditions.

For the acceleration-profile approach, [66] presented a method that is based on a sinusoidal profile of the lateral acceleration. The vehicle gets a lateral acceleration command at every instance, which produces a sinusoidal acceleration profile, in order to change lanes. The major drawback of this method is that the maximum distance the vehicle should travel for the smooth lane changing should be known a *priori* depending on the velocity of the vehicle. Also, this method is an off-line solution as it cannot react to changing conditions.

In [75], a method based on trapezoidal acceleration profile, for the lateral acceleration, was presented. It is shown that this method yields a better solution when compared to the sinusoidal-acceleration-profile method in terms of time taken and distance travelled for the same comfort rating, however, this method too has the same limitations as the sinusoidal-acceleration-profile method.

[67] focused on the platoon lane-changing manoeuvre. It presented two lane-changing methodologies for a platoon under coordinated and un-coordinated infrastructures. In the coordinated environment, the platoon leader may dictate the action sequence to be followed, while in un-coordinated infrastructure, the front vehicle should notify the vehicle behind of the timing and force of the lane-changing manoeuvre. Therefore, each vehicle starts to perform a lane-changing manoeuvre with a delayed of communication time. For the lane-changing manoeuvre, they use a sinusoidal-acceleration-profile methodology.

All the methodologies presented above deal with lane changing without considering any other vehicle in the passing lane, which may not be a useful assumption in the case of a highway environment. [77] presented a methodology in which they consider other vehicles in the passing

lane. They examined various alternative scenarios for merging and lane changing and presented an algorithm for calculating the Minimum Safety Spacing for Lane Changing (MSSLC); namely, they calculate the necessary inter-vehicle spacing during a merging or lane-changing manoeuvre so that in the case where one of the vehicles executes an emergency braking manoeuvre, the rest of the vehicles have enough time and space to stop without any collision taking place. In the scenario where there is another vehicle in the passing lane and the lane gap available is unsafe for lane changing, the merging vehicle starts adjusting its longitudinal velocity (by decelerating or accelerating) to make the spacing large enough; then, it starts adjusting its longitudinal velocity (again by decelerating or accelerating) in order to make its longitudinal velocity equal to the velocity of the destination lane. They used sinusoidal-acceleration-profile method for the generation of the lane-changing path.

In [68], a distributive strategy for calculating the gap in the target lane for executing a safe lane-changing manoeuvre was presented. For lane-changing path generation, it uses a quintic polynomial equation.

1.3 Research Objective

The primary objective of this Thesis is the development and implementation of a novel time-optimal guidance-based on-line trajectory-planning algorithm for the guidance of a pursuer vehicle overtaking a slower obstacle vehicle on a highway setting in the potential presence of other (obstacle) vehicles travelling in the passing lane. The Thesis demonstrates the successful applicability of the rendezvous-guidance technique [114] for overtaking a slower-moving vehicle in the presence of obstacle vehicles in the passing lane. The implementation was performed in two phases: simulation in a Visual Basic environment and experimentation with autonomous robotic vehicles. The simulation phase of the implementation assumed perfect knowledge of the workspace conditions, which includes pursuer and obstacle vehicles' positions. Commands to the vehicles are specified in lateral acceleration and executed perfectly. In the experimental phase, the proposed method was evaluated for its robustness in a noisy environment.

1.4 Thesis Organization

This Chapter presented an introduction to the motivation behind this Thesis and the need for the proposed trajectory planner. A literature review of the relevant topics has also been presented. Lastly, the research objective of the thesis has been stated.

In Chapter 2, the overall problem is defined and the review of guidance laws is presented. This chapter also discussed in detail the proposed overtaking methodology along with the implementation of the algorithm.

Chapter 3 presents the simulation phase of the implementation of the proposed algorithms. First, the methodology, including the software platform and simulation parameters, is discussed. The results of the simulations are subsequently presented. Also, the comparison of the proposed methodology is carried out with the original rendezvous-guidance method and with an off-line method that uses sinusoidal-acceleration-profile approach. Some special cases, like aborting overtaking manoeuvre, overtaking multiple vehicles, and vehicle joining a highway from a ramp are also discussed in this Chapter.

Chapter 4 presents the experimentation phase of the implementation. The set-up is presented first, which includes a system overview, discussion of the vision system, communication system, and robotic vehicles. Discussions of the results of the experimentation follow.

Lastly, in Chapter 5, the conclusions of the thesis and recommendations for future work are given.

2 OPTIMAL OVERTAKING MANOEUVRE

This Chapter presents the problem definition for an overtaking manoeuvre by an autonomous vehicle along with the proposed methodology to address it. Section 2.2 reviews the existing guidance laws along with their different variants. Section 2.3 discusses motion planning using guidance laws. In Section 2.4, a guidance based path planning solution approach is presented along with the implementation methodology under different scenarios: overtaking in the potential presence of an obstacle vehicle in the passing lane, aborting the overtaking manoeuvre, overtaking multiple vehicles, and joining a highway from a ramp.

2.1 Problem Definition

Let us first consider the simplest 2-lane highway-overtaking scenario, namely, where a vehicle (hereafter referred to as the *Pursuer*, *P*) is driving with a velocity v_p, while in front of it, another vehicle (hereafter referred to as the *Obstacle in the Driving Lane*, O_D) is travelling with a slower velocity, v_{od}, (i.e., $v_p > v_{od}$). There exists no (obstacle) Vehicle in the Passing Lane, O_P, that would influence the overtaking manoeuvre, which can be performed by *P* in three phases: (1)

move from the driving lane to the passing lane, (2) travel in the passing lane and, thereafter, (3) return to the driving lane, Figure 2.1.

In the more complex scenario, one could be forced to consider the presence of O_P, which would not allow P to immediately overtake O_D due to safety considerations. In this case, an additional velocity-adjustment phase would need to be included: during this phase, P would adjust its velocity according to the velocity of O_D until the passing lane becomes free of obstacles, Figure 2.1.

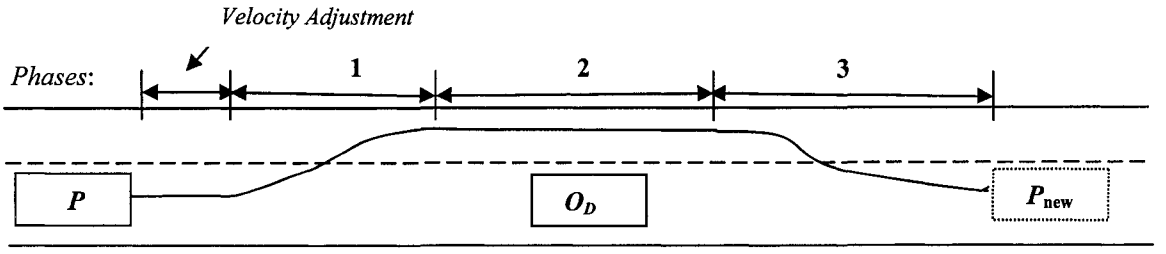

Figure 2.1: The Overtaking Maneuver.

2.2 Review of Guidance Laws

Guidance theory of missiles is a mature field with an abundance of guidance laws already implemented in real systems. Current missile-guidance techniques are, typically, classified into five main categories [90]: Line-Of-Sight (LOS) guidance, Pure Pursuit (PP), Proportional Navigation Guidance (PNG), optimal guidance and, other guidance methods including the use of differential game theory.

2.2.1 LOS Guidance

LOS is the most widely used guidance strategy today. In fact, almost all guidance laws in use have some form of LOS guidance because of its simplicity and ease of implementation [88]. The LOS guidance requires that the interceptor (i.e., pursuer) remains on a hypothetical line connecting the point of control to the target. The basic disadvantage of LOS guidance is that it does not work well with manoeuvring targets. Also, the interception time is high, which can be abridged using different strategies.

2.2.2 Pure-Pursuit Guidance

In PP trajectory, the interceptor moves directly toward the target at all times. Thus, the heading is maintained along the *LOS* between the interceptor and the target by the guidance system. An interceptor moving along a PP course usually ends up in a tail-chase situation. The basic disadvantage of the PP method is that it requires that the speed of the interceptor must be considerably greater than the target's speed.

2.2.3 Proportional Navigation Guidance

The Lark missile that was tested in 1950 was the first interceptor to use PNG [89]. Since then, the PNG law has been used in virtually all tactical radar, and infra-red missiles [90]. It is the most common and effective technique for non-manoeuvring targets, which seeks to nullify the angular velocity of the *LOS* angle. In PNG, the interceptor heading rate is made proportional to the *LOS* rate from the interceptor to the target. The rotation of the *LOS* is measured by a sensor (either on-board or from a ground station), which causes commands to be generated to turn the interceptor in the direction of the target. The advantage of using PNG over LOS guidance is that the interception time can be greatly reduced by adjusting the navigation constant. PNG, like LOS guidance, does not work well in the case of manoeuvring targets. However, the interception time is reduced. Augmented PNG (APNG) [91] is a modified form of PNG to deal with manoeuvring targets. Other forms of PNG are Velocity Compensated PNG (VCPNG), pursuit-plus PNG, and dynamic lead guidance [92].

2.2.4 Optimal Guidance

Recently, some interest has been shown in using optimal control theory for guidance problems. Two important mission parameters, interceptor-target engagement time and the energy needed, can be reduced by utilising optimal control. An optimal guidance law for short-range homing missiles to intercept highly manoeuvrable targets was proposed in [93]. In this law, a guidance problem is addressed to find the optimal interceptor trajectory such that the total time for interception is minimised. The proposed guidance law achieves the best performance in terms of miss distance and interception time in comparison to the True Proportional Navigation Guidance (TPNG) and APNG laws [93]. However, a major disadvantage of this law is that the target's

future trajectory must be known in advance, which would be impossible to evaluate in a realistic environment. A comprehensive review of optimal guidance laws is also presented in [92].

2.2.5 Other Guidance Laws

Some derivatives of the above basic laws have also been employed, exploiting various design concepts, over the years to include Command-to-Line-Of-Sight (CLOS) guidance, optimal guidance laws based on linear quadratic regulator theory, linear/quadratic Gaussian theory, and linear/quadratic exponential Gaussian theory [94-97]. In [90], a guidance law using fuzzy logic to implement PNG law was proposed. The fuzzy law generates acceleration commands for the interceptor using closing velocity and *LOS* rate as input variables. A fuzzy-logic based guidance law was also proposed in [98] using an evolutionary computing-based approach. The proposed law uses a genetic algorithm to generate a set of rules for the guidance law. In [99], a fuzzy-logic weighting is used to blend multiple guidance laws to obtain enhanced homing performance. This law evaluates the weights of each of the guidance laws to obtain a blended guidance command for the interceptor. An H1-based guidance law was implemented in [100]. Unlike other guidance laws, it does not require information about the target acceleration, while ensuring acceptable interception performance for arbitrary target motion with finite acceleration.

2.3 Motion Planning using Missile Guidance Laws

The utilization of guidance-based techniques in the on-line motion planning of autonomous robotic vehicles was first proposed in the late 1990s [101,102]. The tools used to compute guidance laws are similar to those used in dynamic robot-motion planning. In particular, the PNG law uses the homing triangle for computing the acceleration of a missile pursuing an evading target. The homing triangle is defined by the pursuer, the target, and the point of interception. This control law makes the pursuer's acceleration normal to its path and proportional to the rate of change of *LOS* vector to the target. This ensures that the angle between the velocity vector of the pursuer and the *LOS* is constant. This in turn results in a homing triangle with fixed angles, which collapses to a point at interception. Guidance laws assume that the future trajectory of the target is completely defined either analytically, or by a probabilistic model [103-105].

Due to its low computational requirements, simplicity of on-board implementation and time optimality characteristics, PNG has been the most widely used and researched guidance technique among all guidance methods [106]. However, the problem of velocity matching has not been an issue in missile-guidance applications. The need for Rendezvous-Guidance (RG) methods arose from spaceship rendezvous missions with asteroids or space stations. In this context, rendezvous is defined as the simultaneous matching of the position and velocity vectors of the vehicle with those of the target. Most of the available RG techniques incorporate a velocity-matching algorithm in conjunction with a guidance technique, which is usually PNG. A PN-based RG method for the docking problem of two space vehicles was proposed in [107]. In [108], the use of exponential-type guidance was suggested, which is a special form of PN-based RG, for asteroid rendezvous.

The problem of rendezvous with a target capable of performing evasive manoeuvres in order to avoid rendezvous was addressed in [109]. The utilization of a guidance-based technique in robot-motion planning, with the purpose of improving upon the interception time achievable by visual-servoing techniques, was first reported in [110]. However, final velocity matching was only presented as an issue in subsequent works, [101] and [111]: A PNG-based method was used during the first phase of the interception, and later a conventional tracking method was invoked as the robot's end-effector approached the object, for a stable velocity matching. Although this work considered the full dynamics of the robot for minimum-time trajectory planning, it suffered from two drawbacks: First, the navigation-guidance method determines optimal motion commands regardless of the robot dynamics. These commands, then, need to be checked against the robot constraints and required modifications made to ensure their feasibility. The modified commands may not be time efficient any longer according to the original navigation criterion. Second, the trajectory planner must continually look ahead and switch to the conventional tracking method at an optimal time. A delayed switch may result in a loss of optimality achieved via the utilization of a navigation-guidance method in the first phase of robot-motion planning.

The above PN guidance was augmented with a RG method for a robot manipulator to ensure fast interception and velocity matching in [112]. This work once again showed that for fast-manoeuvring objects, guidance-based methods yield shorter interception times compared to other

available techniques. However, the algorithm presented in [112] has an additional limitation; it does not take into account the presence of static or dynamic obstacles in the workspace.

2.4 Proposed Methodology

2.4.1 Guidance Based Solution Approach

In autonomous vehicle trajectory-planning, the time-optimal trajectory depends on the kinematics of the vehicle as well as its initial and final states. Although a global time-optimal solution can be found off-line, on-line planning for unpredictable environments may not yield a time-optimal solution. Thus, one has to resort to other methods in order to obtain a near-optimal, on-line solution.

The proposed on-line motion-planning method, determines a pursuer vehicle trajectory to perform an optimal overtaking manoeuvre based on RG technique [113]. RG has been shown analytically to yield an optimal solution for *rendezvous* with non-manoeuvring targets: which can be assumed to be the case for vehicles travelling on highways. However, there still exist two major issues that restrict the use of RG in trajectory planning for autonomous vehicles. First, RG is designed for matching velocity with a target and not to overtake it. Therefore, a fictitious target needs to be defined in our case. Second, there would be numerous constraints on the motion of a pursuer vehicle, which may not exist for spaceships-rendezvous manoeuvres.

In order to address the first issue, the concept of a *shadow* target, S, is introduced herein, which is used to guide the pursuer, P, during all the phases of the overtaking manoeuvre. The location of S is defined according to the obstacle vehicle, O_D, that is being overtaken. In order to address the second issue, the proposed method uses RG [108,109,113,114]: namely, information about P, O_D, and O_P is used to generate a single acceleration command for the pursuer, P, to avoid O_P and overtake O_D in a time-optimal manner. This acceleration command is calculated based on velocity-matching capability with S, keeping in mind the constraints imposed due to P's dynamics and passenger comfort. The concept of *shadow* target is also utilized for obstacle avoidance in the passing lane to ensure a collision-free path.

A Trajectory Based on RG Law

Let us consider a two-dimensional engagement geometry, in which P and S are moving at velocities v_p and v_s, respectively. The angle formed between an imaginary line joining P and S with the fixed reference, λ, is defined by

$$\lambda = \tan^{-1}\frac{h}{l} \quad , \tag{2.1}$$

where h is the distance between P and S in the lateral direction and l is distance in axial direction, LOS is defined as a range, r, connecting P to S.

The parallel-navigation law states that the direction of LOS should remain constant relative to a non-rotating frame, while, the interceptor (pursuer) approaches the object (target) [90]. Namely, the relative velocity, $\dot{r}$, between P and S should remain parallel to the LOS, r, at all the times. If this rule holds throughout the motion of P, the distance between P and S would decrease until they collide. Furthermore, if S moves with a constant velocity, parallel navigation would result in global-time-optimal interception.

The parallel-navigation law is expressed by the following two relationships

$$r \times \dot{r} = 0, \tag{2.2}$$

and

$$r \cdot \dot{r} < 0. \tag{2.3}$$

Equation (2.2) ensures that r and $\dot{r}$ remain co-linear, while (2.3) ensures that P is not receding from S. The above equations can be solved in a parametric form to yield

$$\dot{r} = -ar, \tag{2.4}$$

where a is a positive real number. The instantaneous relative velocity can then be written in terms of P's and S's velocities, v_p and v_s as follows:

$$\dot{r} = v_s - v_p \ . \tag{2.5}$$

Substituting (2.4) into (2.5) and solving for P's velocity yields

$$v_p = v_s + ar \ . \tag{2.6}$$

The goal of the proposed trajectory planner is to obtain an optimal v_p command according to the parallel-navigation law for the next command instant. The value of r is obtained based on

the data received from proximity sensors on P. Substituting this vector into (2.6) would result in a locus for P's velocity vectors, v_p, all lying on a semi-line parameterized by a. This semi-line is referred to herein as the *Rendezvous Line* (*RL*), Figure 2.2. The end-points of the velocity vectors show the positions of S and P, after one unit of time has passed, should they adopt the corresponding velocities. If P continually adopts a velocity command that falls on the instantaneous *RL*, the direction of *LOS* remains constant and positional matching between P and S is guaranteed.

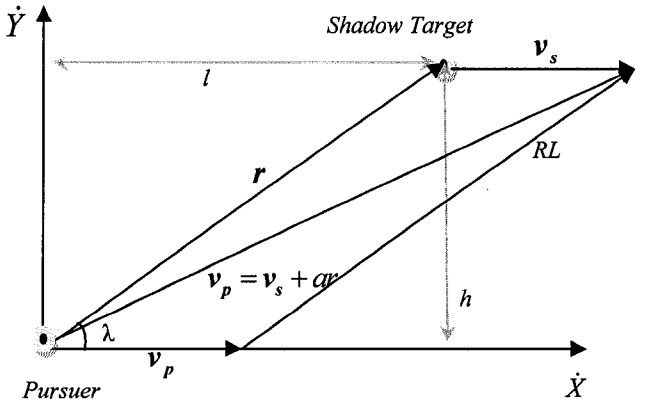

Figure 2.2: The *Rendezvous Line* (*RL*).

As mentioned earlier, unlike in missile-guidance applications, for rendezvous with S, the velocity of P must also match the velocity of S at the time of interception. The velocity commands generated based on (2.6) guarantee position matching. The next task is to find the value of α, such that velocity matching is also assured. An early attempt to match S's velocity may unnecessarily increase interception time. Thus, it is desirable to determine the maximum allowable closing velocity without violating the velocity-matching condition

Let us suppose that from the current instant until the achievement of interception tolerances, P is guided by velocity commands that lie on the instantaneous *RL*. This assumption allows us to consider the interception problem only in the direction of *LOS*. Let us further consider that the acceleration capability of the P in this direction is given by A. This acceleration would be used to bring the closing velocity down to zero. Assuming a constant acceleration for the rest of the

motion of P, the simultaneous reduction of velocity and position differences in the direction of *LOS* for interception may, then, be written as:

$$\begin{cases} \dot{r}_{\max}^{rend} - At_r = 0, \\ r - \dot{r}_{\max}^{rend} tr + \frac{1}{2} At_r^2 = 0 \ , \end{cases} \tag{2.7}$$

where $\dot{r}_{\max}^{rend}$ is the magnitude of the maximum allowable closing velocity, and t_r is the remaining *time-to-intercept* from the current instant. The maximum instantaneous allowable *closing velocity* is obtained by solving (2.7):

$$\dot{r}_{\max}^{rend} = \sqrt{2rA} \ . \tag{2.8}$$

The maximum *closing velocity*, as imposed by the frequency of velocity command generation by the trajectory planner for a fast asymptotic interception, is given by

$$\dot{r}_{\max}^{cr} = r / n.\Delta t \ . \tag{2.9}$$

The value of n above is determined empirically. The final allowable *closing velocity* component of the velocity command is, then, obtained by considering (2.8) and (2.9) simultaneously:

$$v_{\max}^{rel} = \min\left\langle \dot{r}_{\max}^{rend}, \dot{r}_{\max}^{cr} \right\rangle \ . \tag{2.10}$$

The end points of all velocity command vectors on *RL* that have a *closing velocity* component smaller than $v_{\max}^{rel}$ constitute a line segment extending from $v_p = v_s$ to $v_p = v_{p,\max}\left(= v_s + v_{\max}^{rel}\left(r / \|r\| \right) \right)$. This set of points is referred to herein as the *Rendezvous Set* (*RS*), Figure 2.3.

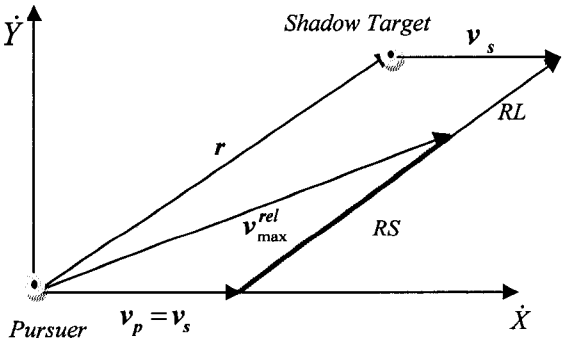

Figure 2.3: The *Rendezvous Set* (*RS*).

The velocity represented by $v_{\max}^{rel}$ in Figure 2.3 may not be achievable by P within the time interval Δt due to constraints of vehicle dynamics. Therefore, a *Feasible Velocity Region* (*FVR*), Figure 2.4, representing all velocities physically reachable by P within the time interval Δt is defined herein. Assuming that the current heading angle of P is δ, and considering all the kinematic and dynamic constraints of P, the velocity selected for P for the time interval Δt is the component of the *RS* within *FVR* with the maximum value represented by $v_p(t_i + \Delta t)$. It is, thus, concluded that if P adopts the velocity commands from within the *RS* with the largest allowable velocity components, then, a time-efficient interception can be achieved.

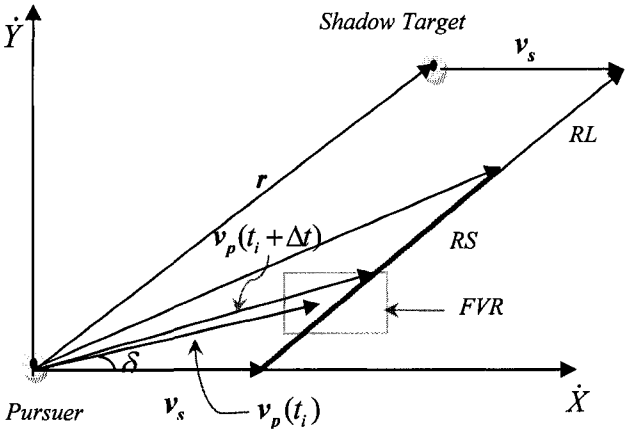

Figure 2.4: Generation of Pursuer-Velocity Command.

Let us assume that the maximum value for the lateral acceleration, $a_{Y\max}$, is defined by

$$a_{Y\max} = \frac{v_p^2}{Kh} 2\sin^2\vartheta\left(1+\frac{\cos\vartheta}{\sqrt{K^2-\sin^2\vartheta}}\right), \tag{2.11}$$

where $K = v_p / v_s$, h is the width of the lane, and ϑ is the maximum angle P can turn with the given set of variables.

Modification of the RG Algorithm

The original RG method described above was further modified to yield *better* overtaking times while remaining within the constraints of passenger comfort. One may note that the limitation on lateral acceleration does not allow P to travel at its optimum velocity by limiting the angular acceleration that it can achieve: namely, RG selects an angular acceleration value that ensures the velocity of P remains on RL, even though it has the capability of selecting a higher value from the FVR.

In the case of S moving on an unknown trajectory, if P tries to achieve a velocity greater than the rendezvous velocity, a situation may arise wherein S is turning away from the direction in which the velocity is increased. This could lead to an increase in the rendezvous time instead of a reduction. However, in the case of an overtaking manoeuvre, the behaviour of the vehicle moving on a highway is predictable. Using this information, the velocity of P can be increased in the forward direction to reduce the overtaking time. However, as noted earlier, the same reduction in time would not be possible if the behaviour of S is unknown.

Taking advantage of this predictability, we define herein a *Velocity Line* (*VL*) which originates from the start point of the RL and makes an angle ϑ with the fixed reference, Figure 2.5. Now, if P were to select and use a velocity command from VL instead of RL, a more time-efficient overtaking could be achieved.

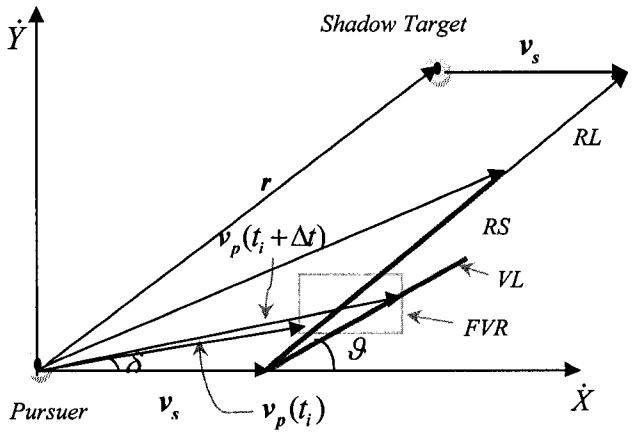

Figure 2.5: The *Velocity Line (VL).*

2.4.2 Implementation

As discussed above, a *shadow target*, *S*, is utilized herein for the guidance of *P*. The location of *S* is dictated by the location of O_D and varied according to the stage of overtaking manoeuvre. Once the manoeuvre starts, the vision module obtains a set of positional and velocity (p, v) quantities about all the vehicles in the workspace namely, *P*, O_D, and O_P. The position and velocity information is passed on to the modified-RG algorithm to compute *RS*, Figure 2.6, and subsequently, the maximum *closing velocity* component, $v_{\max}^{rel}$, Equation (2.10). This represents the desired velocity to be achieved by *P* for the next instance using modified-RG method denoted by v_{RG}.

An acceleration command, a_{RG} , to achieve the desired velocity in the next time instance is passed on to *P*. The proposed method also checks whether the maximum *closing velocity* $v_{\max}^{rel}$ is within the *FVR*. If $v_{\max}^{rel}$ is not within the *FVR*, an optimal velocity from *RS* is required for the next time instance. This velocity is also required to be within the *FVS*, formed by the intersection of *VL* and *FVR*. The *VL* intersects the *FVR* at two points designated as *v1* and *v2*. The set of points on the line bounded by *v1* and *v2* represents the velocities that are both within the *FVR* as well as members of *RS*. Selecting a point from within *FVS* would ensure a rendezvous with *S* with the desired velocity component.

For time-optimal rendezvous, we select the maximum velocity from within *FVS* that takes *P* nearest to *S*, which corresponds to *v1* in this case, Figure 2.6. Thus the required velocity to be achieved by *P* in the next time instant is given by $v_{RG} = v_p(t_i + \Delta t) = v1$. The corresponding lateral acceleration command a_{RG} in order for the robot to achieve this velocity in the interval $(t_i + \Delta t)$ is expressed as:

$$a_{RG} = \frac{v_{RG} - v_p(t_i)}{\Delta t} \tag{2.12}$$

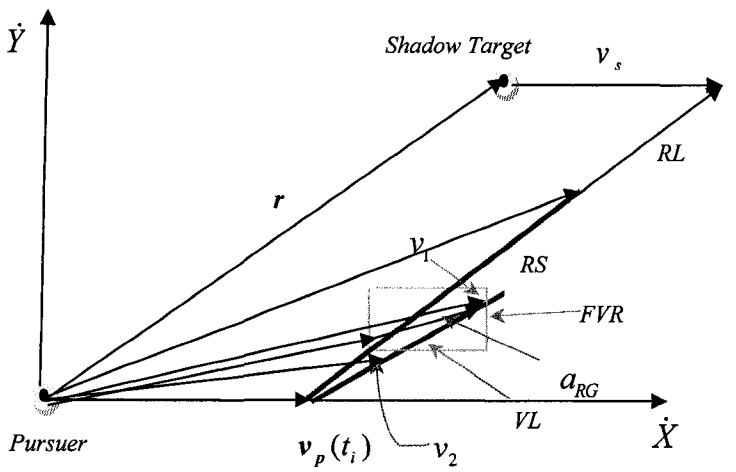

Figure 2.6: Pursuer-Velocity Command.

Case 1: Overtaking in the Absence of An Obstacle Vehicle in the Passing Lane: For Case1, as a first step, when P is 2.5 s behind O_D, the algorithm checks for O_P. If there is no O_P, P continues to travel in the driving lane until the distance between P and O_D is 2 s. At this point, S is created in the passing lane – as shown in Figure 2.7 by Positions 1, 2, and 3, for Phases 1, 2, and 3 of overtaking, respectively. During the complete manoeuvre, the velocity of S is chosen as the original velocity of P, at the start of overtaking, v_{st}. As discussed previously, all position and velocity matching objectives for P (with S) are achieved via the proposed RG algorithm.

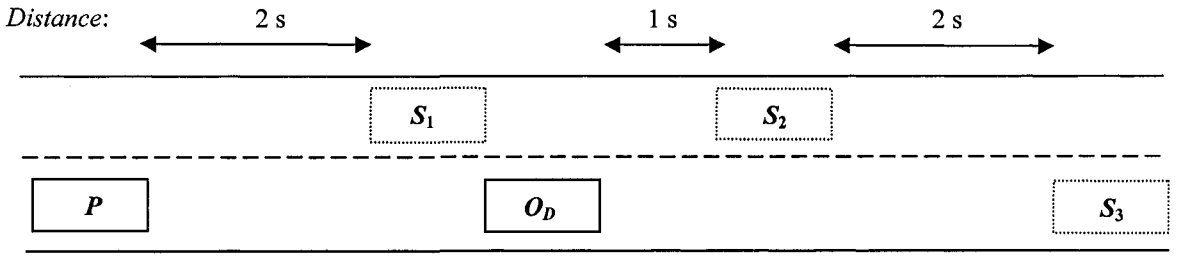

Figure 2.7: Shadow-Target Positions for Case 1.

Case 2: Overtaking in the Presence of An Obstacle Vehicle in the Passing Lane: As in Case 1, as a first step, when P is 2.5 s behind O_D, the algorithm checks for obstacles in the passing lane. If there is an O_P and the gap available between O_P and O_D is deemed as unsafe for overtaking, P must 'wait' until O_P first overtakes O_D. In this case, first, S is created in the driving lane, 2 s

behind O_D having a velocity equal to the velocity of O_D, Position 1, Figure 2.8. Once O_P clears O_D, P may start the overtaking manoeuvre. However, unlike in Case 1, the velocity of S at Positions 2 and 3 is set to either to the original velocity of P, $v_s = v_{st}$, or to the velocity of O_P, $v_s = v_{op}$, whichever is less.

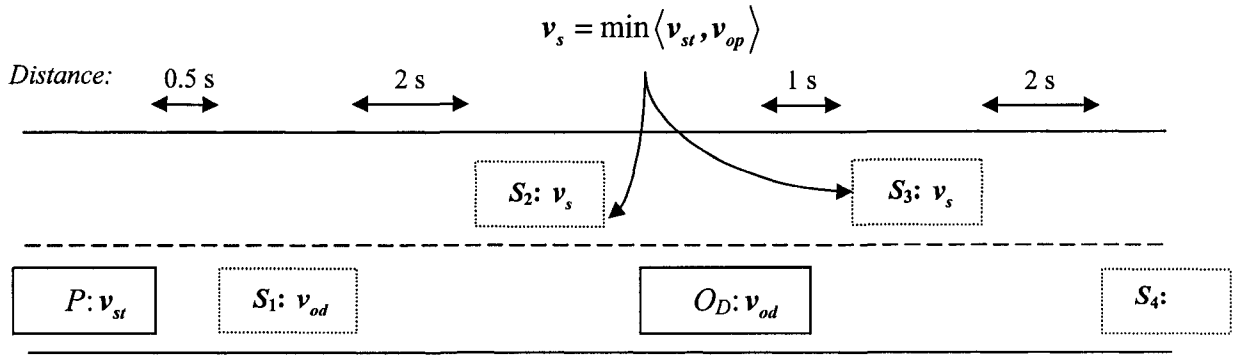

Figure 2.8: Shadow-Target Positions for Case 2.

Case 3: Aborting the Overtaking Manoeuvre: Let us consider a scenario, where P is driving with a velocity v_p in a linear direction. In front of P, O_D is driving with a velocity v_{od}. Initially $v_p > v_{od}$, but as P starts the overtaking manoeuvre, O_D also starts accelerating and its velocity becomes greater than that of P. In this Case, P cannot overtake O_D and has to abort the overtaking process and return back to the driving lane.

The decision to abort the overtaking manoeuvre is taken once the velocity of O_D becomes more than the velocity of S. In this case i.e., $v_{od} > v_s$, once P is in the passing lane, it continues travelling until the distance between P and O_D becomes 3 s (minimum distance required for lane change while ensuring passenger comfort). At this point, S is created in the driving lane which is 3 s ahead of the location of P at that time. The location of S is static and is not moving ahead with the changing location of P. For this Case the location of S and its velocity is shown in Figure 2.9. The velocity of S is set to either to the starting velocity of P, $v_s = v_{st}$, or to the velocity of O_D, $v_s = v_{od}$, whichever is less.

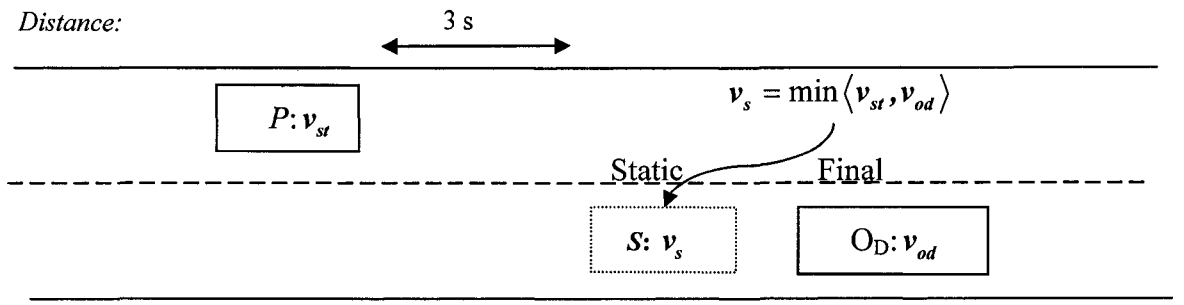

Figure 2.9: Shadow Target Locations.

Case 4: Overtaking Multiple Vehicles: Let us consider a simple Case, where P is driving with a velocity v_p in a linear direction. In front of P, another vehicle, O_{D1} is driving with a velocity v_{od1} . Ahead of O_{D1} another vehicle O_{D2} is moving in the driving lane with a velocity v_{od2}. An O_P is also moving in the passing lane which does not allow P to overtake O_{D1} immediately due to safety considerations. The complete Case is shown in Figure 2.10. The distance O_{D1} and O_{D2} is such that it is not possible for P to come back to the driving lane before overtaking both the vehicles.

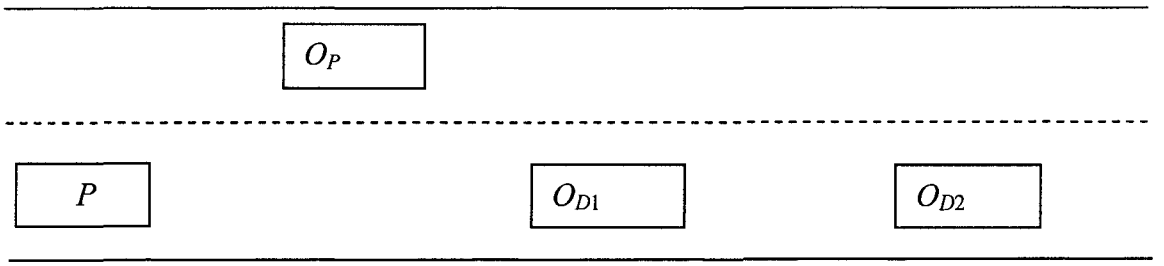

Figure 2.10: Location of Vehicles

In this Case, after Phase 2, the new location of S is 1 s ahead of O_{D2}. P will overtake O_{D2} and returns to the driving lane after overtaking both vehicles. The location and the velocity of the S at different stages are shown in Figure 2.11.

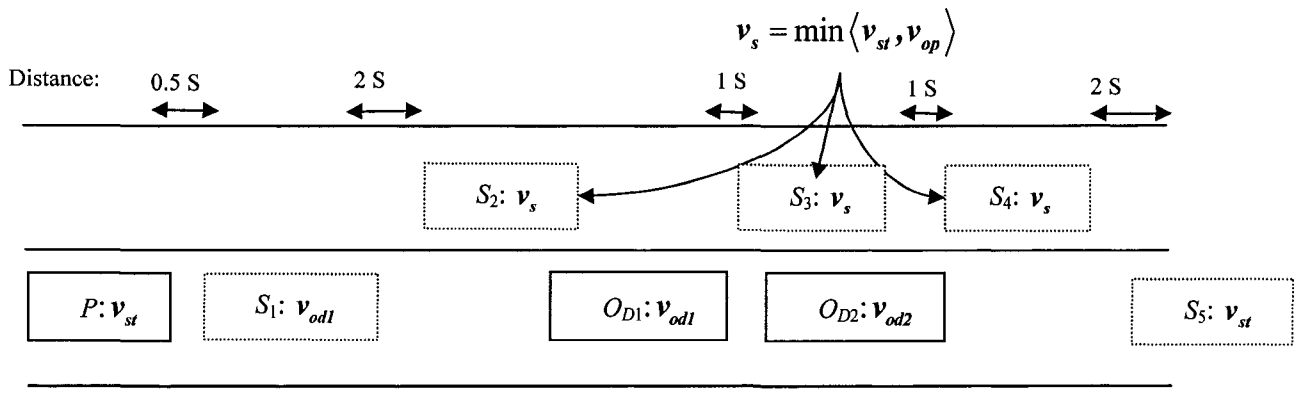

Figure 2.11: Shadow-Target Locations.

Case 5: Joining A Highway from A Ramp: Let us consider a Case, where P is driving with a velocity v_p on a ramp and wants to join the highway. Let the speed limit for the highway be v_{Limit} and the maximum velocity P can achieve, while ensuring safety and remaining within speed limit, be v_{Max} .

Let us divide this manoeuvre in two stages. In Stage 1, P travels on the ramp in a straight line and creates a gap for its safe lane change from ramp to highway, while Stage 2 is the lane-change from ramp to highway.

Once P enters the ramp and is parallel to the highway, S is created at the end of the ramp with a velocity equals to 0, Figure 2.12 and as soon as there is a gap available for the lane changing, Stage 2 starts and the location and velocity of S is shifted accordingly, Figure 2.13: a static S is created 3 s ahead of the location of P at that time (based on the average velocity v_{Ave} , which is the arithmetic average of v_p and that instance and v_{Max}). The velocity of the S is v_{Ave} and is updated after every instance.

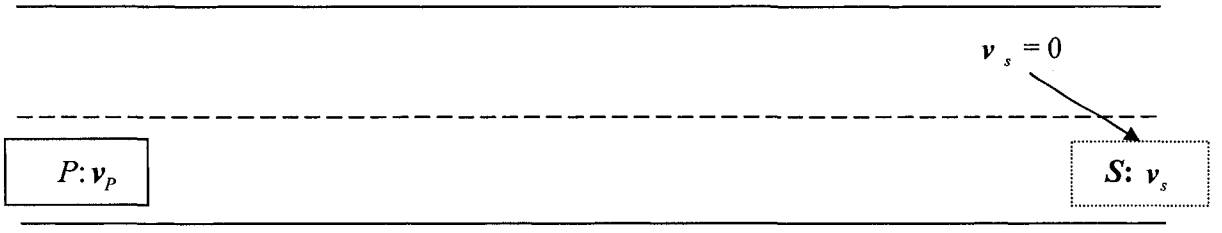

Figure 2.12: Stage 1.

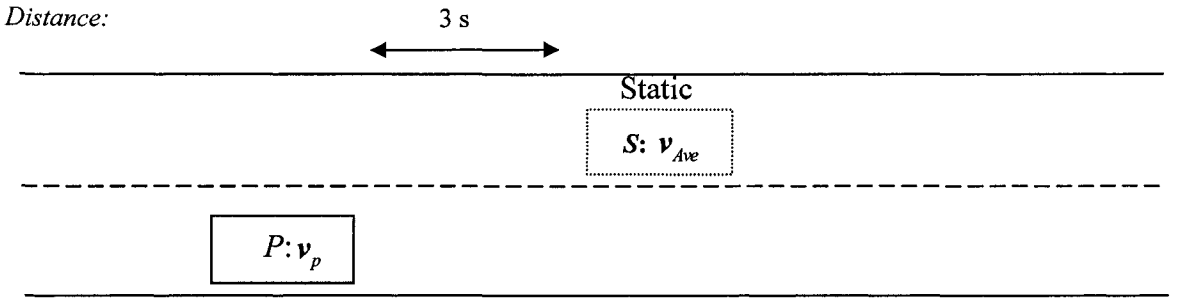

Figure 2.13: Stage 2.

3 IMPLEMENTATION: SIMULATIONS

In Chapter 2, the proposed trajectory-planning algorithm was presented along with the rules for shadow-target location under different cases. This Chapter presents the implementation of the trajectory-planning method via simulations. The overtaking time and obstacle-avoidance ability of the proposed method is analyzed under various ideal conditions. Section 3.1 discusses the methodology used in the simulations. Some simulation results of the proposed methodology are presented in Sections 3.2 to 3.6 with constant and varying velocities of both the obstacle vehicles in the driving lane and passing lane. In Section 3.7, two distinct types of comparisons are carried out: First, the performance of the proposed method is compared to a basic RG method as proposed in [114] and, then, the proposed method is compared to an off-line method presented in [77]. Section 3.8 summarizes the results of the simulations.

3.1 Methodology

All simulations presented in this Chapter were carried out in a VISUAL BASIC environment. For all simulations presented, the starting velocity of the pursuer vehicle, P, is taken as 30 m/s and the starting velocity of the obstacle vehicle in the driving lane, O_D, is taken as 20 m/s. The starting velocity of the obstacle vehicle in the passing lane, O_P, is taken 25 m/s except when it is moving with sinusoidal velocity; in that case, it is taken as 27.5 m/s. The simulations are divided into five Cases: (*i*) overtaking in the absence of an O_P, (*ii*) overtaking in the presence of an O_P, (iii) aborting the overtaking manoeuvre, (iv) overtaking multiple vehicles, and (v) vehicle joining a highway from a ramp.

3.2 Case 1: Overtaking in the Absence of An Obstacle Vehicle in the Passing Lane

In this Case, P is required to overtake a slower moving O_D with no O_P being present. The starting velocity of P is taken as 30 m/s and the starting velocity of O_D is taken as 20 m/s. Once the closing distance between the vehicles is 2 s, P starts its overtaking manoeuvre receiving guidance commands from the modified RG law. The results of the simulations for this Case are presented here for four variations of velocity of O_D, (*i*) constant, (*ii*) accelerating, (*iii*) decelerating, and (*iv*) sinusoidal, Figure 3.1. The results for each case are presented via a set of two figures and one table. The first figure in each set shows P's path and velocity profile and the second figure shows the velocity profiles of P in both the lateral and axial directions. The table shows the summary results.

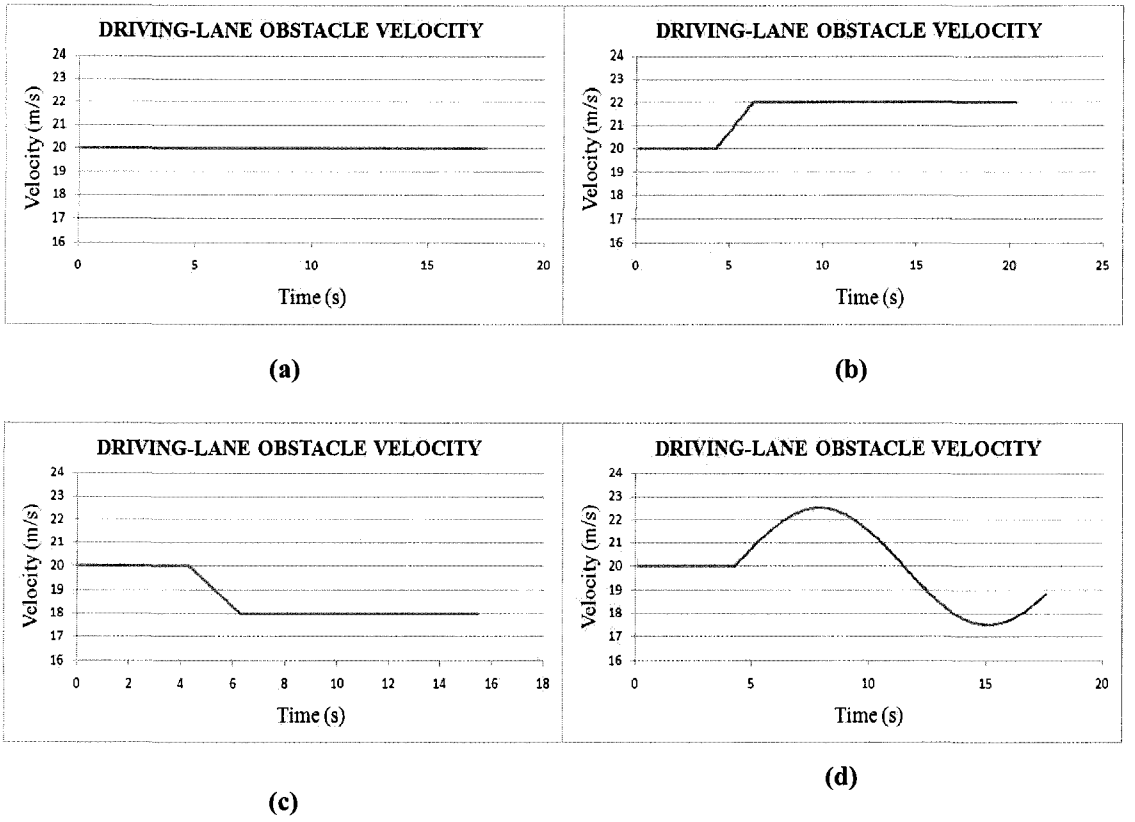

Figure 3.1: (a) Constant, (b) Accelerating, (c) Decelerating, and (d) Sinusoidal Velocity Profiles.

3.2.1 O_D is Moving with Constant Velocity

The results of the simulations for this scenario are presented in Figures 3.2 and 3.3 and Table 3.1. The velocity of O_D is as shown in Figure 3.1 (a). The complete manoeuvre took 13.5 s to complete.

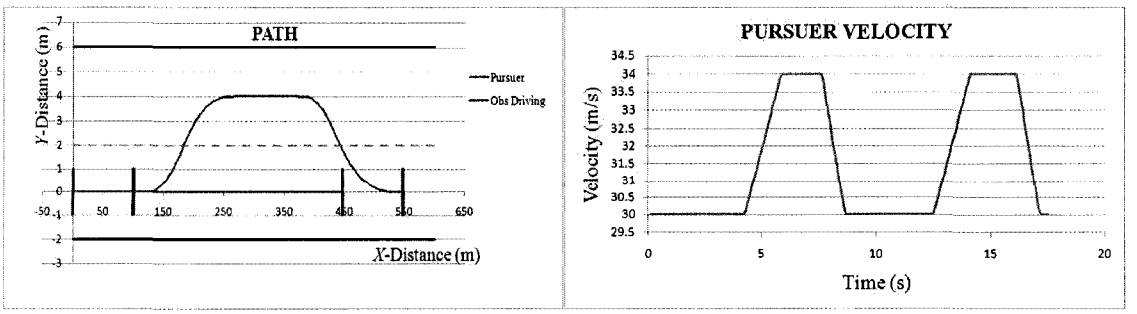

Figure 3.2. Path and Velocity Profile of *P*.

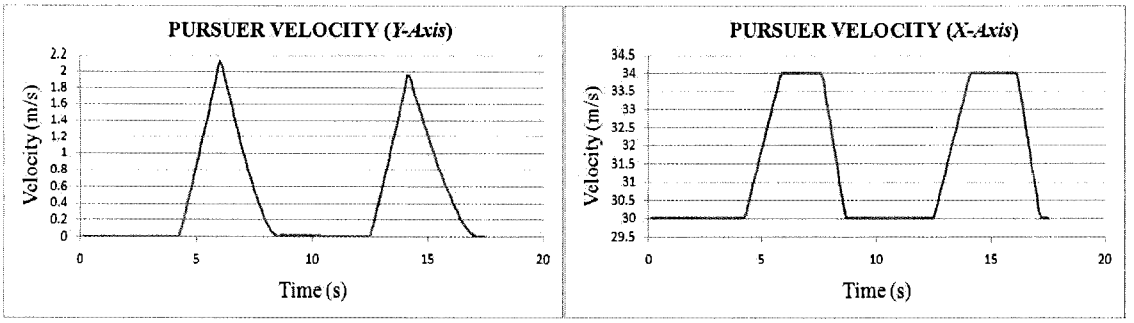

Figure 3.3. Lateral and Axial Velocities of *P*.

Table 3.1. Summary Results for Case 1, Scenario 1.

	Modified RG Technique
Total time taken for overtaking (s)	13.5
Maximum velocity achieved (m/s)	34
Maximum lateral acceleration (m/s^2)	1.1
Maximum axial acceleration (m/s^2)	2.0

3.2.2 O_D is Accelerating

The results of the simulations for this scenario are presented in Figures 3.4 and 3.5 and Table 3.2. The velocity of O_D is as shown in Figure 3.1 (b). The complete manoeuvre took 16.3 s to complete.

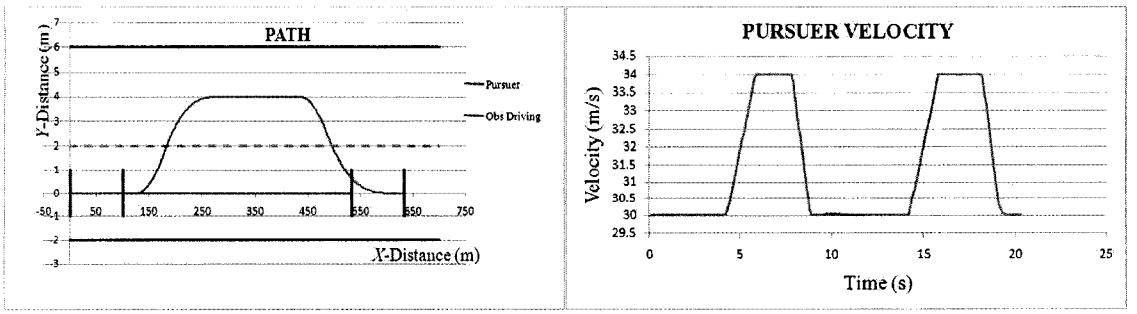

Figure 3.4. Path and Velocity Profile of *P*.

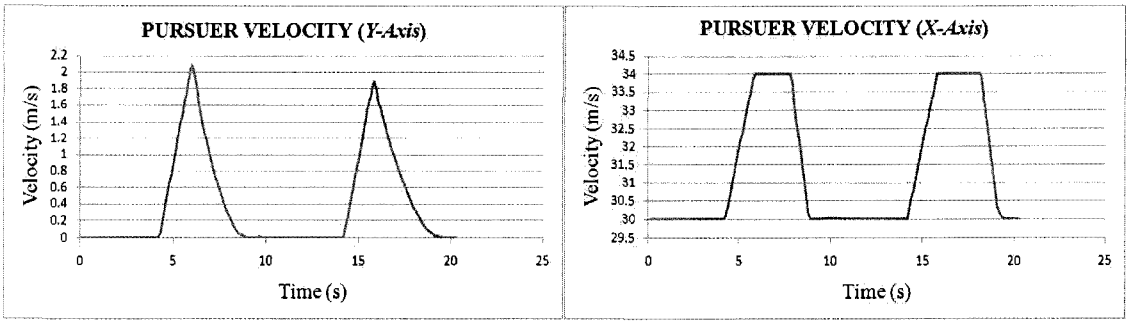

Figure 3.5. Lateral and Axial Velocities of *P*.

Table 3.2. Summary Results for Case 1, Scenario 2.

	Modified RG Technique
Total time taken for overtaking (s)	16.3
Maximum velocity achieved (m/s)	34
Maximum lateral acceleration (m/s^2)	1.04
Maximum axial acceleration (m/s^2)	2.5

3.2.3 O_D is Decelerating

The results of the simulations for this scenario are presented in Figures 3.6 and 3.7 and Table 3.3. The velocity of O_D is as shown in Figure 3.1 (c). The complete manoeuvre took 11.5 s to complete.

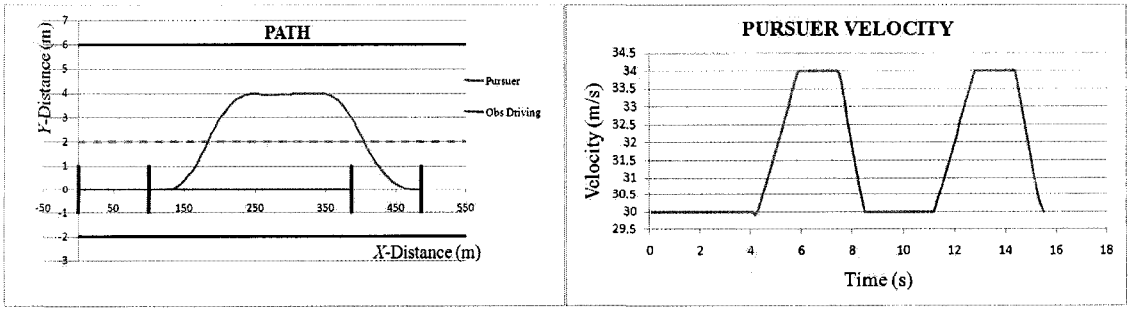

Figure 3.6. Path and Velocity Profile of *P*.

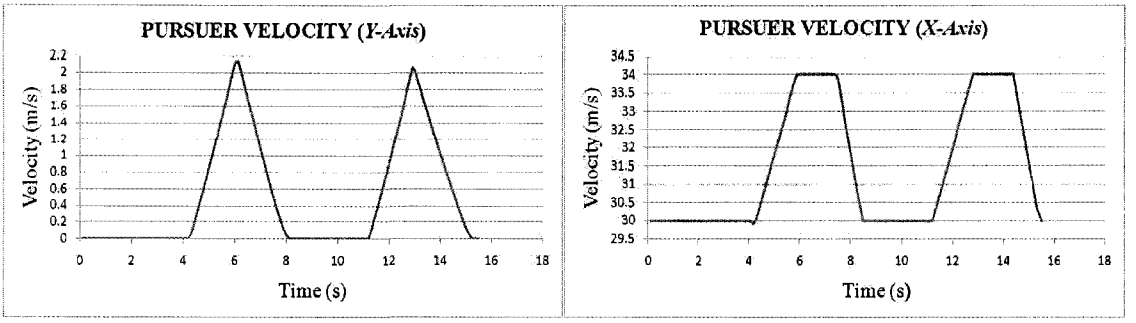

Figure 3.7. Lateral and Axial Velocities of *P*.

Table 3.3. Summary Results for Case1, Scenario 3.

	Modified RG Technique
Total time taken for overtaking (s)	11.5
Maximum velocity achieved (m/s)	34
Maximum lateral acceleration (m/s^2)	1.06
Maximum axial acceleration (m/s^2)	2.5

3.2.4 O_D is Moving with Sinusoidal Velocity

The results of the simulations for this scenario are presented in Figures 3.8 and 3.9 and Table 3.4. The velocity of O_D is as shown in Figure 3.1 (d). The complete manoeuvre took 13.6 s to complete.

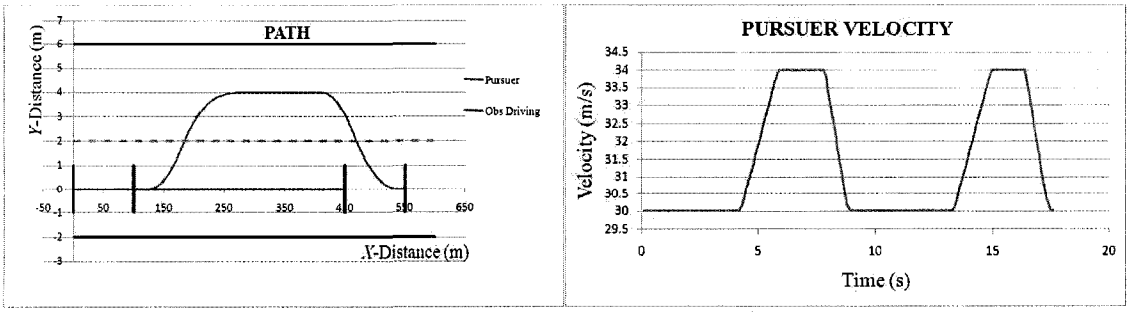

Figure 3.8. Path and Velocity Profile of *P*.

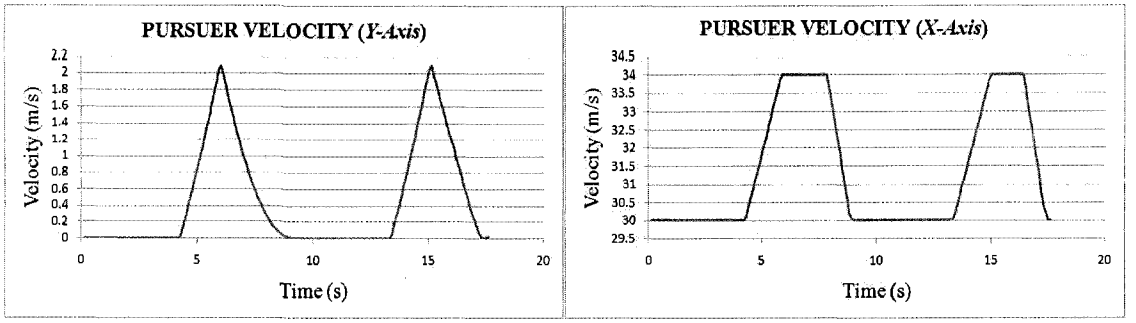

Figure 3.9. Lateral and Axial Velocities of *P*.

Table 3.4. Summary Results for Case 1, Scenario 4.

	Modified RG Technique
Total time taken for overtaking (s)	13.6
Maximum velocity achieved (m/s)	34
Maximum lateral acceleration (m/s^2)	1.04
Maximum axial acceleration (m/s^2)	2.1

3.3 Case 2: Overtaking in the Presence of An Obstacle Vehicle in the Passing Lane

In this Case, *P* is required to overtake a slower moving O_D when an O_P does not allow immediate overtaking. For this Case, the starting velocity of *P* is taken as 30 m/s and the starting velocity of O_D is taken as 20 m/s. The starting velocity of O_P is taken as 25 m/s except in the sinusoidal case where the starting velocity of O_P is taken as 27.5 m/s.

For this Case, the simulations were carried out for four variations of O_D and O_P velocities: (*i*) constant, (*ii*), accelerating, (*iii*) decelerating, and (*iv*) sinusoidal. The complete set of results are presented in Appendix A: two examples are presented here. In the first scenario, O_D is accelerating and O_P is decelerating. In the second scenario, both O_D and O_P are moving with sinusoidal velocity. The results of each example are presented via a set of three figures and one table. The first figure in each set shows *P*'s path and velocity profile, the second figure shows the

velocity profiles of P in both the lateral and axial directions, and the third figure shows the velocity profiles of both O_D and O_P. The table shows the summary results.

3.3.1 O_D is Accelerating and O_P is Decelerating

The results of the simulations for this scenario are presented in Figures 3.10, 3.11, and 3.12 and Table 3.5. An O_P is present and an overtaking manoeuvre by P is not immediately feasible. Hence, due to the presence of O_P, P first undertakes a collision-avoidance manoeuvre and, then, an overtaking manoeuvre. In the obstacle-avoidance manoeuvre, P decelerates in order to match the velocity of O_D while ensuring a 2 s distance between itself and O_D. When O_P is ahead of O_D and the overtaking manoeuvre is collision free, P starts the overtaking manoeuvre. During Phase 1, the velocity of P increases to a value of 30.2 m/s and, then, decelerates to match the velocity of the shadow target, S. During Phase 3, the velocity of P initially increases to a value of 34 m/s and, then, reduces to match the velocity of S. The complete manoeuvre took 52.8 s to complete.

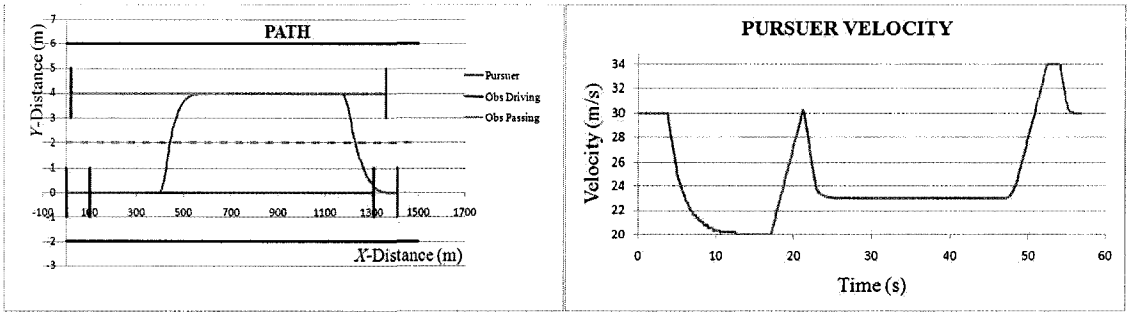

Figure 3.10. Path and Velocity Profile of P.

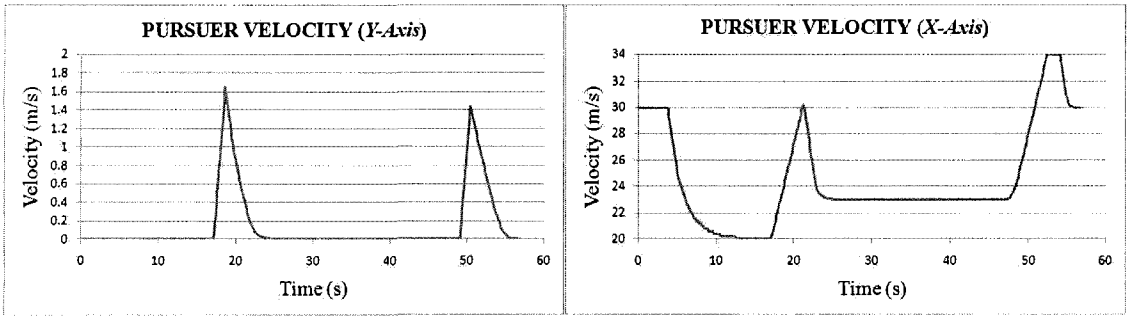

Figure 3.11. Lateral and Axial Velocities of P.

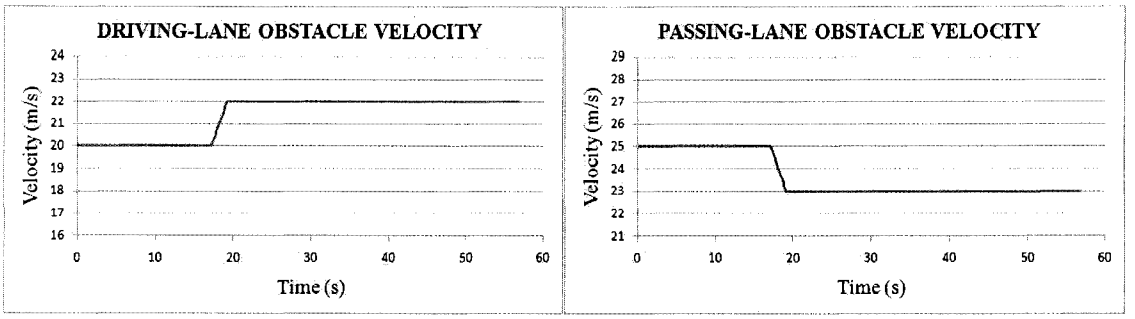

Figure 3.12. Velocities of O_D and O_P.

Table 3.5. Summary Results for Case 2, Scenario 7.

	Modified RG Technique
Total time taken for overtaking (s)	52.8
Maximum velocity achieved (m/s)	34
Maximum lateral acceleration (m/s^2)	0.91
Maximum axial acceleration (m/s^2)	2.42

3.3.2 Both O_D and O_P are Moving with Sinusoidal Velocity

The results of the simulations for this scenario are presented in Figures 3.13, 3.14, and 3.15 and Table 3.6. The complete manoeuvre took 26.8 s to complete.

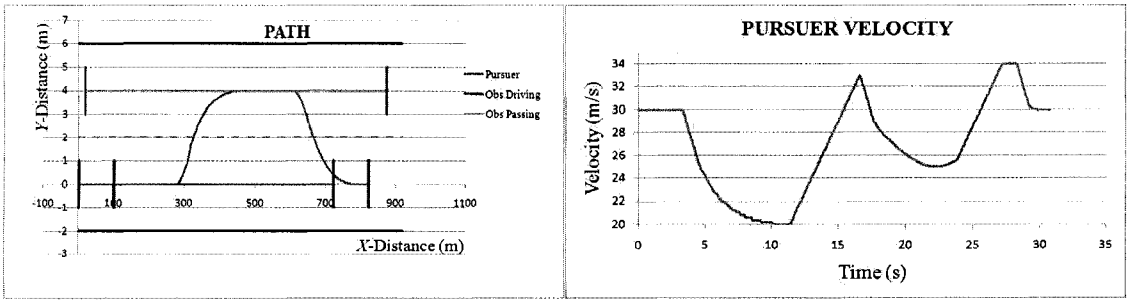

Figure 3.13. Path and Velocity Profile of *P*.

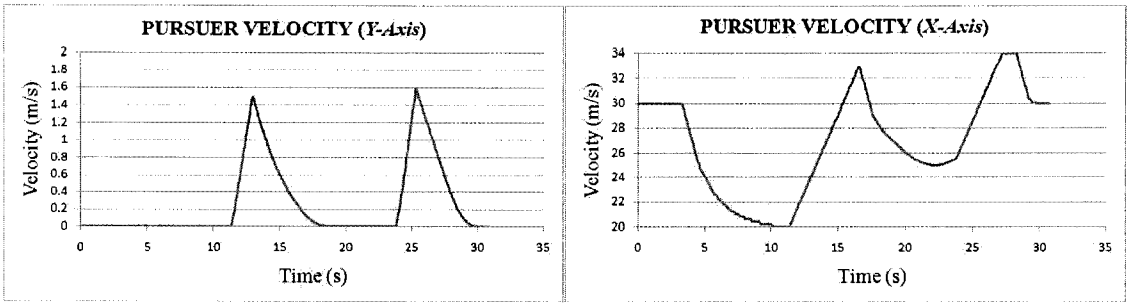

Figure 3.14. Lateral and Axial Velocities of *P*.

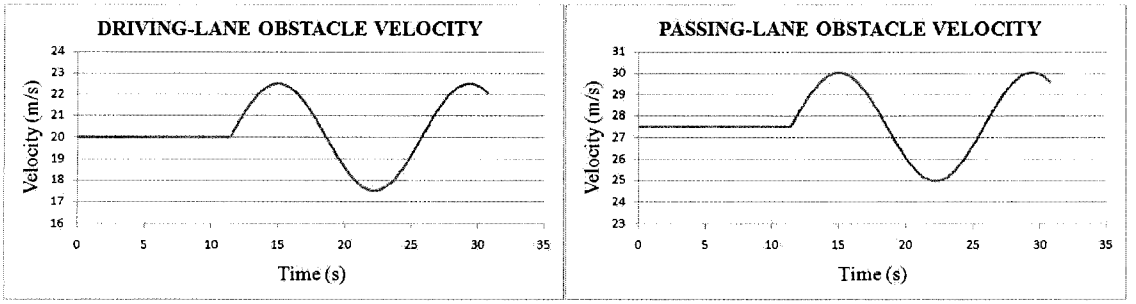

Figure 3.15. Velocities of O_D and O_P.

Table 3.6. Summary Results for Case 2, Scenario 16.

	Modified RG Technique
Total time taken for overtaking (s)	26.8
Maximum velocity achieved (m/s)	34
Maximum lateral acceleration (m/s^2)	0.88
Maximum axial acceleration (m/s^2)	2.35

3.4 Case 3: Aborting the Overtaking Manoeuvre

Two simulations were carried out for this Case: in the first scenario O_D is moving with a constant velocity after accelerating to its maximum velocity, in the second scenario, once P starts returning to the driving lane, O_D also starts decelerating. For both the scenarios, the starting velocity of P is 30 m/s and the velocity of O_D is 20 m/s.

3.4.1 O_D is Moving with A Constant Velocity after Accelerating to Maximum Velocity

In this scenario, once the overtaking manoeuvre starts, O_D accelerates to 34 m/s and, then, continues with this velocity. The path and the velocity profile of P for this scenario are shown in Figure 3.16.

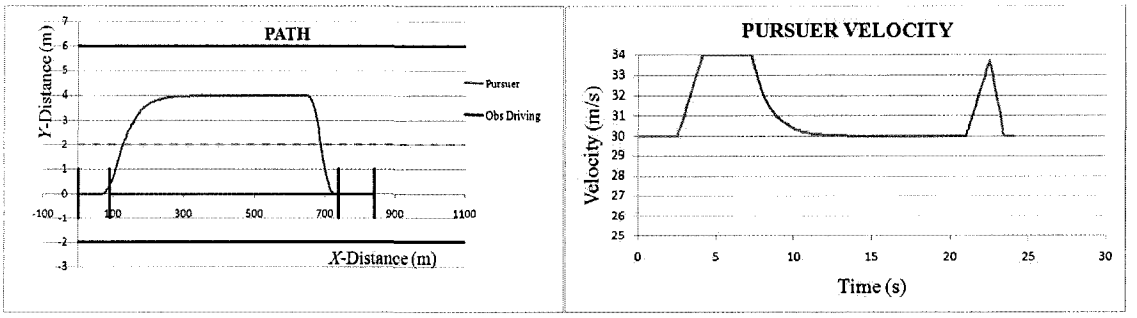

Figure 3.16. Aborting the Overtaking Maneuver: Case 3, Scenario 1.

3.4.2 O_D is Decelerating

In this scenario, once the overtaking manoeuvre starts, O_D accelerates to 34 m/s and as P starts its return manoeuvre, O_D also starts decelerating and its velocity becomes less than the starting velocity of P. The path and the velocity profile of P for this scenario are shown in Figure 3.17.

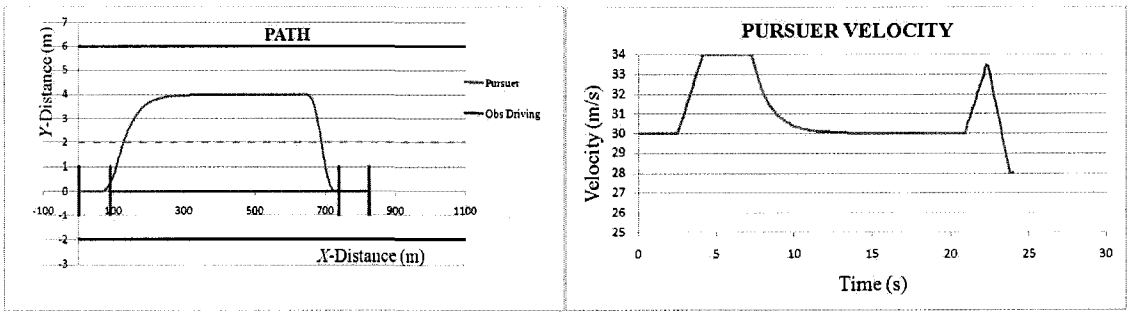

Figure 3.17. Aborting the Overtaking Maneuver: Case 3, Scenario 2.

3.5 Case 4: Overtaking Multiple Vehicles

For this Case, the starting velocity of P is 30 m/s and the velocities of the two O_Ds are 20 m/s. The path and the velocity profile of P are shown in Figure 3.18.

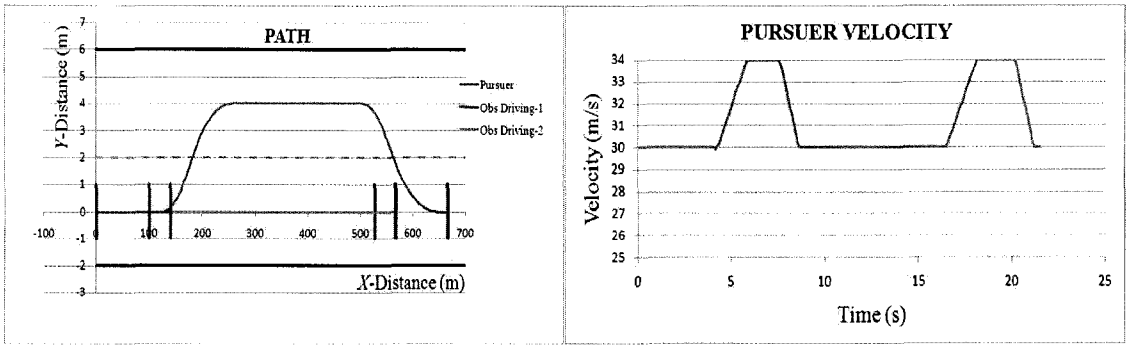

Figure 3.18. Overtaking Multiple Vehicles.

3.6 Case 5: Joining A Highway from A Ramp

3.6.1 No Obstacle Vehicle on Highway

If there is no other vehicle present on the highway, which restricts P from joining the highway, then, as soon as P is on the ramp and is parallel to the highway, Stage 2 starts and P joins the highway by receiving the velocity and direction commands from the modified RG method. In this scenario, $v_{Max} = v_{Limit}$, i.e., the maximum velocity P can achieve is the speed limit for that highway.

For this scenario, the velocity of P once it joins the ramp and is parallel to the highway is taken as 20 m/s and the speed limit for the highway, v_{Limit}, is taken as 30 m/s. At the start of Stage 2, the average velocity, v_{Ave} = 25 m/s. S is created 3 s (based on v_{Ave}) ahead of present location of P. P gets the velocity and direction commands from the modified RG method to rendezvous with S. The path and the velocity profile of P are shown in Figure 3.19.

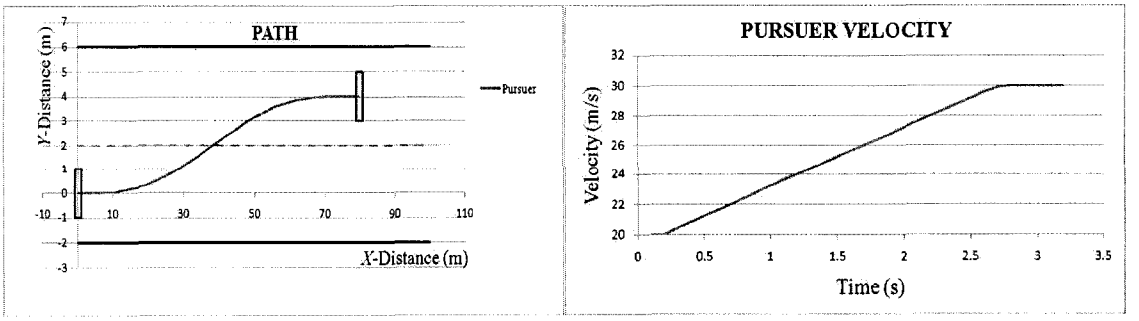

Figure 3.19. Vehicle Joining a Highway: Case 5, Scenario 1.

3.6.2 Obstacle Vehicle on Highway

If there is an obstacle vehicle on the highway and the gap available between the obstacle vehicle and P is deemed as unsafe for joining the highway, P must 'wait' until the obstacle vehicle moves 3 s ahead of it. In this scenario, P remains in Stage 1 until a gap of 3 s is created. While in Stage 1, S is created at the end of the ramp with a velocity of 0. Hence, P starts decelerating in order to match the velocity and location of S in Phase 1. However, as soon as the gap between the vehicles is more than 3 s, Stage 2 starts and P starts the lane-change manoeuvre. However, unlike in scenario 1, the maximum velocity, would be $v_{Max} = \min\langle v_{Limit}, v_{op} \rangle$.

For this scenario the velocity of P, once it joins the ramp and is parallel to the highway, is taken as 20 m/s, the speed limit for the highway, v_{Limit} , is taken as 30 m/s and the velocity of the obstacle vehicle moving on the highway as 25 m/s . Since in this case $v_{op} < v_{Limit}$, $v_{Max} = v_{op}$. For this scenario, the path and the velocity profile of P is shown in Figure 3.20.

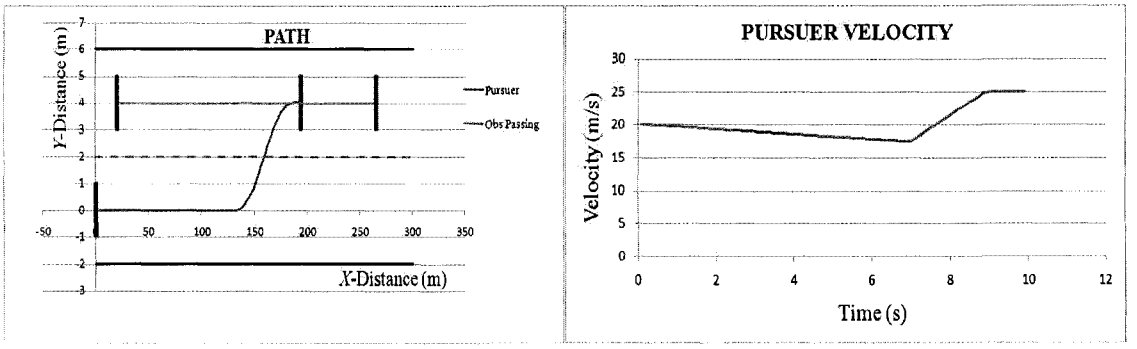

Figure 3.20. Vehicle Joining a Highway: Case 5, Scenario 2.

3.7 Comparison of Proposed Methodology

3.7.1 Comparison with Original RG Method

Simulations which were carried out for the modified RG method were repeated using the original RG method, Appendix B. One example for each case is presented here via a set of two figures and one table. The first figure shows P's path and velocity profile using the modified RG method

and the second figure shows P's path and velocity profile using the original RG method. The table shows the time taken and the distance travelled using both methodologies.

Case 1, Scenario 3

There is no O_P present, which could delay/restrict the overtaking manoeuvre. In this scenario, O_D is decelerating from 20 m/s to 18 m/s. The results obtained from the simulation are presented in Figures 3.21 and 3.22 and Table 3.7.

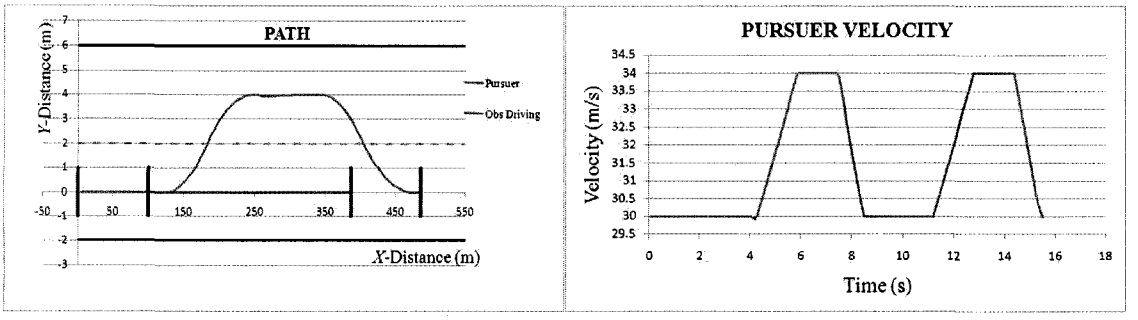

Figure 3.21. Path and Velocity Profile of P Using the Modified RG Method.

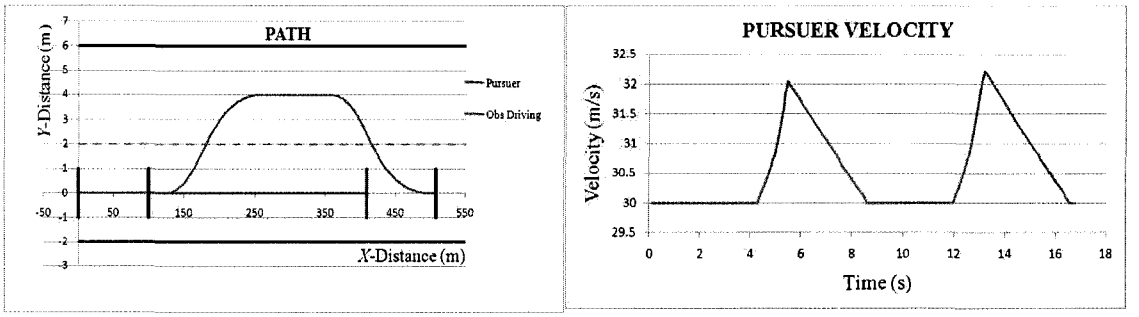

Figure 3.22. Path and Velocity Profile of P Using the Original RG Method.

Table 3.7: Basic Overtaking Parameters for Case 1, Scenario 3 – A Comparison.

	Modified RG Method	Original RG Method
Total time (s)	11.5	12.7
Distance travelled (m)	368	390

Case 2, Scenario 2

There is an O_P present which could delay/restrict the overtaking manoeuvre. In this scenario, O_D is moving with a constant velocity and O_P is accelerating from 25 m/s to 30 m/s. The results obtained from the simulation are presented in Figure 3.23 and 3.24 and Table 3.8.

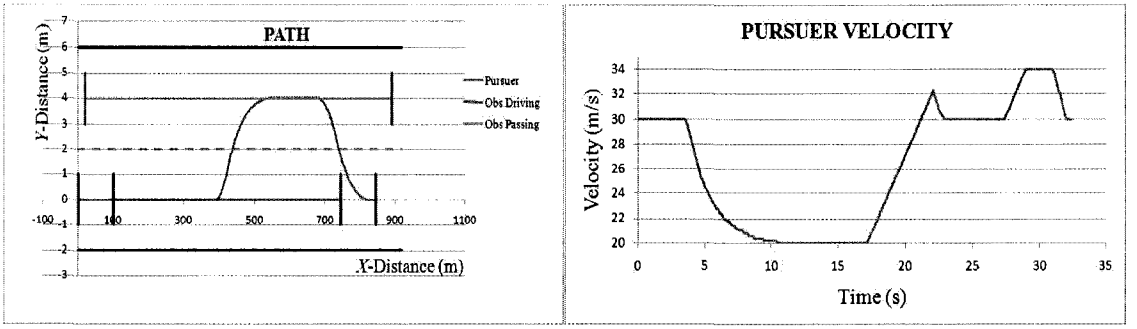

Figure 3.23. Path and Velocity Profile of *P* Using the Modified RG Method.

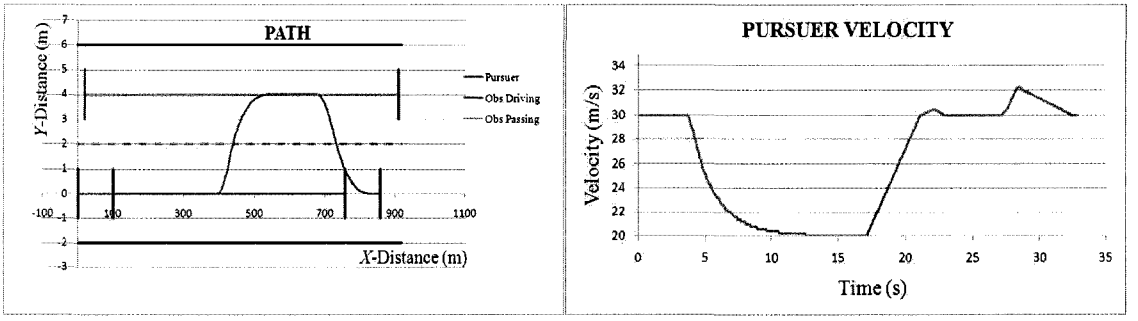

Figure 3.24. Path and Velocity Profile of *P* Using the Original RG Method.

Table 3.8: Basic Overtaking Parameters for Case 2, Scenario 2 – A Comparison.

	Modified RG Method	Original RG Method
Total time (s)	28.4	28.8
Distance travelled (m)	728	736

3.7.2 Comparison with an Off-Line Method

The comparison of the proposed on-line methodology was also carried with an off-line method presented in [77]. Since the technique proposed in [77] cannot cope with variations in obstacle velocity, for this comparison, both O_D and O_P are moving with constant velocities. Two simulations are presented for this comparison: one with no O_P present and another with an O_P present. The results of the simulations for the comparison are presented via a set of two figures and one table. The first figure shows P's path and velocity profile using the proposed modified RG method and the second figure shows P's path and velocity profile using the off-line method presented in [77]. The table shows the time taken and the distance travelled using both methodologies.

Case 1, Scenario 1

There is no O_P present which could delay/restrict the overtaking manoeuvre. In this scenario, O_D is moving with a constant velocity of 20 m/s and the velocity of P is 30 m/s. The results obtained from the simulation are presented in Figures 3.25 and 3.26 and Table 3.9.

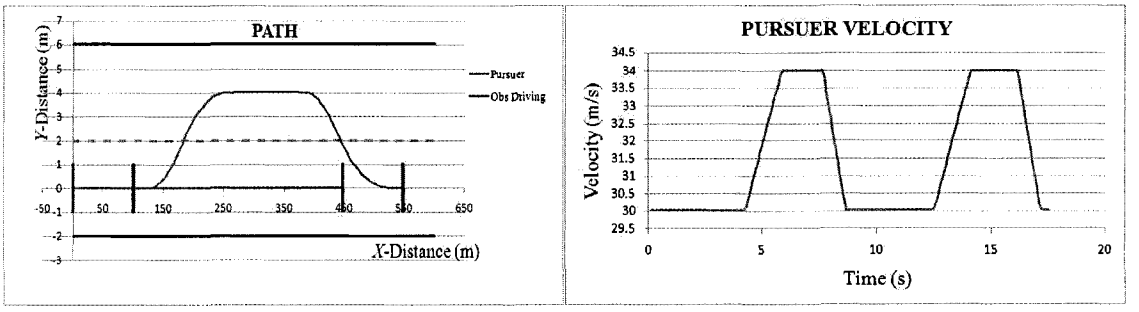

Figure 3.25. Path and Velocity Profile of P Using the Modified RG Method.

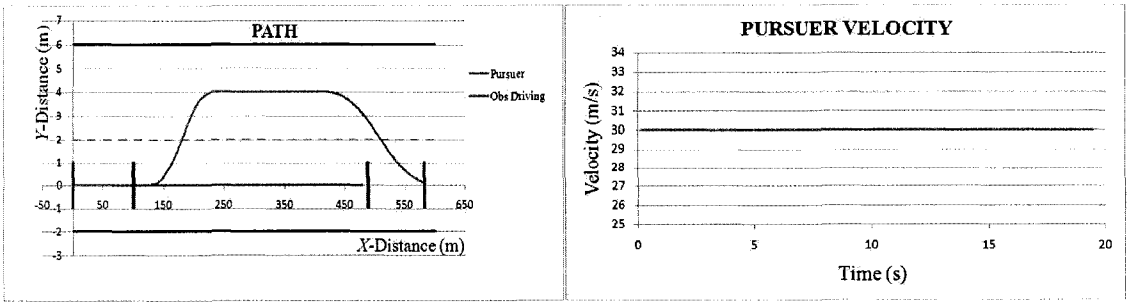

Figure 3.26. Path and Velocity Profile of P Using the Off-Line Method.

Table 3.9: Basic Overtaking Parameters for Case 1, Scenario 1 – A Comparison

	Modified RG Method	Off-Line Method
Total time (s)	13.5	15.5
Distance travelled (m)	430	466

Case 2, Scenario 1

There is an O_P present which could delay/restrict the overtaking manoeuvre. In this scenario, both O_D and O_P are moving with constant velocities of 20 m/s and 25 m/s, respectively. The starting velocity of P is taken as 30 m/s. The results obtained from the simulation are presented in Figure 3.27 and 3.28 and Table 3.10.

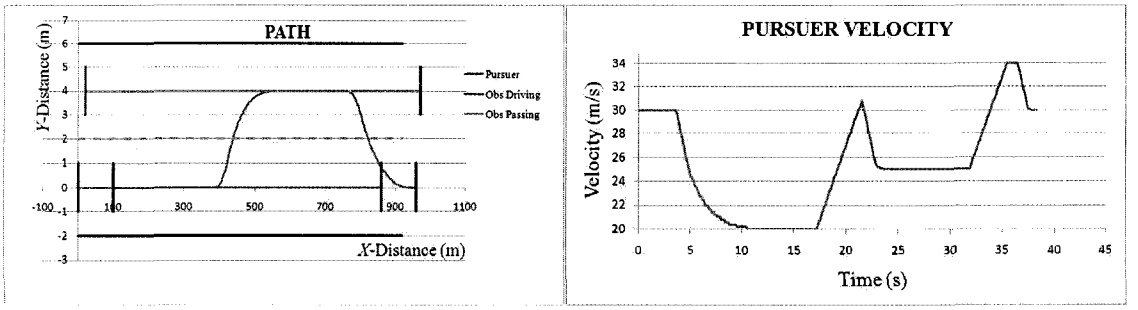

Figure 3.27. Path and Velocity Profile of P Using the Modified RG Method.

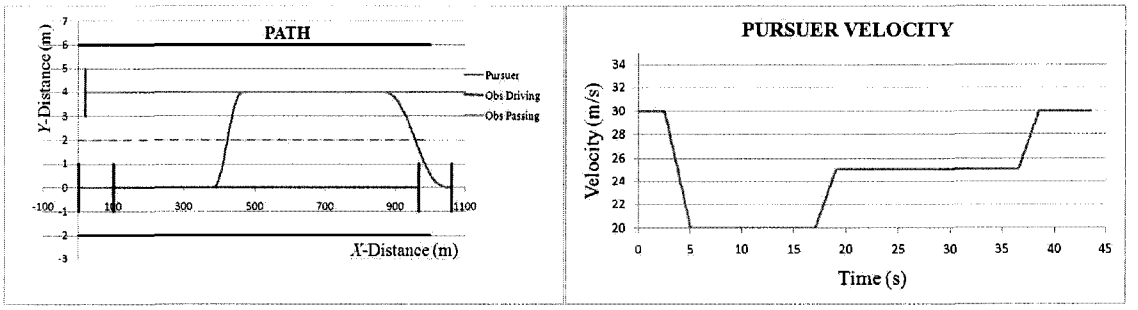

Figure 3.28. Path and Velocity Profile of P Using the Off-Line Method.

Table 3.10: Basic Overtaking Parameters for Case 2, Scenario 1 – A Comparison.

	Modified RG Method	Off-Line Method
Total time (s)	34.2	39.5
Distance travelled (m)	844	966

3.8 Summary of Results

The modified RG method is able to carry out the overtaking manoeuvre in the presence or absence of any other obstacle vehicle in the passing lane while remaining within the constraints of passenger comfort and ensuring a collision-free overtaking. Furthermore, the proposed method has the following added characteristics.

1. The proposed method shows improvement in terms of time taken and the distance required to undertake the overtaking manoeuvre as compared to the original RG method and the off-line methods.
2. The method can be used for both overtaking and obstacle-avoidance thus reducing the complications during overtaking.
3. The method can be used for other manoeuvres required by the autonomous vehicle in addition for its usage for overtaking.

4 IMPLEMENTATION: EXPERIMENTS

The simulations performed in Chapter 3 assumed ideal conditions. In order to examine the performance of the proposed algorithm in more realistic environment, numerous experiments were carried out. Section 4.1 below describes the different aspects of the experimental set-up, including a system overview, and details of the vision system, the communication system, and the autonomous robotic vehicles. The results of some example experiments are presented in Section 4.2. Section 4.3 presents conclusions derived from the experimental results.

4.1 Experimental Set-up

The experimental set-up is illustrated in Figure 4.1. The host PC, a Pentium IV 1.6 GHz processor, incorporates the Visual C++ application with three primary software modules: image acquisition and processing, pursuer's trajectory planning, and communications, Figure 4.2. An analog CCD camera captures the image of the workspace and transfers it to the frame grabber in the PC. The vision algorithm, then, takes the raw image and extracts the positional information

of all objects in the workspace. This information is sent to the trajectory planner, where an acceleration command is calculated for the pursuer vehicle. The communication module broadcasts data to the mobile robotic vehicles via a Bluetooth module connected to the PC.

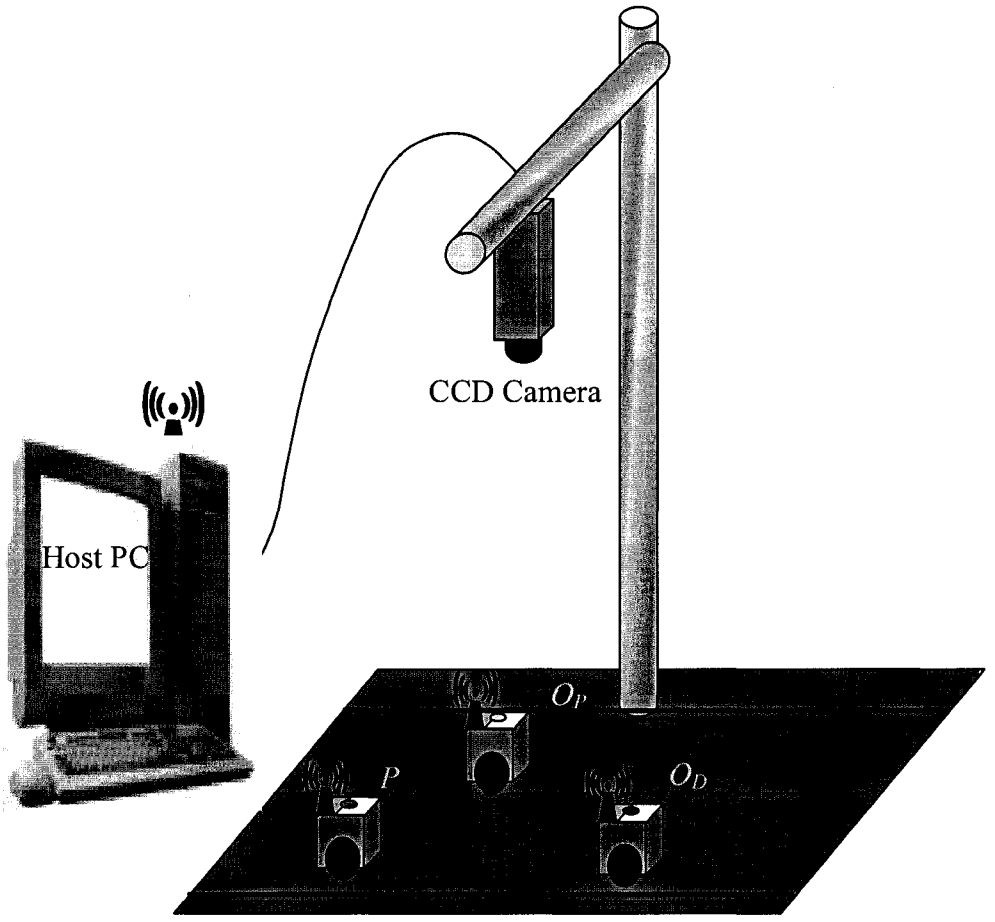

Figure 4.1: Experimental Set-up: Physical Layout.

Three robotic vehicles were controlled by the host PC. The overall dimension of the work floor as seen by the camera is (2700 mm × 1500 mm). The "two-lane road" is configured with a mat-finish black chart paper. The CCD camera is mounted ≈ 2000 mm directly above the centre of the experimental set-up. Two halogen lamps, mounted on each side of the camera, provide the necessary lighting.

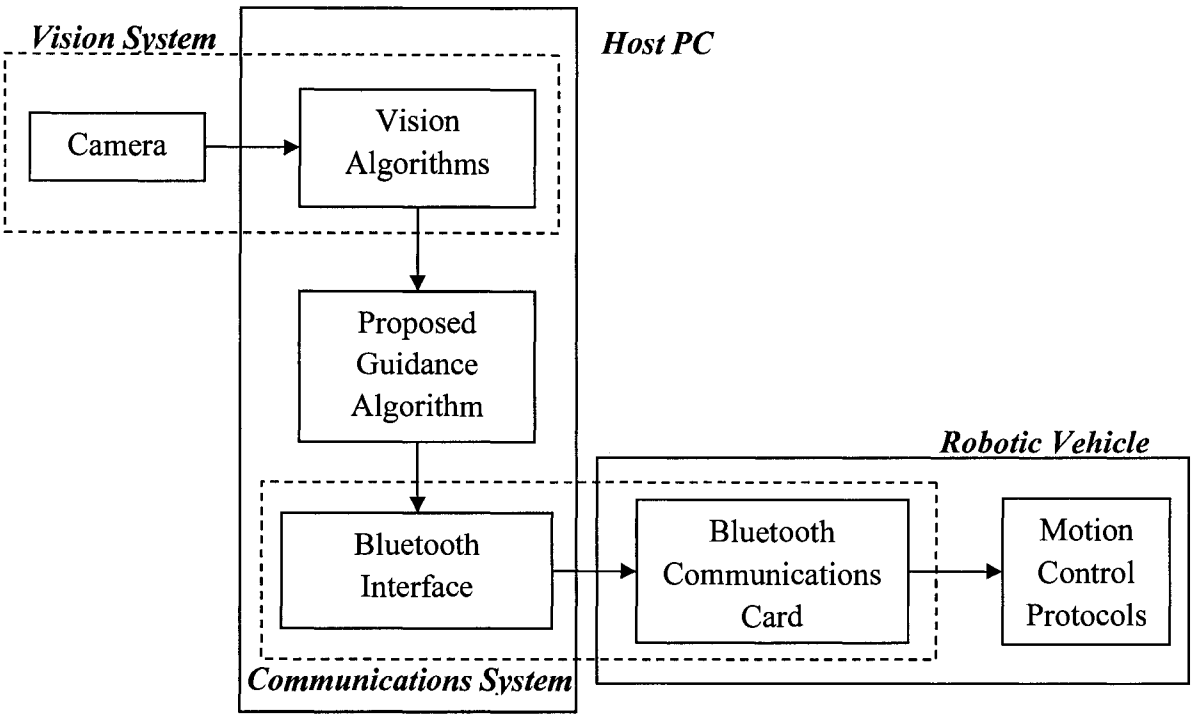

Figure 4.2: Experimental Set-up: Software Configuration.

4.1.1 Vision System

The details of the vision system can be found in [115].

Hardware

The vision system comprises a JVC TK-870U CCD camera with a Cosmicar C60607 wide-angle lens and a Matrox Meteor II frame-grabber. The CCD camera has a resolution of (640 × 480) pixels and a standard composite colour output. The refresh rate of the camera is 30 frames per second (fps). The Cosmicar C60607 wide angle lens has a focal length of 6 mm and provides a Field-of-View (FOV) of (3200 mm × 2400 mm).

The images taken by the camera are transferred to the Matrox Meteor II frame-grabber through a co-axial cable from the composite output. The Meteor II is installed into the PCI slot of the PC. Matrox provides a set of Visual C++ functions that allow access to the memory of the Meteor II to extract image data.

Image-to-world coordinate transformation is done through a camera-calibration model. The overhead camera was calibrated using the same off-line, non-coplanar calibration technique that

was used in [116]. This technique, computes the intrinsic and extrinsic parameters of a camera, and provides a set of equations for coordinate transformation. The intrinsic parameters include focal length, lens distortion, scale factor uncertainty, and 2D camera-image centre coordinates. The extrinsic parameters are the six translation and rotation parameters defining the 3D rigid body transformation from world-to-image coordinate system. A large calibration board, on which evenly spaced circular markers were printed, was used to provide the calibration model with known coordinate points in the workspace. The circles are 80 mm in diameter, and the pitch in the X direction is 279.4 mm and in the Y direction is 215.9 mm. The calibration board is (1157mm × 1118 mm) in size and contains (4 rows × 4 columns) of circles. It was placed at various locations in the workspace and the pixel location of each coordinate point (circle) was taken. The model parameters were then calculated using these coordinate points.

Software

The pursuer and the obstacles are colour coded for identification. The raw image contains three channels of data, indicating the intensities of the Red (R), Green (G) and Blue (B) colours in each pixel. This is more commonly known as the *RGB* colour space. Each channel contains 8 bits of information. Thus, 24-bits of information is embedded into one pixel, representing more than 16 million different colours. However, there are only three colours that are used by the identification markers. Therefore, the 24-bits of information must be categorized into any of the three colours or a non-colour. This is called the *thresholding process*.

A transformation of the entire raw-image to the *YCbCr* colour space is performed because of its ability to separate the luminance or brightness of a pixel from its hue or colour [117]. This property makes it possible to place less importance on the change in brightness of an object, as when the object is affected by shadows but, rather, focus on the colour of the object itself. The *YCbCr* colour space, like the *RGB* space, is also 3-dimensional. The first dimension, *Y*, describes the luminance, or brightness, of the pixel. The second, *Cb*, which stands for Chrominance-blue, describes the hue of the pixel in terms of its intensity of the blue colour. Lastly, *Cr*, which stands for Chrominance-red, refers to the hue of the pixel in terms of the red colour. The transformation is performed by the following equations, [116]:

$$Y = 0.299R + 0.587G + 0.114B, \tag{4.1}$$

$$Cb = (B - Y)/1.772, \quad \text{and} \tag{4.2}$$

$$Cr = (R - Y)/1.402, \tag{4.3}$$

where Y has a range of [0, 255], and Cb and Cr both have a range of [−127.5, 127.5].

As mentioned above, three colours are used by the identification markers: blue, yellow, and white. Before thresholding can be carried out, these colours must be assigned a *YCbCr* value. An image of an identification marker containing these three colours is first taken. From the pixel values, the mean is found for each colour. The mean is now the defined *YCbCr* value of that colour. For example, the blue colour has a Y value of 140, a Cb value of 10.0, and a Cr value of −8.0. The three identification colours are, hereafter, referred to as the *predefined colour set.*

When an image is examined, the Euclidean distances, in the *YCbCr* colour space, between each pixel in the image and the predefined colour set are calculated. Since it is desirable to lessen the effects of uneven lighting or shadows, a weighted Euclidean distance is used. Less weight is placed on the Y channel because it refers to the brightness of the pixel, while more weight is put on the Cb and Cr channels because they refer to the hue of the pixel. Through experimentation in [115], it was found that the weights in the following equation perform well to lessen the effects of shadows:

$$D = \sqrt{0.15\left(Y_{pixel} - Y_{colour}\right)^2 + 0.425\left(Cb_{pixel} - Cb_{colour}\right)^2 + 0.425\left(Cr_{pixel} - Cr_{colour}\right)^2}, \tag{4.4}$$

where D is the weighted Euclidean distance, Y_{pixel}, Cb_{pixel}, and Cr_{pixel}, are measured *YCbCr* values of the pixel, and Y_{colour}, Cb_{colour}, and Cr_{colour} are the values of the predefined colour set.

It was found that the pixels on the identification marker varied no more than 18.0″ weighted Euclidean distance from the defined *YCbCr* value. This value was, therefore, set as the threshold distance. Thus, if a pixel is within a threshold distance of 18.0″ of a certain colour in the predefined colour set, then it is considered to be that colour. If the distance is more than this threshold for all the colours of the predefined colour set, the pixel is considered a non-colour. This thresholding operation effectively transforms each pixel to contain 2 bits of information, indicating that the pixel is blue, yellow, white or a non-colour.

After the image has gone through the thresholding operation, the positions of the pursuer and the obstacles are determined. A search through the work floor is performed to find the markers on the vehicles. In order to minimize the search time, sampling is done according to markers. The dimension of the smallest marker is used to achieve the smallest sampling rate, denoted here as l pixels. Starting from pixel location (0, 0) in the work floor, every $0.5l$ pixels are sampled along the X and Y directions. If the sampled pixel has the colour of the predefined set, a search frame is placed over that pixel. The size of the search frame is dependent on the colour of interest, but it is twice that of the diameter of the marker. This search frame size ensures that the marker, regardless of its orientation, would be within the frame. Every pixel in the search frame is examined and if the number of pixels of a certain colour in the search frame exceeds a pre-determined threshold, then, a marker of that colour is considered to be located in that search frame. The centroid of that colour blob is, then, calculated to sub-pixel accuracy using the Centroid Method [118]. This operation continues throughout the whole work floor to locate all colour markers. Figure 4.3 illustrates this search process.

With all the markers located, object identification can be performed. Each of the three vehicles, which can be the pursuer or obstacles in the driving or passing lane, is identified by a colour-coded marker. The marker contains a coloured circle in the centre of the marked pattern, and a pink strip in front of the robotic vehicle as shown in Figure 4.4. The rest of the vehicle is coloured in black. The vision program first searches for coloured circle markers (in this case blue markers). Once a blue marker is found, the algorithm looks for a pink marker within a distance of the radius of the vehicle. If a corresponding pink marker is located, then, a vehicle has been successfully found. An imaginary line is then drawn between the centre of the blue circle to the centroid of the pink pattern. This line indicates the bearing of the vehicle. The colour of the circular markers pattern differs as such the identification of different coloured markers on the detected vehicle helps to identify whether the vehicle detected is the pursuer or an obstacle in the driving or passing lane. In this regard P is identified with a blue circle whereas O_D and O_P are identified with red and yellow circles, respectively.

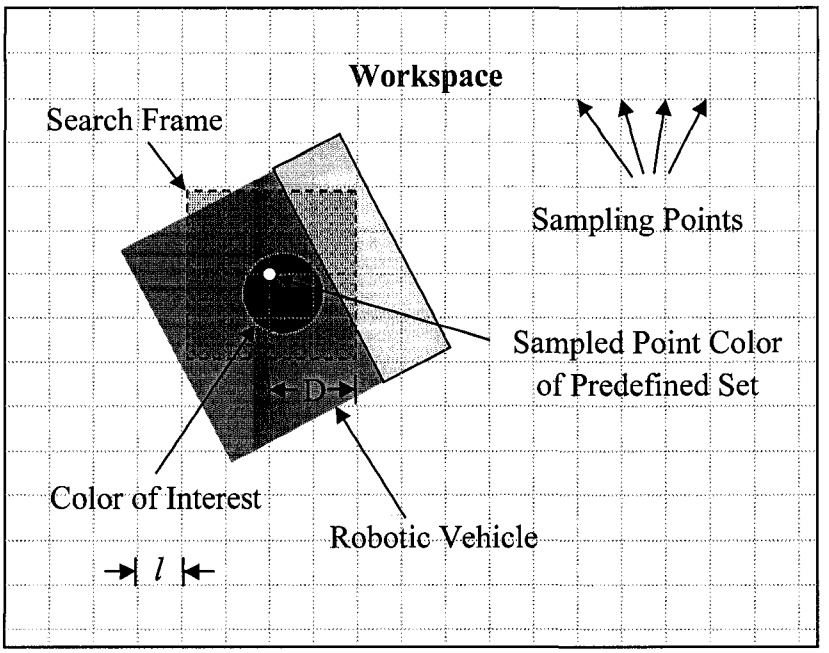

Figure 4.3. Color Marker Search [115].

4.1.2 Robotic Vehicles

Three identical robotic vehicles were used in the implementation of this thesis work. For the purpose of the experiments, one vehicle acts as P and the other two as O_D and O_P respectively.

The vehicles are the MIABOT Pro-robots developed by Merlin Systems, Figure 4.4. These vehicles are fully autonomous and have a differential-drive system that provides an ease of implementation and compactness. They have a base plate, a top plate, two DC-motors, two gear assemblies, and two ball casters. The motors are driven by 6 × 1.2 V (AA) cells through a low-resistance driver integrated circuit with a slow-acting current limit at about 5A. Maximum speed of an unloaded motor is in the range of 6-8000 rpm.

The motor shafts drive the wheels through an 8:1 gearing. The motors incorporate quadrature encoders giving 512 position-pulses per rotation. The wheels are 52 mm in diameter, so one encoder pulse corresponds to just under 0.04 mm of movement. The top plate is marked with a coloured pattern to provide the vision system with the position and orientation (pose) of the vehicle.

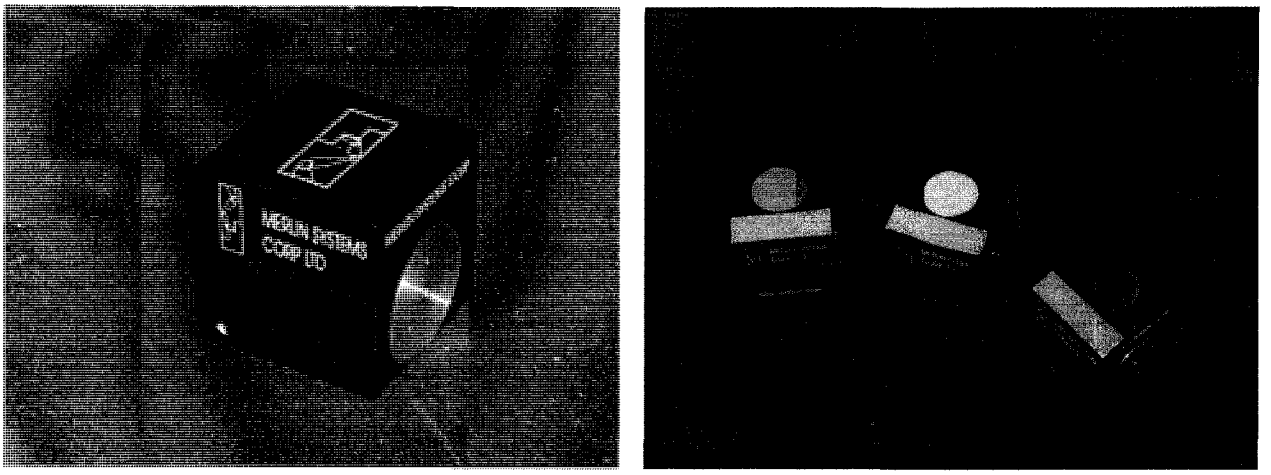

(a) (b)

Figure 4.4. (a) Robotic Vehicle (b) Vehicles with Markers .

4.1.3 Communication System

The communication system of the MIABOT Pro-robot consists of a bi-directional Bluetooth communications module, which provides a robust frequency hopping wireless communications protocol at 2.4GHz. A Bluetooth communications card is incorporated within each vehicle. This enables the host PC to communicate with the vehicle by converting the Bluetooth link to logic-level serial signals connecting to the main board processor.

A PC Bluetooth dongle is supplied that plugs into the USB port on the PC. This can support wireless links with up to 7 vehicles at once. Each Bluetooth link is a dedicated, secure two-way channel established exclusively between the two devices (the 'pairing'). It appears to PC applications programs as a *virtual COM port*, which can be connected to like an ordinary serial port. At the vehicle end, it appears as logic-level serial signals. The PC dongle acts a Bluetooth *master* device (which can establish links) while each vehicle is a separate *slave* device. A slave device can only be paired with one master at any one time. If radio contact is lost, the link will be automatically restored when it is regained. However, whenever the vehicle or computer is powered off, the link must generally be re-established.

4.2 Results and Discussion

Experiments for two Cases i.e., with the absence or presence of an obstacle vehicle in the passing lane, were performed. The experiments were performed with only constant obstacle-vehicle velocities since the vehicles can only receive the velocity commands in integers and in the multiples of 2, i.e., 2, 4, and 6. Thus, if variable obstacle-vehicle velocities were to be used then it can only show when the vehicle instantaneously accelerated or decelerated to a different velocity.

Each Case was performed three times to examine the repeatability of the trajectory planner. The results are given by sets of two figures: The first two figures plot P's path, and the last two figures plot P's overall velocity profile, obtained through simulation and through three repetitive experiments.

4.2.1 Case 1: No Op Present

In this experiment, P is required to overtake O_D with no O_P, being present. Due to the dimensions of the robotic vehicles (80 × 80 mm) and the availability of limited workspace, the width of the lane was set as 160 mm, the velocity of P was set to 8 mm/s, and the velocity of O_D was set to 6 mm/s. The shadow-target, S, positions for this experiment are shown in Figure 4.5. The simulation and experimental results are shown in Figures 4.6 to 4.9. The experiments were repeated three times under identical conditions.

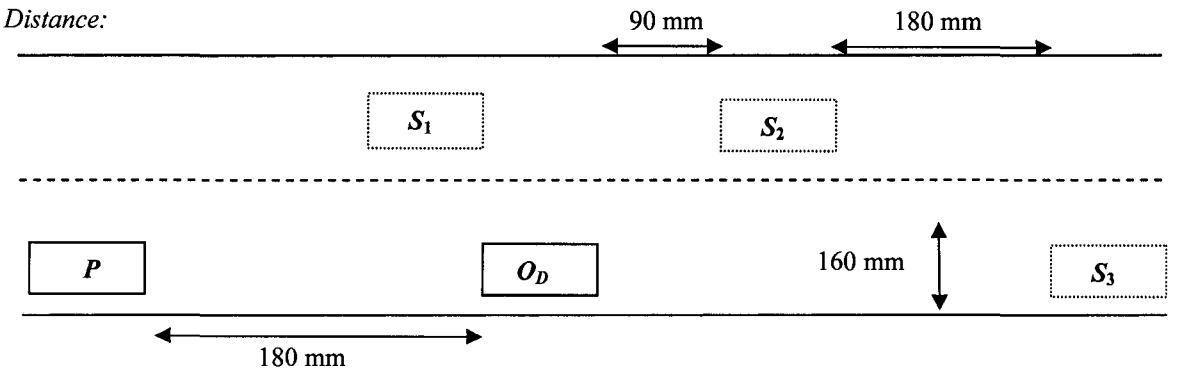

Figure 4.5: Shadow-Target Positions for Case 1.

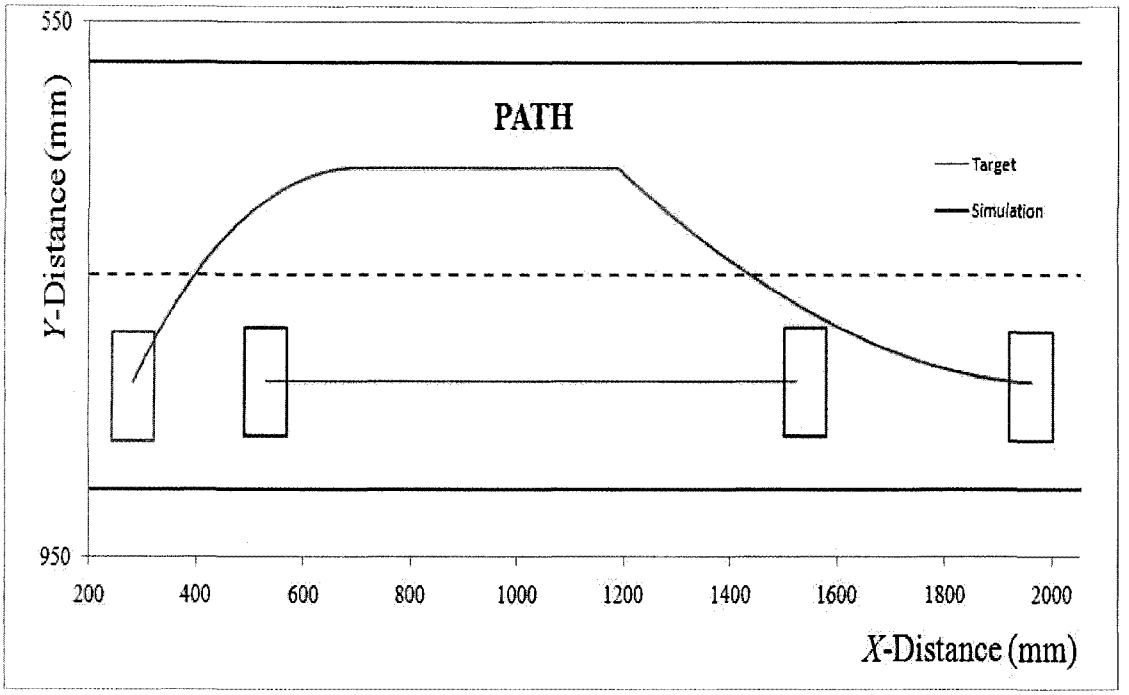

Figure 4.6: Case 1: Path of *P*: Simulation.

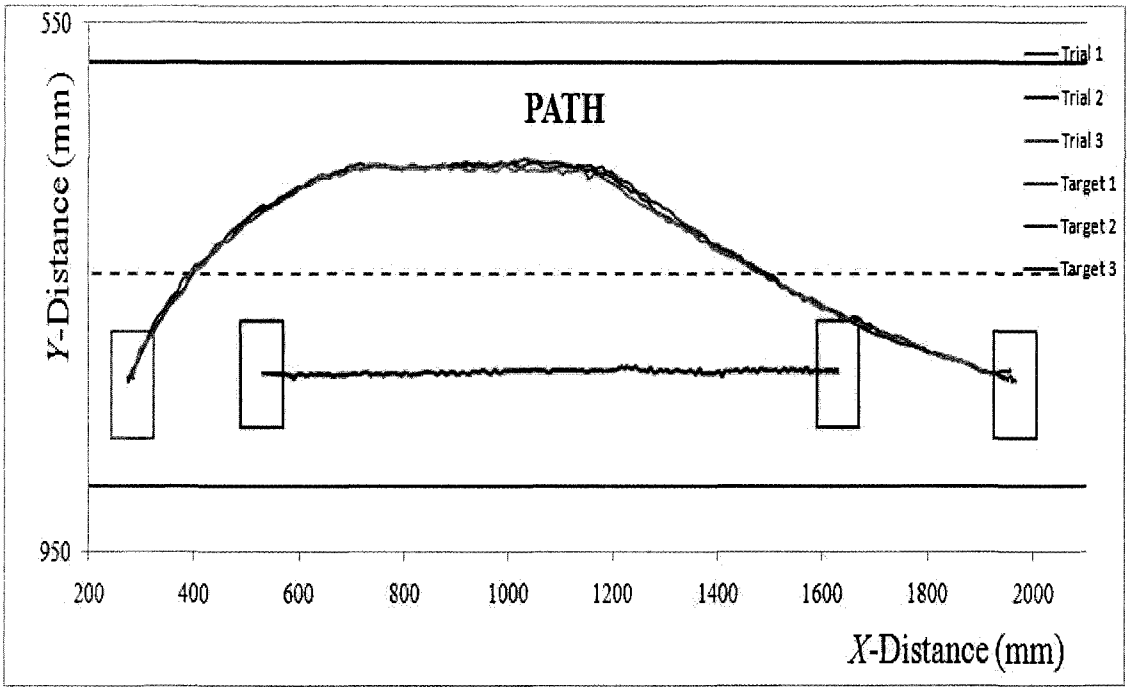

Figure 4.7: Case 1: Path of *P*: Experiment.

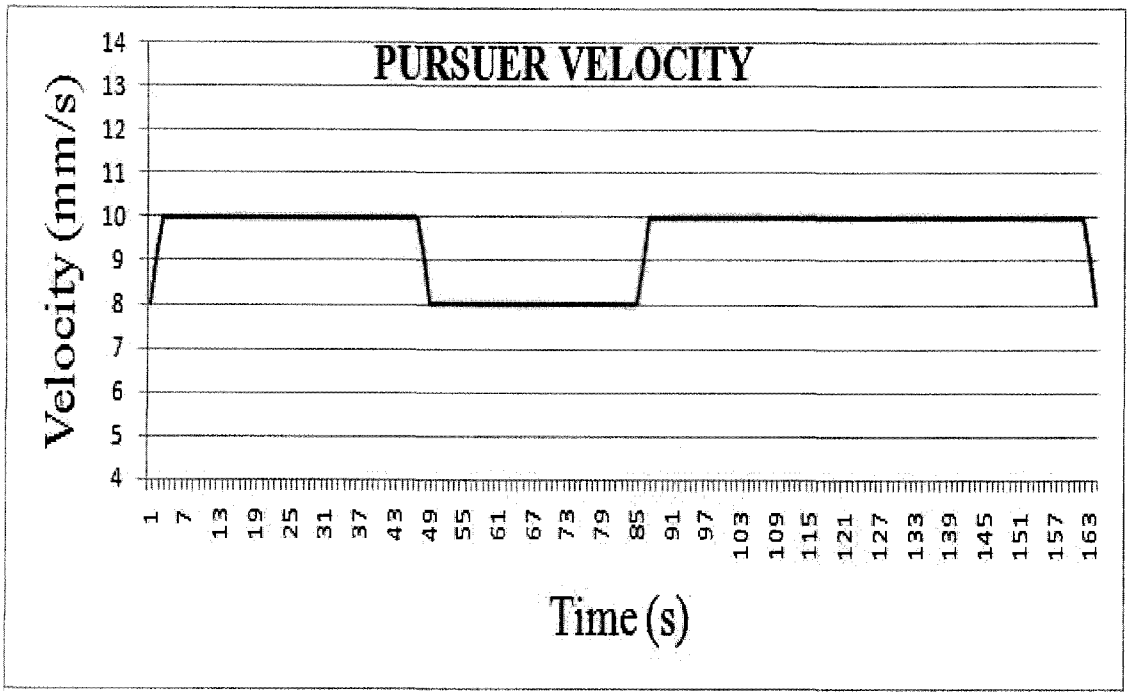

Figure 4.8: Case 1: Overall Velocity Profile of *P*: Simulation.

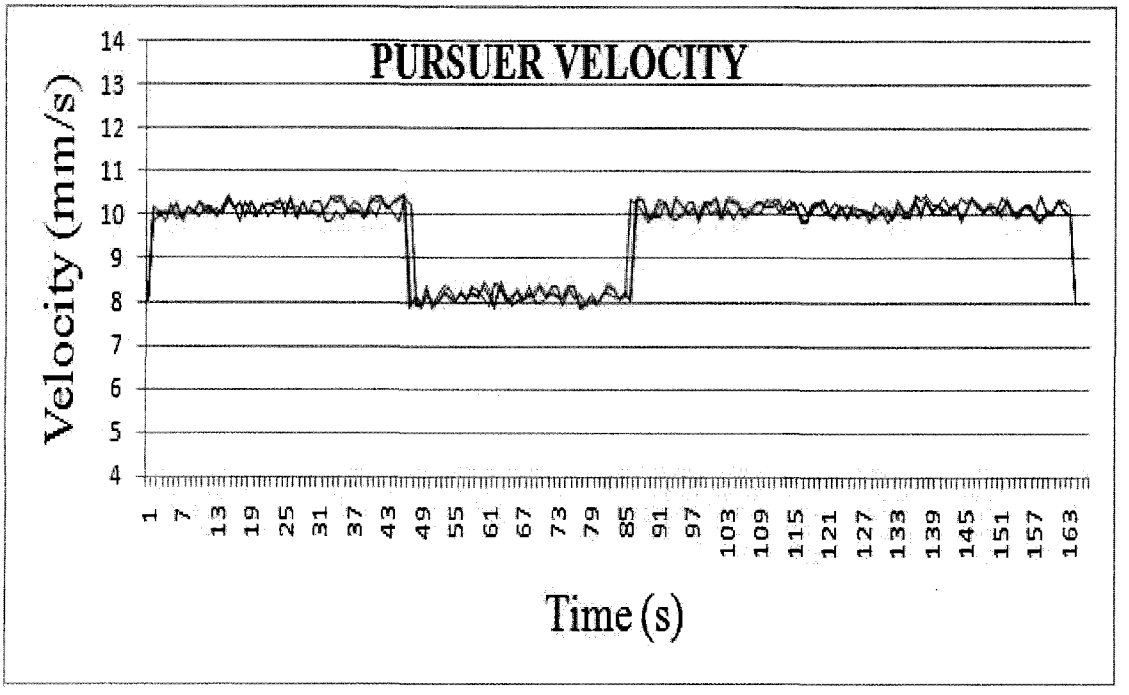

Figure 4.9: Case 1: Overall Velocity Profile of *P*: Experiment.

4.2.2 Case 2: Op Present

In this experiment, an O_P is present and an overtaking manoeuvre by P is not immediately feasible. O_P is moving with a constant velocity of 8 mm/s and O_D is moving with a constant velocity of 6 mm/s. The starting velocity of P is 10 mm/s. The positions of S for this experiment are shown in Figure 4.10.

Due to the presence of O_P, P first undertakes a collision-avoidance manoeuvre by reducing its velocity and ensuring a safe distance between itself and O_D. Once O_P is ahead of O_D, P starts the overtaking manoeuvre. The simulation and experimental results are shown in Figures 4.11 to 4.14. The experiments were repeated three times under identical conditions.

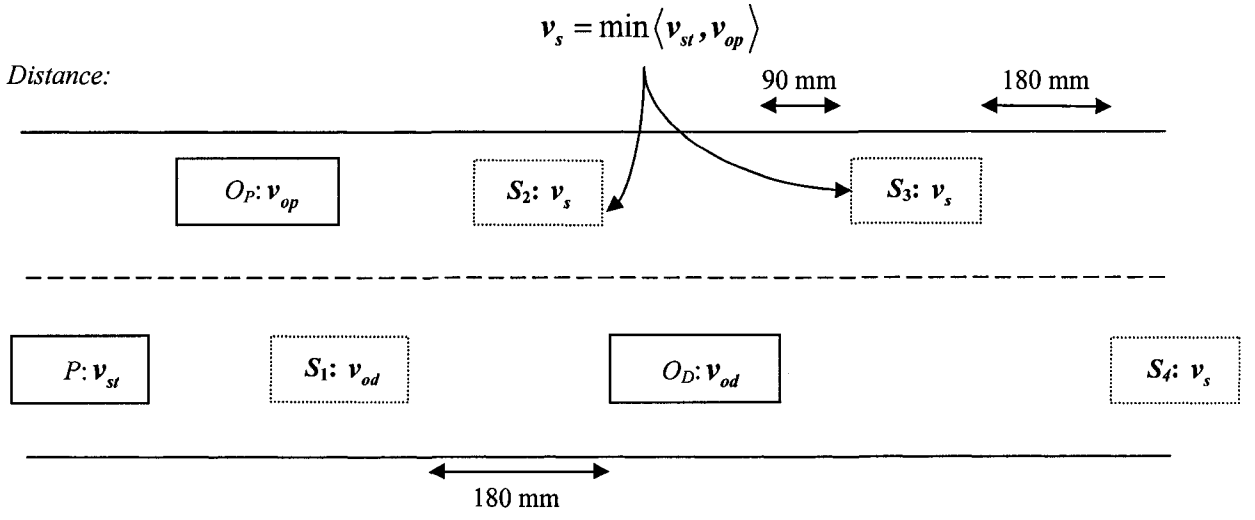

Figure 4.10: Shadow-Target Positions for Case 2.

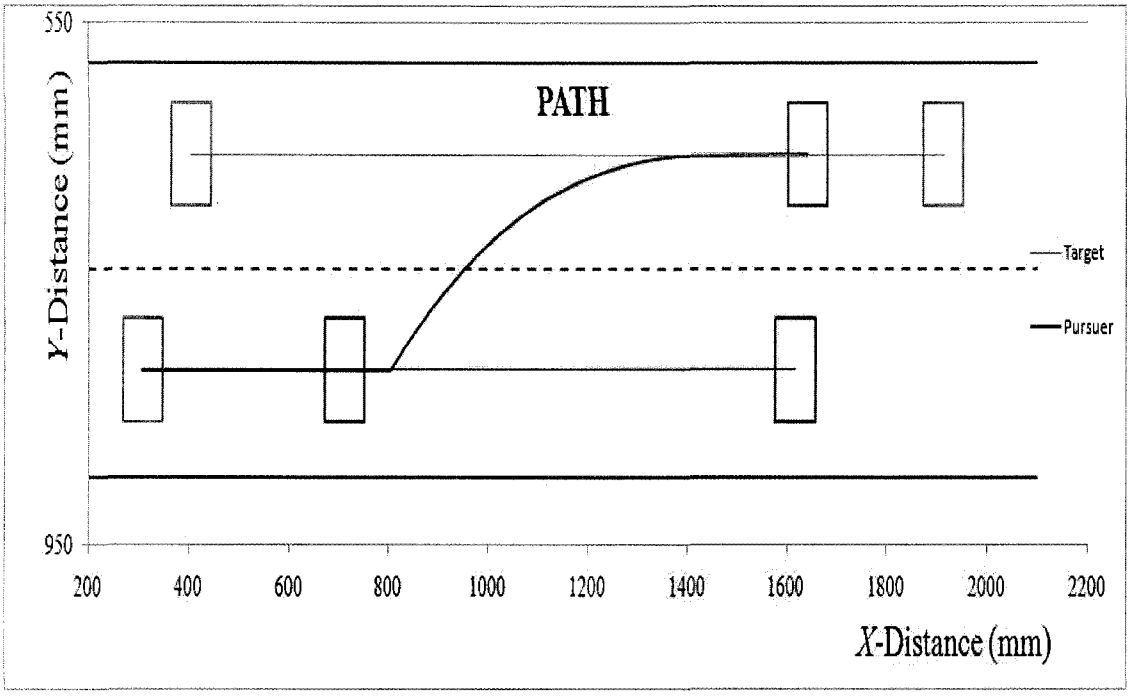

Figure 4.11: Case 2: Path of *P*: Simulation.

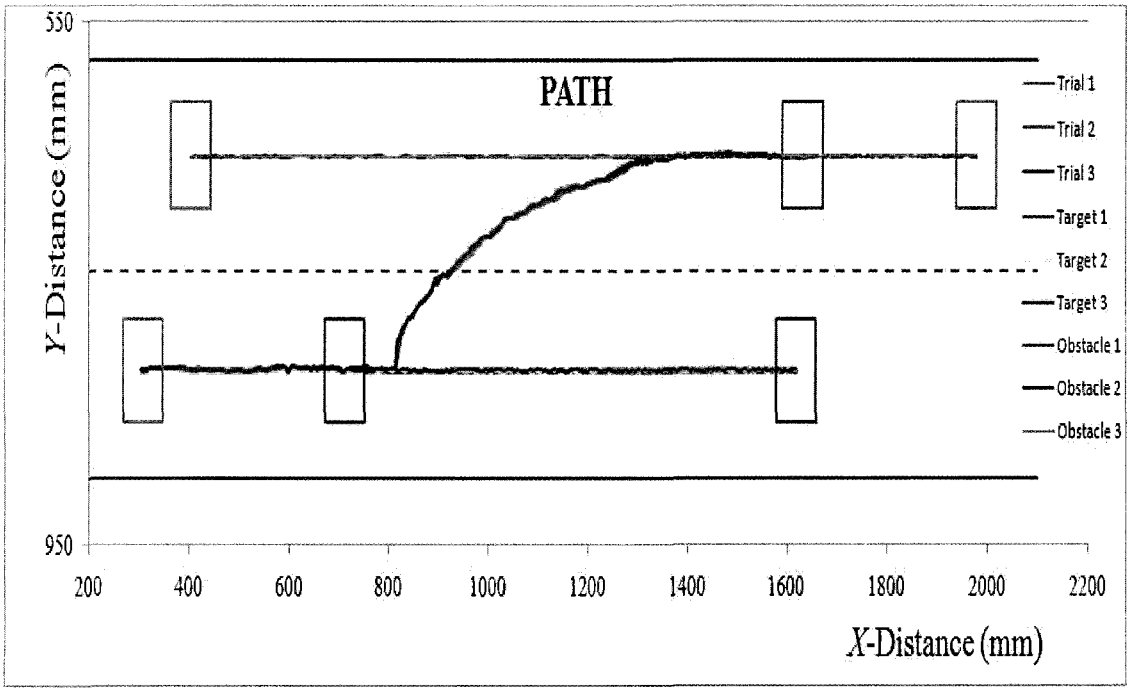

Figure 4.12: Case 2: Path of *P*: Experiment.

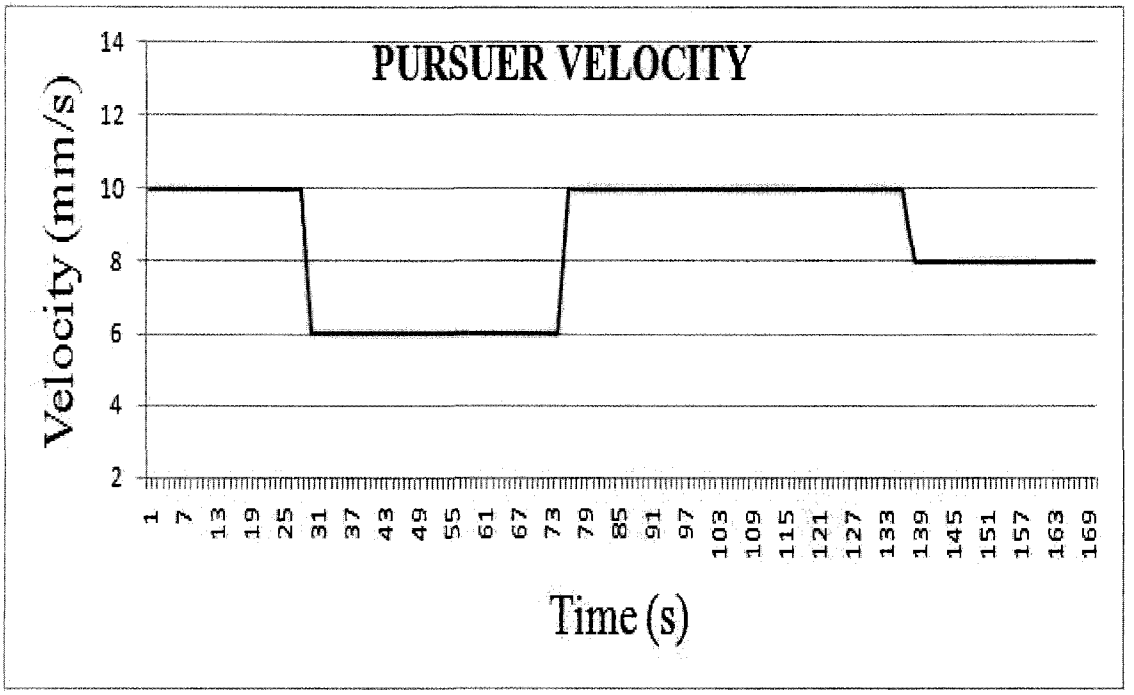

Figure 4.13: Case 2: Overall Velocity Profile of *P*: Simulation.

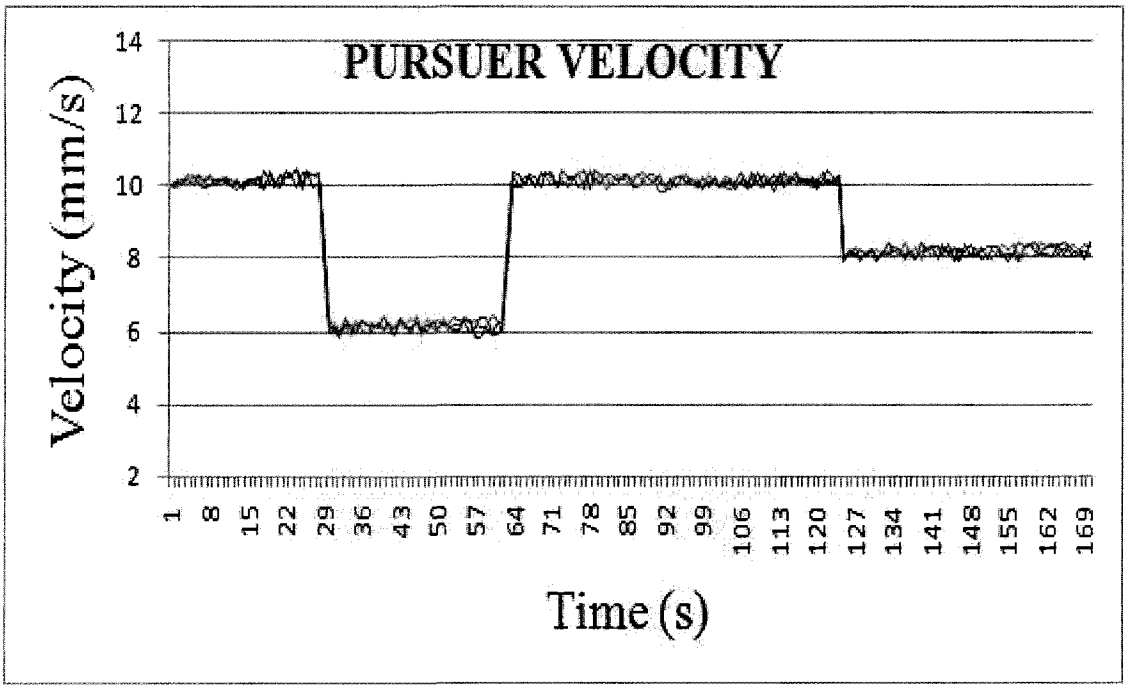

Figure 4.14: Case 2: Overall Velocity Profile of *P*: Experiment.

4.3 Conclusions

The primary conclusions that can be drawn from the experimental results are as follows:

- The proposed navigation algorithm has been successfully implemented for the path generation for the overtaking manoeuvre of an autonomous vehicle in a noisy environment, thus, showing robustness.
- The experimental results confirm the results obtained by the simulations. They show that the proposed method is able to overtake a slower moving vehicle in the presence, or absence, of another obstacle vehicle in the passing lane, with near-optimal overtaking time.

5 CONCLUSIONS AND RECOMMENDATIONS

5.1 Summary and Conclusions

In this Thesis, a novel time-optimal guidance based on-line trajectory-planning algorithm is presented for the guidance of a pursuer vehicle, P, overtaking a slower vehicle, O_D, on a highway setting in the presence of other (obstacle) vehicles, O_P, travelling in the passing lane. The focus has been on two autonomy aspects of overtaking manoeuvre: (*i*) time-optimal overtaking in the possible presence of obstacle vehicles in the passing lane while ensuring passenger comfort and (*ii*) ensuring that a safety distance is always maintained between vehicles in order to avoid any collision.

Both above aspects were addressed by using a modified Rendezvous Guidance (RG) law. The (original) RG developed in [114] was shown analytically to yield an optimal solution for *rendezvous* with non-manoeuvring targets, which can be assumed to be the case for vehicles travelling on highways. However, there still existed two major issues that restricted the use of

original RG law in trajectory planning for overtaking cases. First, RG is designed for matching velocity with a target and not to overtake it. Therefore, a target needs to be defined. Second, there would be numerous constraints on the motion of P.

In order to address the first issue, the concept of a *shadow* target, S, was introduced in this Thesis, which is used to guide P during all the phases of the overtaking manoeuvre. The location of S is defined according to O_D that is being overtaken. In order to address the second issue, this Thesis proposed an on-line trajectory-planning method based on a modified RG method. The information about P, O_D, and O_P is used to generate a single acceleration command for P to avoid O_P and overtake O_D in a near time-optimal manner. This acceleration command is calculated based on velocity-matching capability with S keeping in mind the constraints imposed due to P's dynamics and passenger comfort.

The RG law implements the parallel-navigation geometrical rule, which requires the angle of the *Line-Of-Sight*, (*LOS*) between the interceptor and the target to remain constant. Utilization of the parallel-navigation law herein assures the matching of position between P and S.

The RG law yields a set of velocity commands that can be followed to achieve velocity-matching, denoted as the *Rendezvous Set* (*RS*). However, due to the dynamic properties of P, not all velocities in this set can be executed. Therefore, *RS* is limited to a *Feasible Rendezvous Set* (*FRS*) that comprises velocity commands within the acceleration capacity of P having both position and velocity-matching components. The largest component from *FRS* is selected to ensure efficient rendezvous with the target. RG has also been shown to be robust and easily implementable.

However, in the case of overtaking, the limitation on lateral acceleration does not allow P to travel at its optimum velocity by limiting the angular acceleration that it can achieve: namely, RG selects an angular acceleration value that ensures the velocity of P remains on *RL*, even though the vehicle has the capability of selecting a higher value of velocity from the *FVS*. Thus, in order to ensure that P always selects an optimum velocity, this Thesis introduced the concept of *Velocity Line* (*VL*). *VL* originates from the start point of the *RL* and makes an angle, ϑ, with the fixed reference. ϑ is the maximum angle P can turn while ensuring that the angular

acceleration remains within limits. Now, if P were to select and use a velocity command from VL instead of RL, a more time-efficient overtaking could be achieved.

The utilization of VL is only possible if the movement of the target is predictable, which is the case with the vehicle moving on a highway. In the case of a target moving on unknown trajectory, if P tries to achieve a velocity greater than the rendezvous velocity a situation may arise wherein S is turning away from the direction in which the velocity is increased. This could lead to an increase in the rendezvous time instead of a reduction.

The implementation of the proposed method was performed in two phases: simulation in a Visual Basic environment and experimentation with three robotic vehicles. The simulation phase of the implementation assumes perfect knowledge of the workspace conditions, which includes the P, O_D, and O_P positions. The motion command to P is specified in lateral-acceleration terms and executed perfectly. The concept was tested for changing velocities of both O_D and O_P. Also, in order to analyze the performance of the trajectory planners, computer simulations were performed and results were compared with the original RG method [114] and to an off-line path-generation method proposed in [77]. The results showed that the proposed method yields shorter overtaking times than would the original RG and off-line methods.

In order to further verify the findings of the simulations, and to demonstrate the robustness of the algorithms in a noisy system, the proposed methodology was implemented via the use of robotic vehicles in experiments. The experimental results confirmed the results obtained by the simulations. They showed that the proposed method is able to overtake a slower moving vehicle in the presence, or absence, of any other obstacle vehicle in the passing lane, thus, provide near-optimal overtaking time.

The proposed methodology was also tested for its implementation in miscellaneous other cases, such as, aborting the overtaking manoeuvre, overtaking multiple vehicles and vehicle joining a highway. In all these cases, the proposed methodology was able to perform the task in a near time-optimal and collision free manner.

5.2 Recommendations

Some improvements to the algorithms and suggestions for future work are discussed below:

1. The system implemented in the experiments described herein had a refresh rate of approximately 6.5 fps, operating on a PC with a Pentium IV processor running at 1.6 GHz. A faster PC would improve the refresh rate and efficiency of the system.
2. The CCD camera currently used in the experimental set-up has a resolution of (680 × 480). The use of a camera with a higher resolution would increase the accuracy of the vision algorithm by reducing system noise.
3. Optimization of the computer code could also be made. The most time-consuming operation in the proposed algorithm is the acquisition and analysis of the object's images by the vision algorithm. The code for the vision system can be optimized to increase the algorithm efficiency in implementation on physical systems by reducing the computation time.
4. The proposed method gives a near time-optimal solution for a highway in the presence or absence of an O_P, however, it only considers obstacles that are moving in the same direction in which P is moving. The proposed method can be implemented for a non-highway case, where O_P may not have the same direction as P instead, it may be travelling in the opposite direction.
5. The proposed method can be further developed for complete trajectory planning of an autonomous vehicle, which may include all the driving tasks, e.g., crossing intersections or responding to a traffic light, that are required to be performed by the autonomous vehicle.
6. The integration of different sensors to get the parameters of all relevant vehicles, instead of using only the vision sensor, may improve the performance of the proposed system in a "real-world" environment.

5.3 Final Concluding Statement

In conclusion, a novel guidance-based on-line trajectory-planning algorithm was developed for autonomous ground-vehicle overtaking manoeuvres in dynamic two-lane highway environments.

The focus has been on three primary aspects: (*i*) time-optimal overtaking, (*ii*) obstacle avoidance, and (*iii*) passenger comfort. The proposed algorithm uses a modified RG method to obtain optimal vehicle-acceleration commands for the overtaking manoeuvre. A *shadow* target concept is utilized to adjust the driving parameters of the pursuer vehicle in real-time in response to changes in the driving parameters of obstacle vehicles in the driving lane as well as in the passing lane – this ability presents the primary novelty of the proposed method in contrast to previous off-line methods presented in the literature. Numerous simulations and experiments have verified the proposed methodology to be robust and time efficient.

References

[1] R. Bishop, "*Intelligent Vehicle Technology and Trends*," Chapter 10, Norwood, MA: Artech House, 2005.

[2] J. Michon, *Human Behavior and Traffic Safety,* New York: Plenum Press, 1985.

[3] T-Y. Sun, S-J. Tsai, and V. Chan, "HSI Color Model Based Lane-Marking Detection," *Proceedings of the IEEE Intelligent Transportation Systems Conference*, Toronto, Canada, September 17-20, 2006, pp. 1168-1172.

[4] K.A. Redmill, T. Kitajima, and U. Ozguner, "DGPS/INS Integrated Positioning for Control of Automated Vehicle," *Proceedings of the IEEE Intelligent Transportation Systems*, Oakland, CA, August 2001, pp. 172-178.

[5] K. Yamada, T. Nakano, and S. Yamamoto, "Effectiveness of Video Camera Dynamic Range Expansion for Lane Mark Detection," *Proceedings of the IEEE Intelligent Transportation System,* Boston, MA, November 1997, pp. 584-588.

[6] K-Y. Chiu and S-F. Lint, "Lane Detection using Color-Based Segmentation," *Proceedings of the IEEE Intelligent Vehicles Symposium,* Tokyo, Japan, June 2006, pp. 706-711.

[7] C. Tan, T. Hong, T. Chang, and M. Shneier, "Color Model-Based Real-Time Learning for Road Following," *Proceedings of the IEEE Intelligent Transportation Systems Conference*, Toronto, Canada, September 17-20, 2006, pp. 939-944.

[8] K. Kluge, "Extracting Road Curvature and Orientation from Image Edge Points without Perceptual Grouping into Features," *Proceedings of IEEE Intelligent Vehicles Symposium*, Paris, France, October 1994, pp. 109-114.

[9] X. Yu, S. Beucher, and M. Bilodeau, "Road Tracking, Lane Segmentation and Obstacle Recognition by A Mathematical Morphology," *Proceedings of IEEE Intelligent Vehicles Symposium*, Detroit, MI, June 1992, pp. 166-172.

[10] S. Beucher and M. Bilodeau, "Road Segmentation and Obstacle Detection by a Fast Watershed Transformation," *Proceedings of IEEE Intelligent Vehicles Symposium*, Paris, France, October 1994, pp. 296-301.

[11] D.A. Pomerleau, "RALPH: Rapidly Adapting Lateral Position Handler," *Proceedings of IEEE Intelligent Vehicles Symposium*, Detroit, MI, September 1995, pp. 506-511.

[12] M. Bertozzi and A. Broggi, "Real-Time Lane and Obstacle Detection on the Gold System," *Proceedings of IEEE Intelligent Vehicles Symposium*, Tokyo, Japan, September 1996, pp. 213-218.

[13] M. Bertozzi and A. Broggi, "Gold: A Parallel Real-time Stereo Vision System for Generic Obstacle and Lane Detection," *IEEE Transactions on Image Processing*, Vol. 7, No. 1, 1998, pp. 62-81.

[14] N. Apostoloff and A. Zelinsky, "Robust Based Lane Tracking Using Multiple Cues and Particle Filtering," *Proceedings of IEEE Intelligent Vehicles Symposium*, Columbus, OH, June 2003, pp. 558-563.

[15] W. Enkelmann, G. Struck, and J. Geisler, "Roma: A System for Model-Based Analysis of Road Markings," *Proceedings of IEEE Intelligent Vehicles Symposium*, Detroit, MI, September 1995, pp. 356-360.

[16] Y. Wang, D. Shen, and E. Teoh, "Lane Detection Using Catmull-Rom Spline," *Proceedings of IEEE Intelligent Vehicles Symposium*, Stuttgart, Germany, October 1998, pp. 51-57.

[17] Y.Wang, D. Shen, and E. Teoh, "Lane Detection Using Spline Model," *Pattern Recognition Letters*, Vol. 21, June 2000, pp. 677-689.

[18] R. Risack, N. Mohler, and W. Enkelmann, "A Video-Based Lane Keeping Assistant," *Proceedings of IEEE Intelligent Vehicles Symposium*, Dearborn, MI, October 2000, pp. 506-511.

[19] J. Park, J. Lee, and K. Jhang, "A Lane-Curve Detection Based on an LCF," *Pattern Recognition Letters*, Vol. 24, October 2003, pp. 2301-2313.

[20] Y. Wang, E. Teoh, and D. Shen, "Lane Detection and Tracking using B-Snake," *Image and Vision Computing*, Vol. 22, April 2004, pp. 269-280.

[21] J. Lee, "A Machine Vision System for Lane-Departure Detection," *Computer Vision and Image Understanding*, Vol. 86, April 2002, pp. 52-78.

[22] J.W. Lee, C.D. Kee, and U.K. Yi, "A New Approach for Lane Departure Identification," *Proceedings of IEEE Intelligent Vehicles Symposium*, Columbus, OH, June 2003, pp. 100-105.

[23] F. Guichard and J.P. Tarel. "Curve Finder Combining Perceptual Grouping and a Kalman Like Fitting" *Proceedings of IEEE International Conference on Computer Vision*, Kerkya, Greece, September 1999, pp. 1003-1008.

[24] C. R. Jung and C. R. Kelber. "A Robust Linear-Parabolic Model for Lane Following," *Proceedings of SIBGRAPI*, Curitiba, PR, October 2004, pp. 72-79.

[25] D. Pomerleau, "ALVINN: An Autonomous Land Vehicle in A Neural Network," **Technical Report, CM-CS-89-107**, Carnegie Mellon, 1989.

[26] M. Födish and A. Takeuchi, "Adaptive Real-Time Road Detection Using Neural Networks," *Proceedings of the 7th International IEEE Conference on Intelligent Transportation Systems*, Washington, DC, October 2004, pp. 167-172.

[27] C. Chen, "Backstepping Design of Nonlinear Control Systems and its Application to Vehicle Lateral Control in Automated Highway Systems," **Ph.D. dissertation**, University of California, Berkeley, CA, 1996.

[28] P. Hingwe and M. Tomizuka, "Robust and Gain Scheduled H Controllers for Lateral Guidance of Passenger Vehicles in AHS," *Proceedings of the ASME Dynamic Systems and Control Division*, Vol. 61, November 1997, pp. 707-713.

[29] J.Y. Wang and M. Tomizuka, "Analysis and Controller Design Based on Linear Model for Heavy-Duty Vehicles," *Proceedings of the International Mechanical Engineering Congress and Exposition, ASME Symposium on Transportation Systems*, Anaheim, CA, November 1998, pp. 729-735.

[30] J.Y. Wang and M. Tomizuka, "Dynamics Analysis and Robust Steering Controller Design for Automated Lane Guidance of Heavy-Duty Vehicles," *Asian Journal on Control*, Vol. 2, No. 3, September 2000, pp. 140-154.

[31] Y-J. Ryoo, "Design of Magnet Based Position Sensing System for Autonomous Vehicle Robot" *Proceedings of the IEEE Intelligent Robots and Systems*, Sendai, Japan, October 2004, pp. 2378-2383.

[32] J. Guldner, H.S. Tan, S. Patwardhan, C. Chen,and B. Bougler, "Development of an Automated Steering Vehicle Based on Roadway Magnets – A Case of Study of Mechatronic System Design, " *IEEE/ASME Transactions on Mechatronics*, Vol. 4, September 1999, pp. 258-272.

[33] H.G. Xu, C.X. Wang, R.Q. Yang, and M. Yang, "Extended Kalman Filter Based Magnetic Guidance for Intelligent Vehicles," *Intelligent Vehicles Symposium 2006*, Tokyo, Japan, June 13-15, 2006, pp. 169-175.

[34] G. Lu and M. Tomizuka, "Vehicle Following as Backup Control Schemes for Magnet-Magnetometer-Based Lateral Guidance," *IEEE Transactions on Control Systems Technology*, Vol. 13, No. 2, March 2005 , pp. 274-285.

[35] M. Nakamura, "Vehicle Lateral Control System Using Laser Radar," *Intelligent Vehicle Highway Systems*, Vol. 2344, November 1994, pp. 267-277.

[36] M. Omae and T. Fujioka, "DGPS-Based Position Measurement and Steering Control for Automatic Driving," *Proceedings of the American Control Conference*, San Diego, California, June 1999, pp. 3685-3690,

[37] S.Y. Chang, and J.C. Gerdes, "Differential Geometric Structures in Vehicle Lane Keeping and Roll Mitigation," *Proceedings of the American Control Conference*, Portland, OR, June 2005, pp. 441-446.

[38] M. Tsogas, A. Polychronopoulos, and A. Amditis, "Using Digital Maps to Enhance Lane Keeping Support Systems," *Proceedings of the IEEE Intelligent Vehicles Symposium,* Istanbul, Turkey, June 2007, pp. 148-153.

[39] W.P. Zhang, and T. West, "An Intelligent Roadway Reference System for Vehicle Lateral Guidance/Control," *Proceedings of the American Control Conference*, San Diego, CA, May 1990, pp. 281-286.

[40] H. Peng, and M. Tomizuka, "Preview Control for Vehicle Lateral Guidance in Highway Automation," *Proceedings of the American Control Conference*, Boston, MA, June 1991, pp. 3090-3095.

[41] H. Peng, T.M. Hessburg, M. Tomizuka, W. Zhang, Y. Lin, P. Devlin, S. Shladover, and A. Arai, "A Theoretical and Experimental Study on Vehicle Lateral Control," *Proceedings of the American Control Conference*, Chicago, IL, June 1992, pp. 1738-1742.

[42] J. Ackermann, and W. Sienel, "Automatic Steering of Vehicles with Reference Angular Velocity Feedback," *Proceedings of the American Control Conference*, Baltimore, MD, June 1994, pp. 1957-1958.

[43] J. Guldner, V.I. Utkin, and J. Ackermann, "A Sliding Mode Control Approach to Automatic Car Steering," *Proceedings of the American Control Conference*, Baltimore, MD, June 1994, pp. 1969-1973.

[44] M.M.M. Brackstone, "Car-Following: A Historical Review," *Journal of Transportation Research*, Vol. 2, 1990, pp. 181-196.

[45] T. Jochem, D. Pomerleau, and C. Thorpe, "Vision Guided Lane Transition," *Proceedings of the Intelligent Vehicles Symposium*, September 1995, pp. 30-35.

[46] T. Jochem and M. Todd, "Using Virtual Active Vision tools to Improve Autonomous Driving Tasks," **CMU Technical Report CMU-RI-TR-94-39**, October 1994.

[47] K. Shin, T. Kohji and T. Sadayuki, "Lane-Change Manoeuvres For Vision-Based Vehicle," *Proceedings of Intelligent Transportation Systems*, Boston, MA, November 1997, pp. 129-134.

[48] S. Kato, K. Tomita, and S. Tsugawa, "Visual Navigation Along Reference Lines and Collision Avoidance for Autonomous Vehicles," *Proceedings of the IEEE Intelligent Vehicles Symposium*, Tokyo, Japan, September 1996, pp. 385-390.

[49] J.K. Hedrick, M. Tomizuka, and P. Varaiya, "Control Issues in Automated Highway Systems," *IEEE Control Systems Magazine*, Vol. 14, 1994, pp. 21-32.

[50] P. Varaiya, "Smart Cars on Smart Roads: Problems of Control," *IEEE Transactions on Automatic Control*, Vol. 38, 1993, pp. 195-207.

[51] T.Q. Tang, H.J. Huang, S.C. Wong, and X.Y. Xua, "A New Overtaking Model and Numerical Tests," *Physica A: Statistical Mechanics and its Applications,* Vol. 376, March 2007, pp. 649-657.

[52] T. Hsiao and M. Tomizuka, "Design of Position Feedback Controllers for Vehicle Lateral Motion," *Proceedings of the American Control Conference*, Minneapolis, MN, June 2006, pp. 5855-5860.

[53] T. Srinivasan, J.B. Siddharth, and A. Chandrasekhar, "Sentient Autonomous Vehicle Using Advanced Neural Net Technology", Proceedings of the *IEEE Conference on Cybernetics and Intelligent Systems*, Singapore, December 2004, pp. 827-832.

[54] J. Frankel, L. Alvarez, R. Horowitz, and P. Li, "Safety Oriented Manoeuvres for IVHS," *Proceedings of the American Control Conference*, Seattle, WA, June 1995, pp. 668-672.

[55] H. Jula, E. Kosmaropoulos, and P. Ioannou , "Collision Avoidance Analysis for Lane Changing and Merging," *IEEE Transaction on Vehicular Technology*, Vol. 49, No. 6, 2000, pp. 2295-2308.

[56] J. Lygeros, and D. Godbole, "An Interface Between Continuous & Discrete-Event Controllers for Vehicle Automation," *IEEE Transaction on Vehicular Technology*, Vol. 46, No. 1, 1997, pp. 229-241.

[57] T. Jochem, D. Pomerleau, and C. Thorpe, "Vision Guided Lane Transition," *Proceedings of the Intelligent Vehicles Symposium*, Detroit, MI, September 1995, pp. 30-35.

[58] S. Jamison and M. McCartney, "A Vehicle Overtaking Model of Traffic Dynamics," *CHAOS : An Interdisciplinary Journal of Nonlinear Science,* Vol. 17, No. 3, September 2007, pp. 1-7.

[59] W. Chee, and M. Tomizuka, "Lane Change Manoeuvres for AHS Applications," *Proceedings of the International Symposium on Advanced Vehicle Control*, Tsukuha, Japan, October 1994, pp. 420-425.

[60] N.H. Sledge and K.M. Marshek, "Comparison of Ideal Vehicle Lane-Change Trajectories, *SAE Transactions, Research into Vehicle Dynamics and Simulation*, Vol. 62, 1997, pp. 233-256.

[61] Z. Shiller, and S. Sundar, "Emergency Lane-Change Manoeuvres of Autonomous Vehicles," *ASME Journal of Dynamic Systems, Measurement and Control*, Vol. 120, No. 1, March 1998, pp. 36-44.

[62] C.G. Bianco, A. Piazzi, and M. Romano, "Velocity Planning for Autonomous Vehicles," *Proceedings of IEEE Intelligent Vehicles Symposium,* Parma, Italy, June 2004, pp. 413-418.

[63] N. Montés, C. Mora, and J. Tornero, "Trajectory Generation Based on Rational Bezier Curves as Clothoids," *Proceedings of the IEEE Intelligent Vehicles Symposium,* Istanbul, Turkey, June 13-15, 2007, pp. 505-510.

[64] T. Shamir, "How Should an Autonomous Vehicle Overtake a Slower Moving Vehicle: Design and Analysis of an Optimal Trajectory," *IEEE Transaction on Automatic Control,* Vol. 49, No. 4, April 2004, pp. 607-610.

[65] I. Papadimitriou and M. Tomizuka, "Fast Lane Changing Computations Using Polynomials," *IEEE Proceedings of the American Control Conference,* Denver, CO, June 2003, pp. 48-53.

[66] S.E. Shladover, C.A. Desoer, J.K. Hedrick, M. Tomizuka, J. Walrand, W.B. Zhang, D. McMahon, and S. Sheikholeslam, "Automatic Vehicle Control Development in the PATH Program," *IEEE Transaction on Vehicle Technology*, Vol. 40, Feburary 1991, pp. 114-130.

[67] C-H. Hsu and A. Liu, "Kinematic Design for Platoon-Lane-Change Manoeuvres," *IEEE Transactions on Intelligent Transportation Systems*, Vol. 9, No. 1, March 2008, pp 185-190.

[68] J. Kaneko and A. Shimamura, "A Design of Lane Change Manoeuvre for Automated Vehicles," *Proceedings of the 37th IEEE Conference on Decision and, Control,* Tampa, Florida, December 1998, pp. 1031-1033.

[69] Z. Shiller, and S. Sundar ,"Emergency Manoeuvres of AHS Vehicles," *SAE Transactions, Journal of Passenger Cars*, Vol. 104, 1995, pp. 2633-2643.

[70] R.S. Sharp, "Stability, Control and Steering Responses of Motorcycles," *Vehicle System Dynamics,* Vol. 35, No. 4-5, 2001, pp. 291-318.

[71] N. Sledge and K. Marshek, "Development and Validation of an Optimized Emergency Lane-Change Trajectory," *SAE Transactions, Research into Vehicle Dynamics and Simulation*, Vol. 31, August 1998, pp. 103-121.

[72] F. Jinxiang, R. Jiuhong, and L. Yibin, "Study on Intelligent Vehicle Lane Change Path Planning and Control Simulation," *Proceedings of the IEEE International Conference on Information Acquisition*, Weihai, China, August 2006, pp. 683-688.

[73] J.Y. Huang , H-X. Pan, X-W. Yang, J-D. Li, "Fuzzy Controller Design of Autonomy Overtaking System," *Proceedings of the International Conference on Intelligent Engineering Systems* ,Miami, FL, Feburary 2008, pp. 281-285.

[74] W. Caywood, H. Donnely, and N. Rubinstein, "Guideline for Ride-Quality Specifications Based on Transpo '72 Test Data," **Applied Physics Laboratory, John Hopkins University,** Washington, 1977.

[75] M.R. Koopman, and L.J.J. Kusters, "The Development of a Path Planning Strategy for Obstacle Avoidance and Crash Impact Minimisation for an Automatic Guided Vehicle," **Advanced Chassis and Transport Systems**, Netherlands, June 2003.

[76] H. Jula, E. Kosmaropoulos, and P. Ioannou , "Collision Avoidance Analysis for Lane Changing and Merging," *IEEE Transaction on Vehicular Technology*, Vol. 49, No. 6, 2000, pp. 2295-2308.

[77] A. Kanaris, E.B. Kosmatopoulos, and P.A. Ioannou, "Strategies and Spacing Requirements for Lane Changing and Merging in Automated Highway Systems," *IEEE Transactions on Vehicle Technology*, Vol. 50, No. 6, November 2001, pp. 1568-1581.

[78] A. Levitt, "Autonomous Vehicles: Motion Planning and Control", **M.Eng. Project Report**, Department of Mechanical and Industrial Engineering, University of Toronto, 2006.

[79] R.S. Bucy and P.D. Joseph, *Filtering for Stochastic Processes with Applications to Guidance,* Hoboken, NJ: John Wiley & Sons, 1968.

[80] N.C. Griswold, "A Transportable Neural Network Controller for Autonomous Vehicle Following," *Proceedings of the Intelligent Vehicles Symposium*, Paris, France, October 1994, pp. 195-200.

[81] S.K. Gehrig and F.J. Stein, "A Trajectory-Based Approach for the Lateral Control of Car Following Systems," *Proceedings of the IEEE Systems, Man, and Cybernetics Conference*, San Diego, CA, October 1998, pp. 3596-3601.

[82] A. Renfrew, V.A.G. Villasenor, and P. Brunn, "Application of the "Contact Convoy" Concept to Hybrid-Electric Vehicles," *Proceedings of the IEEE Vehicle Power and Propulsion Conference*, Chicago, IL, September 2005, pp. 419-426.

[83] K. Tamura and Y. Furukawa, "Autonomous Vehicle Control System of ICVS City Pal: Electrical Tow-Bar Function," *Proceedings of the IEEE Intelligent Vehicles Symposium,* Dearborn, MI, October 2000, pp. 702-707.

[84] J.C. Gerdes and J.K. Hedrick, "Brake System Requirements for Platooning on an Automated Highway," *Proceedings of the American Control Conference*, Seattle, Washington, June 1995, pp. 165-169.

[85] D.H. McMahon, J.K. Hedrick, and S.E. Shladover, "Vehicle Modeling and Control for Automated Highway Systems," **Technical Report UCB-ITS-PRR-93-24**, University of California, Berkley, CA, 1993.

[86] D.H. McMahon, J.K. Hedrick, and S.E. Shladover, "Longitudinal Vehicle Controllers for IVHS: Theory and Experiment," *Proceedings of the American Control Conference*, Chicago, IL, June 1992, pp.1753-1757.

[87] X-Y. Lu and K.J. Hedrick, "Longitudinal Control Algorithm for Automated Vehicle Merging," *Proceedings of the IEEE Decision and Control Conference*, Sydney, Australia, December 2000, pp. 450- 455.

[88] N.A. Shneydor, *Missile Guidance and Pursuit,* Chichester, England: Horwood Publishing, 1998.

[89] W. Naeem and R.Sutton "A Review to Guidance Laws Applicable to Unmanned Underwater Vehicles," *Journal of Navigation*, Vol. 5, No. 6, 2003, pp. 15-29.

[90] V. Rajasekhar and A.G. Sreenatha, "Fuzzy Logic Implementation of Proportional Navigation Guidance," *Acta Astronautic,* Vol. 46, No. 1, 2000, pp. 17-24.

[91] P. Zarchan, *Tactical and Strategic Missile Guidance*, 2nd Ed., Washington DC: AIAA, Inc., 1994.

[92] C.F. Lin, *Modern Navigation, Guidance and Control Processing,* Upper Saddle River, NJ: Prentice-Hall, 1991.

[93] L.P. Tsao and C.S. Lin, "A New Optimal Guidance Law for Short-Range Homing Missiles," *Proceedings of the National Science Council Republic of China,* Vol. 24, No. 6, 2000, pp. 422- 426.

[94] A.E. Bryson and Y.C. Ho, *Applied Optimal Control,* Washington, DC: Hemisphere Publishing, 1975.

[95] G.J. Nazaroff, "An Optimal Terminal Guidance Law," *IEEE Transaction on Automatic Control*, Vol. 21, No. 6, 1976, pp. 407- 408.

[96] J.E. Potter, "A Guidance-Navigation Separation Theorem" **Technical Report, NASA-CR-58341, RE-11, NASA**, USA, 1964.

[97] J.L. Speyer, W.M. Greenwell and D.G. Hull, "Adaptive Noise Estimation and Guidance for Homing Missile," *AIAA Guidance and Control Conference*, Washington DC, USA, September 1982, pp 48-56.

[98] P.A. Creaser, B.A. Stacey and B.A. White, "Evolutionary Generation of Fuzzy Guidance Laws," *UKACC International Conference on Control'98*, Swansea, UK, September 1-4, 1998, pp. 883-888.

[99] P.K. Menon and V.R. Iragavarapu, "Blended Homing Guidance Law Using Fuzzy Logic," *AIAA Guidance, Navigation and Control Conference,* Boston, MA, August 10-12, 1998, pp. 1-9.

[100] C.D. Yang and H.Y. Chen, "Three-Dimensional Nonlinear H-1 Guidance Law," *International Journal of Robust and Nonlinear Control*, Vol. 11, No. 2, 2001, pp. 109-129.

[101] M. Mehrandezh, M.N. Sela, R.G. Fenton, and B. Benhabib, "Robotic Interception of Moving Objects Using an Augmented Ideal Proportional Navigation Guidance Technique," *IEEE Transactions on Systems, Man and Cybernetics*, Vol. 30, No. 1, 2000, pp. 238-250

[102] F. Agah, M. Mehrandezh, R.G. Fenton, and B. Benhabib, "Rendezvous-Guidance Based Robotic Interception," *Proceedings of the IEEE International Conference on Intelligent Robots and Systems*, Las Vegas, NV, October 2003, pp. 2998-3003.

[103] G.M. Anderson, "Comparison of Optimal Control and Differential Game Intercept Missile Guidance Law," *AIAA Journal of Guidance and Control*, Vol. 4, No. 2, March 1981, pp. 109-115.

[104] D. Ghose, "True Proportional Navigation with Manoeuvring Target," *IEEE Transactions on Aerospace and Electronic Systems*, Vol. 1, No. 30, January 1994, pp. 229-237.

[105] T.J. Speyer, K. Kim and M. Tahk, "Passive Homing Missile Guidance Law Based on New Target Manoeuvre Models," *Journal of Guidance*, Vol. 1, No. 13, September 1990, pp. 803-812.

[106] C.D. Yang, and C.C. Yang, "A Unified Approach to Proportional Navigation," *IEEE Transactions on Aerospace and Electronic Systems*, Vol. 33, No. 2, 1997, pp. 557-567.

[107] P.J. Yuan, and S.C. Hsu, "Rendezvous Guidance with Proportional Navigation," *Journal of Guidance, Control, and Dynamics*, Vol. 17, No. 2, 1993, pp. 409-411.

[108] M. Guelman, "Guidance for Asteroid Rendezvous," *Journal of Guidance, Control, and Dynamics*, Vol. 14, No. 5, 1990, pp. 1080-1083.

[109] D.L. Jensen, "Kinematics of Rendezvous Manoeuvres," *Journal of Guidance*, Vol. 7, No. 3, 1984, pp. 307-314.

[110] H. R. Piccardo, and G. Hondered, "A New Approach to On-Line Path Planning and Generation for Robots in Non-Static Environment," *Journal of Robotics and Autonomous Systems*, Vol. 8, No. 3, 1991, pp. 187-201.

[111] J. Borg, M. Mehrandezh, R.G. Fenton, and B. Benhabib, "Navigation-Guidance-Based Robotic Interception of Moving Objects in Industrial Settings," *Journal of Intelligent and Robotic Systems*, Vol. 33, No. 1, January 2002, pp. 1-23.

[112] F. Agah, M. Mehrandezh, R.G. Fenton, and B. Benhabib, "On-line Robotic Interception Planning Using Rendezvous-Guidance Technique," *Journal of Intelligent and Robotic Systems: Theory and Applications*, Vol. 40, No. 1, May 2004, pp. 23- 44.

[113] F. Kunwar, and B. Benhabib, "Motion Planning for Autonomous Rendezvous with Vehicle Convoys" *Proceedings of the IEEE Intelligent Transportation Systems Conference,* Toronto, Canada, September 2006, pp. 1568-1573

[114] F. Kunwar, F. Wong, R. Ben Mrad, and B. Benhabib, "Rendezvous Guidance for the Autonomous Interception of Moving Objects in Cluttered Environments," *Proceedings of the IEEE International Conference of Robotics and Automation*, Barcelona, Spain, April 2005, pp. 3787-3792

[115] K.Faraz, "Prediction Based Guidance for Real-Time Navigation of Mobile Robots in a Dynamic Cluttered Environment", **Ph.D. dissertation**, Department of Mechanical and Industrial Engineering, University of Toronto, 2008.

[116] D. Chai and A. Bouzerdoum, "A Bayesian Approach to Skin Color Classification in *YCbCr* Color Space," *IEEE, TENCON*, Kuala Lumpur, Malaysia, September 2000, pp. 421-424.

[117] D. Bourgin, , "Color space FAQ," http://www.neuro.sfc.keio.ac.jp/~aly/polygon/info/color-space-faq.html, August 2004.

[118] C. B. Bose and J. Amir, "Design of Fiducials For Accurate Registration Using Machine Vision," *IEEE Transactions on Pattern Analysis and Machine Intelligence*, Vol. 12, No. 12, December 1990, pp. 1196-1200.

APPENDIX A: SIMULATION RESULTS: MODIFIED RG METHOD

All simulations presented in this Appendix were carried out in a VISUAL BASIC environment. The starting velocity of P is taken as 30 m/s and the starting velocity of O_D is taken as 20 m/s. The starting velocity of O_P is taken 25 m/s except when it is moving with sinusoidal velocity; in that case, it is taken as 27.5 m/s. The simulations are divided into two main cases: (*i*) no O_P present and (*ii*) O_P present, which does not allow P to immediately overtake O_D.

A.1 Case 1: Overtaking in the Absence of An Obstacle Vehicle in the Passing Lane

In this Case, P is required to overtake a slower moving O_D with no O_P being present. Once the closing distance between the vehicles is 2 s, P starts its overtaking manoeuvre receiving guidance commands from the modified RG law. The results of the simulations for this Case are presented here for four variations of velocity of O_D, (*i*) constant, (*ii*) accelerating, (*iii*) decelerating, and (*iv*) sinusoidal, Figure A.1. The results for each case are presented via a set of

two figures and one table. The first figure in each set shows P's path and velocity profile and the second figure shows the velocity profiles of P in both the lateral and axial directions. The table shows the summary results.

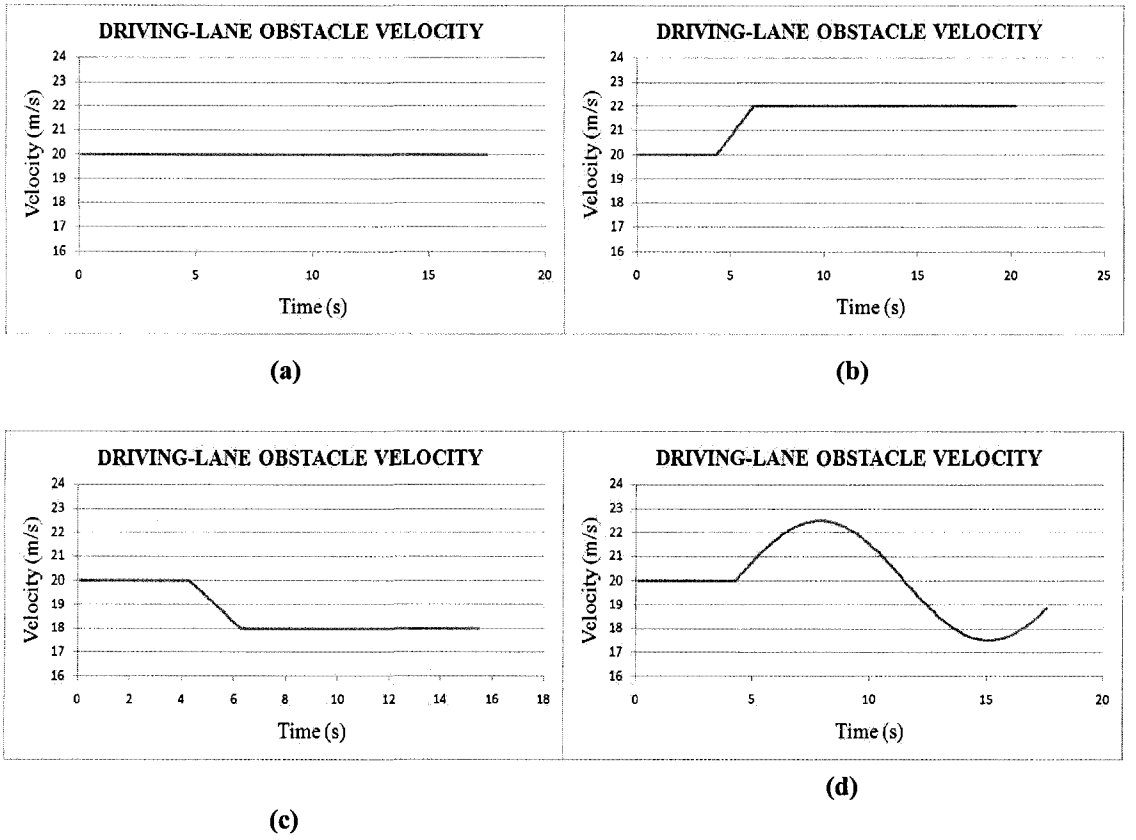

Figure A.1: (a) Constant, (b) Accelerating, (c) Decelerating, and (d) Sinusoidal Velocity Profiles.

A.1.1 O_D is Moving with Constant Velocity

The results of the simulations for this scenario are presented in Figures A.2 and A.3 and Table A.1. The velocity of O_D is as shown in Figure A.1 (a). The complete manoeuvre took 13.5 s to complete.

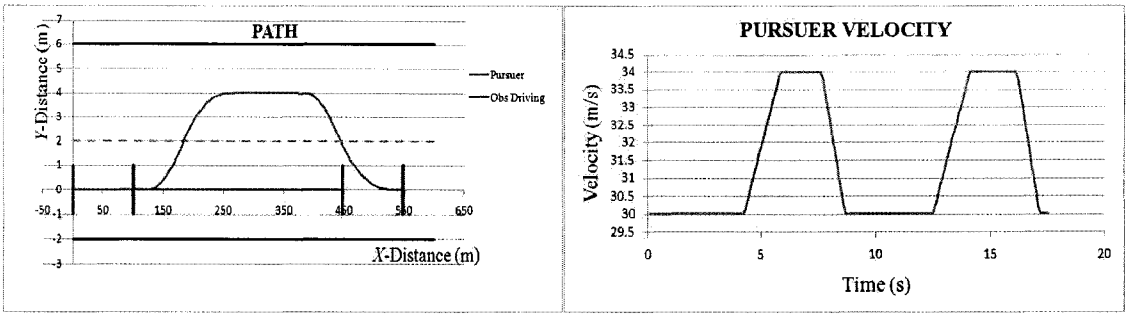

Figure A.2. Path and Velocity Profile of *P*.

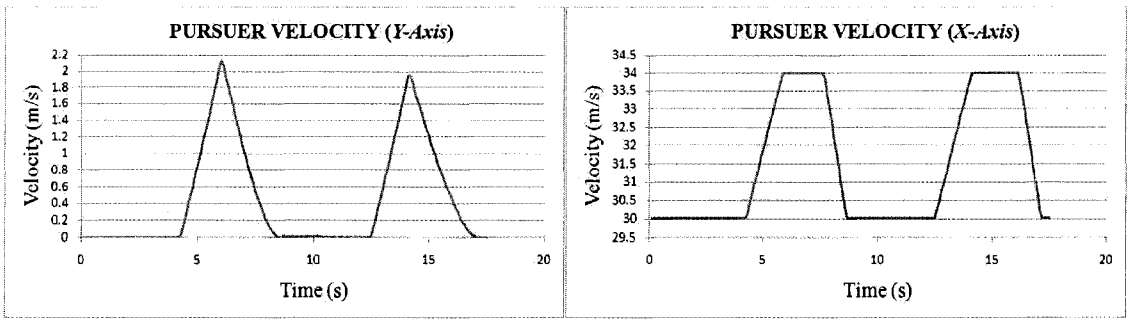

Figure A.3. Lateral and Axial Velocities of *P*.

Table A.1. Summary Results for Case 1, Scenario 1.

	Modified RG Technique
Total time taken for overtaking (s)	13.5
Maximum velocity achieved (m/s)	34
Maximum lateral acceleration (m/s^2)	1.1
Maximum axial acceleration (m/s^2)	2.0

A.1.2 O_D is Accelerating

The results of the simulations for this scenario are presented in Figures A.4 and A.5 and Table A.2. The velocity of O_D is as shown in Figure A.1 (b). The complete manoeuvre took 16.3 s to complete.

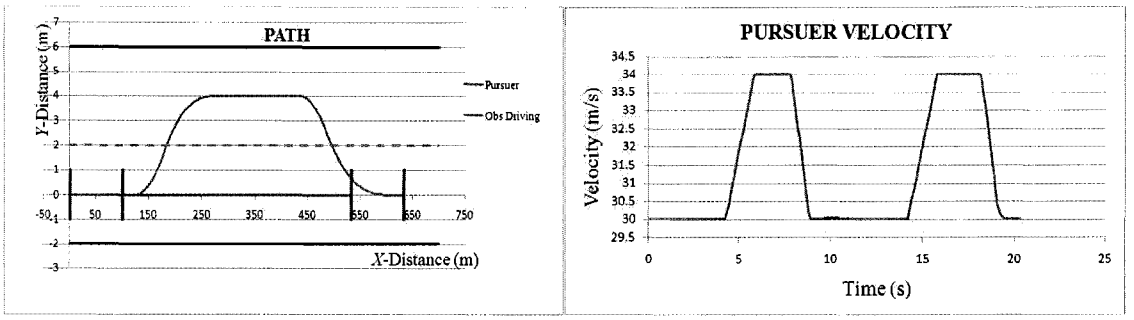

Figure A.4. Path and Velocity Profile of *P*.

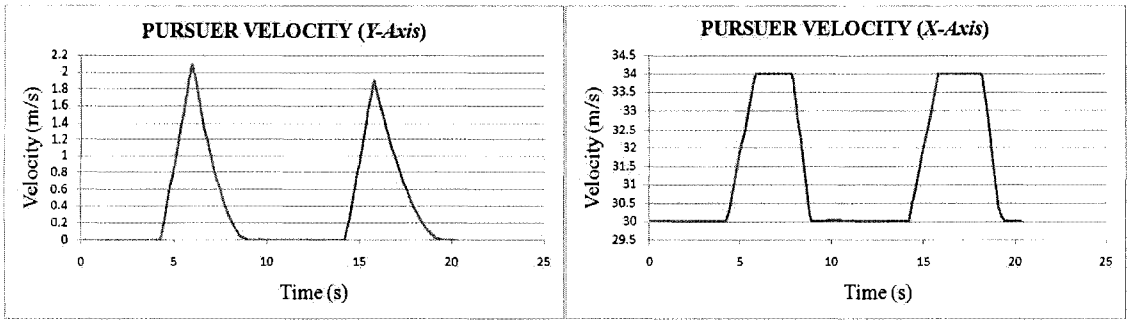

Figure A.5. Lateral and Axial Velocities of *P*.

Table A.2. Summary Results for Case 1, Scenario 2.

	Modified RG Technique
Total time taken for overtaking (s)	16.3
Maximum velocity achieved (m/s)	34
Maximum lateral acceleration (m/s^2)	1.04
Maximum axial acceleration (m/s^2)	2.5

A.1.3 O_D is Decelerating

The results of the simulations for this scenario are presented in Figures A.6 and A.7 and Table A.3. The velocity of O_D is as shown in Figure A.1 (c). The complete manoeuvre took 11.5 s to complete.

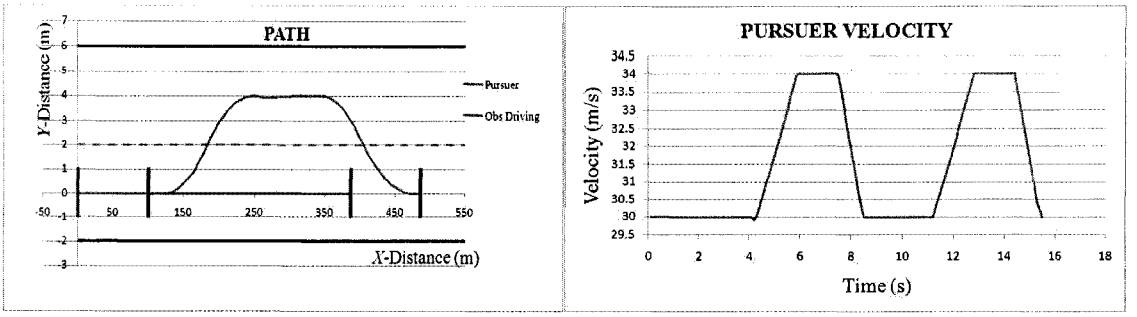

Figure A.6. Path and Velocity Profile of *P*.

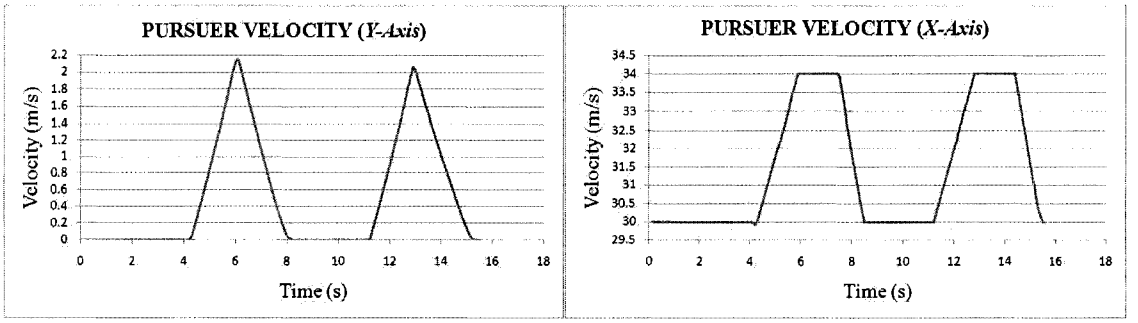

Figure A.7. Lateral and Axial Velocities of *P*.

Table A.3. Summary Results for Case1, Scenario 3.

	Modified RG Technique
Total time taken for overtaking (s)	11.5
Maximum velocity achieved (m/s)	34
Maximum lateral acceleration (m/s^2)	1.06
Maximum axial acceleration (m/s^2)	2.5

A.1.4 O_D is Moving with Sinusoidal Velocity

The results of the simulations for this scenario are presented in Figures A.8 and A.9 and Table A.4. The velocity of O_D is as shown in Figure A.1 (d). The complete manoeuvre took 13.6 s to complete.

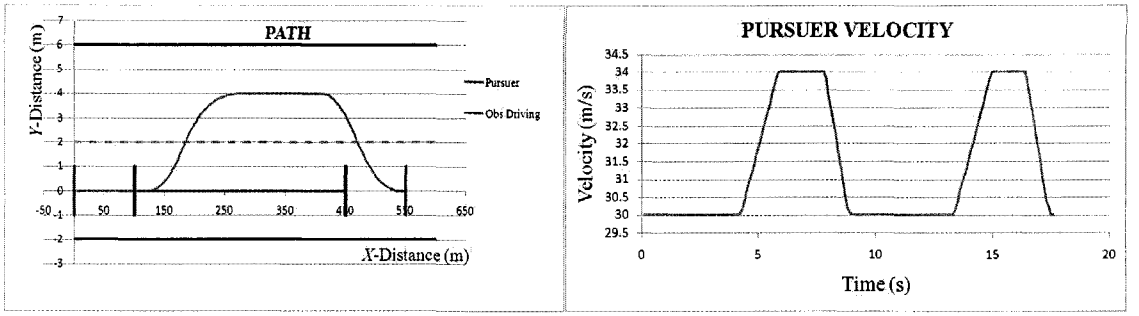

Figure A.8. Path and Velocity Profile of *P*.

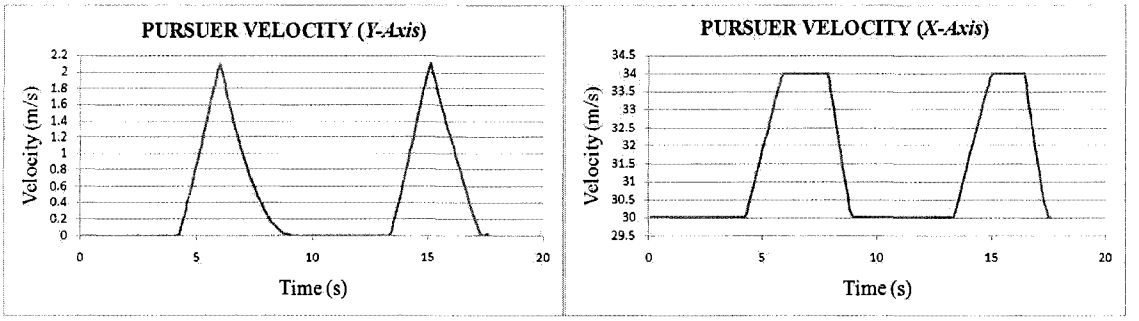

Figure A.9. Lateral and Axial Velocities of *P*.

Table A.4. Summary Results for Case 1, Scenario 4.

	Modified RG Technique
Total time taken for overtaking (s)	13.6
Maximum velocity achieved (m/s)	34
Maximum lateral acceleration (m/s^2)	1.04
Maximum axial acceleration (m/s^2)	2.1

A.2 Case 2: Overtaking in the Presence of An Obstacle Vehicle in the Passing Lane

In this Case, *P* is required to overtake a slower moving O_D when an O_P is present, which does not allow *P* to immediately overtake O_D. For this Case, the results of simulations are presented here for four variations of velocities of both O_D and O_P: (*i*) constant, (*ii*), accelerating, (*iii*)

decelerating, and (*iv*) sinusoidal. The results of each scenario are presented via a set of three figures and one table. The first figure in each set shows *P*'s path and velocity profile, the second figure shows the velocity profiles of *P* in both the lateral and axial directions and the third figure shows the velocity profiles of both O_D and O_P. The table shows the summary results.

A.2.1 Both O_D and O_P are Moving with Constant Velocity

The results of the simulations for this Scenario are presented in Figures A.10, A.11, and A.12 and Table A.5. The complete manoeuvre took 34.2 s to complete.

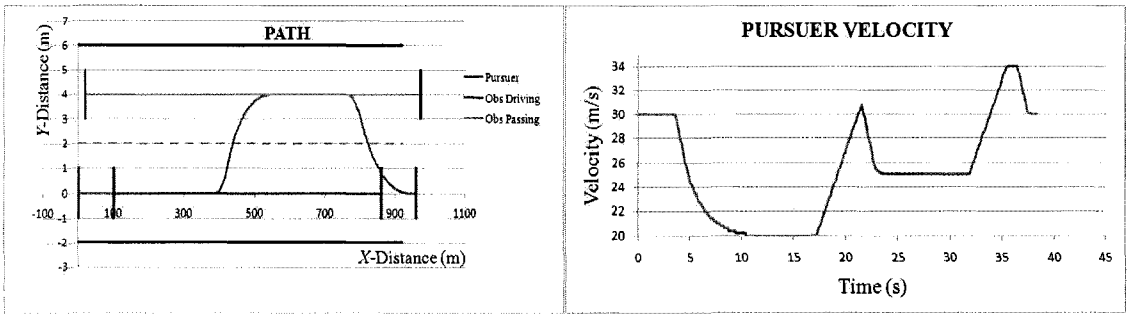

Figure A.10. Path and Velocity Profile of *P*.

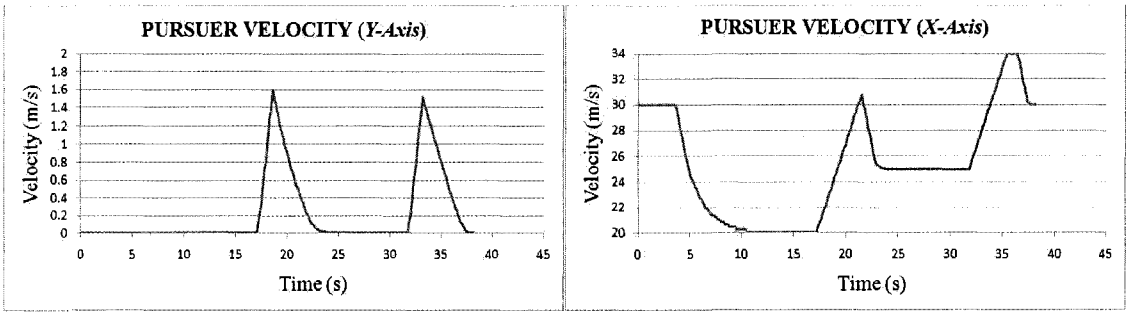

Figure A.11. Lateral and Axial Velocities of *P*.

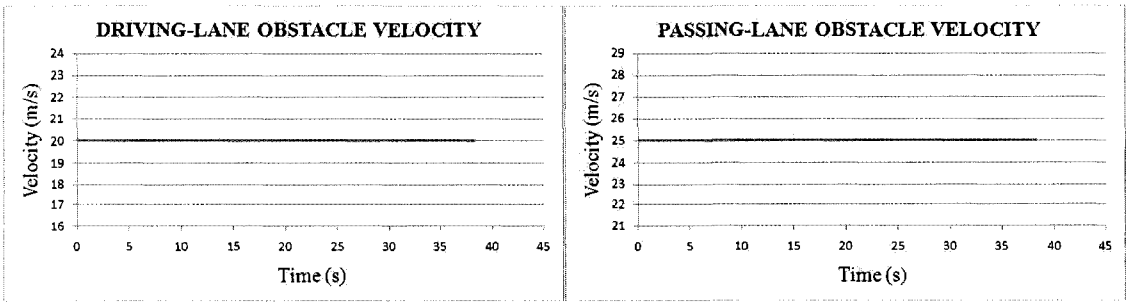

Figure A.12. Velocities of O_D and O_P.

Table A.5. Summary Results for Case 2, Scenario 1.

	Modified RG Technique
Total time taken for overtaking (s)	34.2
Maximum velocity achieved (m/s)	34
Maximum lateral acceleration (m/s^2)	0.88
Maximum axial acceleration (m/s^2)	2.45

A.2.2 O_D is Moving with Constant Velocity and O_P is Accelerating

The results of the simulations for this scenario are presented in Figures A.13, A.14, and A.15 and Table A.6.The complete manoeuvre took 28.4 s to complete.

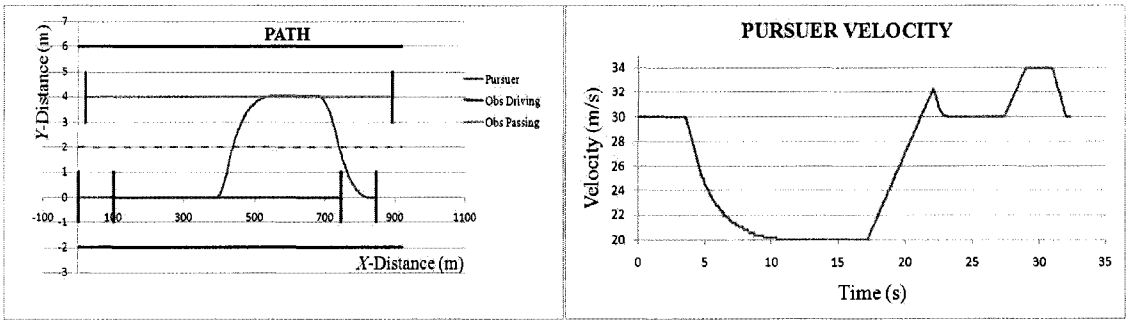

Figure A.13. Path and Velocity Profile of *P*.

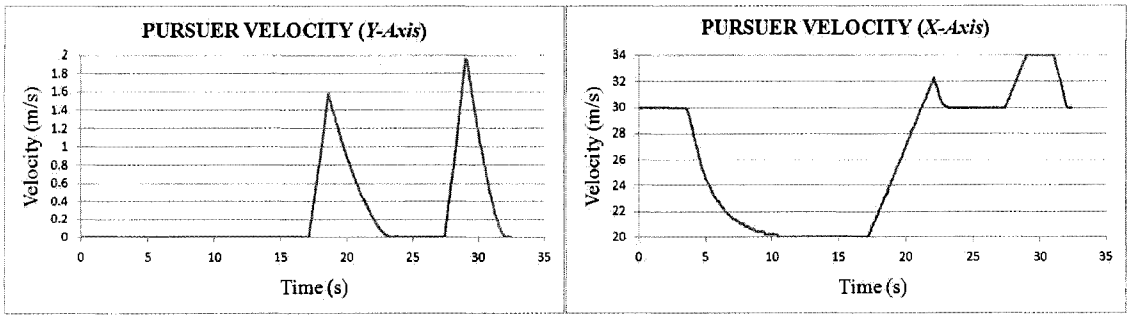

Figure A.14. Lateral and Axial Velocities of *P*.

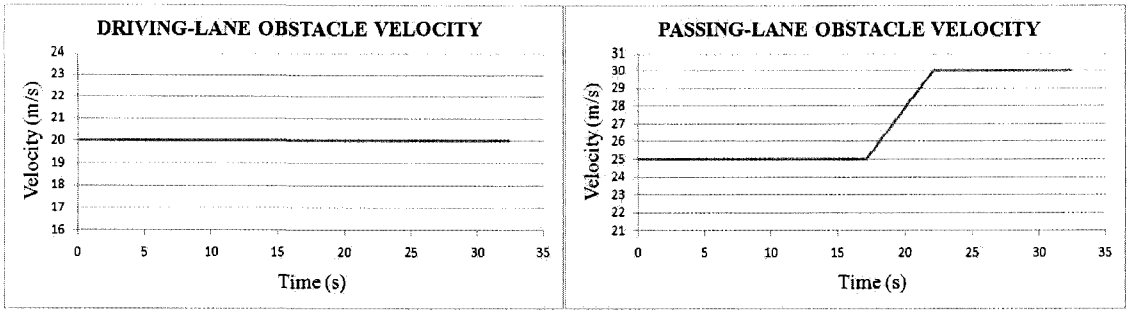

Figure A.15. Velocities of O_D and O_P.

Table A.6. Summary Results for Case 2, Scenario 2.

	Modified RG Technique
Total time taken for overtaking (s)	28.4
Maximum velocity achieved (m/s)	34
Maximum lateral acceleration (m/s^2)	0.95
Maximum axial acceleration (m/s^2)	2.4

A.2.3 O_D is Moving with Constant Velocity and O_P is Decelerating

The results of the simulations for this scenario are presented in Figures A.16, A.17, and A.18 and Table A.7. The complete manoeuvre took 35.8 s to complete.

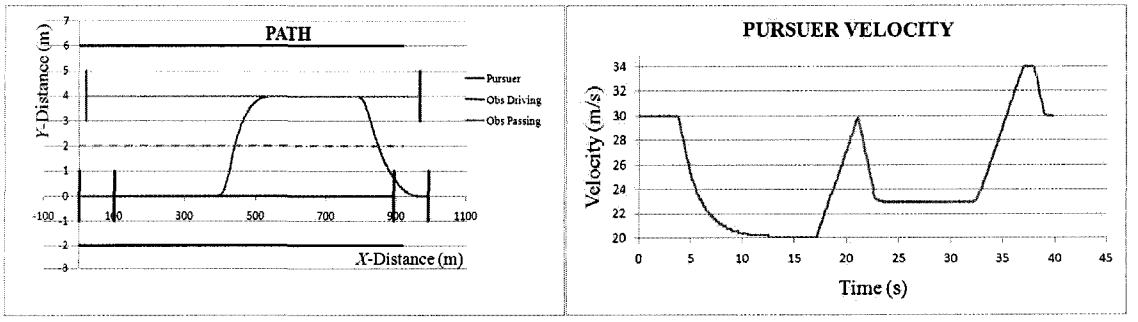

Figure A.16. Path and Velocity Profile of *P*.

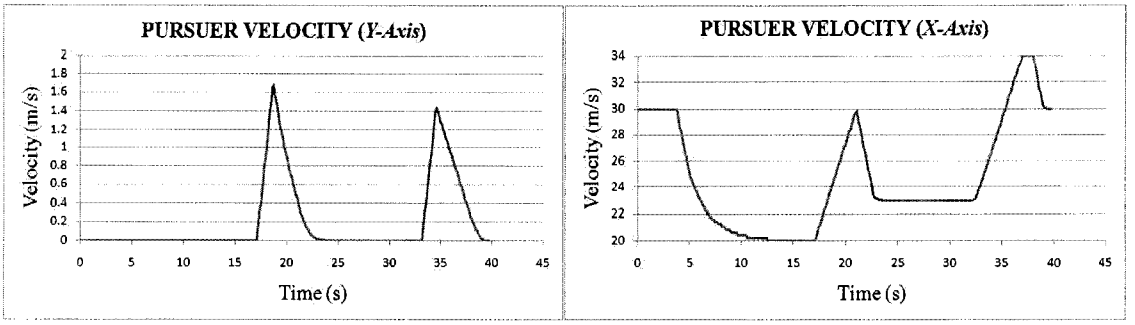

Figure A.17. Lateral and Axial Velocities of *P*.

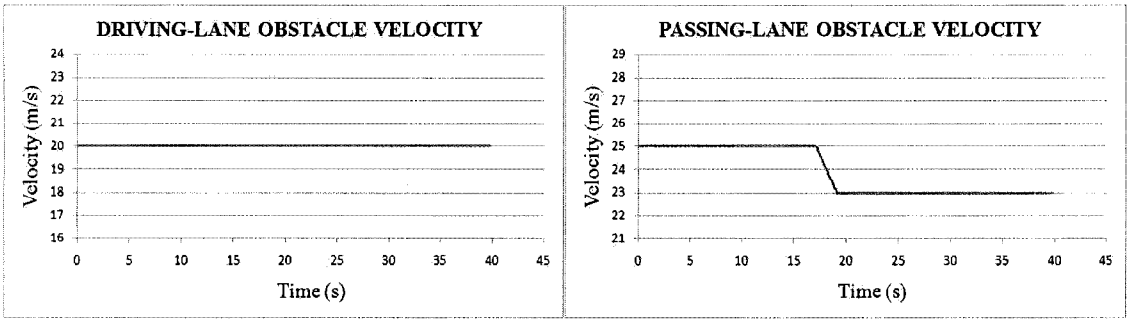

Figure A.18. Velocities of O_D and O_P.

Table A.7. Summary Results for Case 2, Scenario 3.

	Modified RG Technique
Total time taken for overtaking (s)	35.8
Maximum velocity achieved (m/s)	34
Maximum lateral acceleration (m/s^2)	0.88
Maximum axial acceleration (m/s^2)	2.48

A.2.4 O_D is Moving with Constant Velocity and O_P is Moving with Sinusoidal Velocity

The results of the simulations for this scenario are presented in Figures A.19, A.20, and A.21 and Table A.8. The complete manoeuvre took 26.0 s to complete.

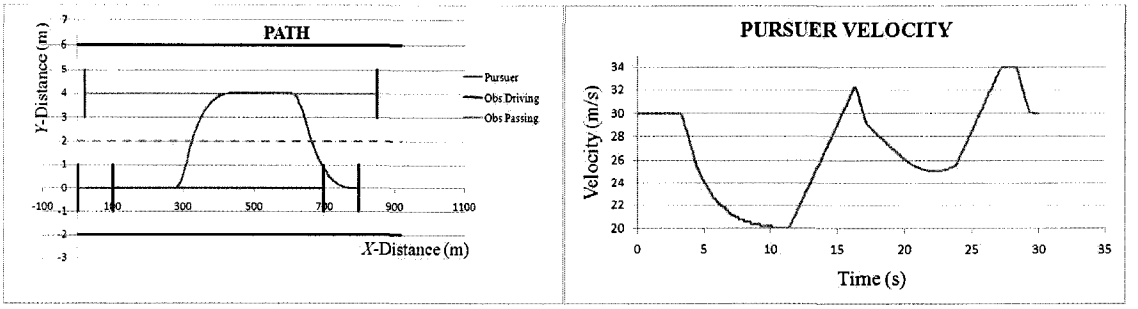

Figure A.19. Path and Velocity Profile of *P*.

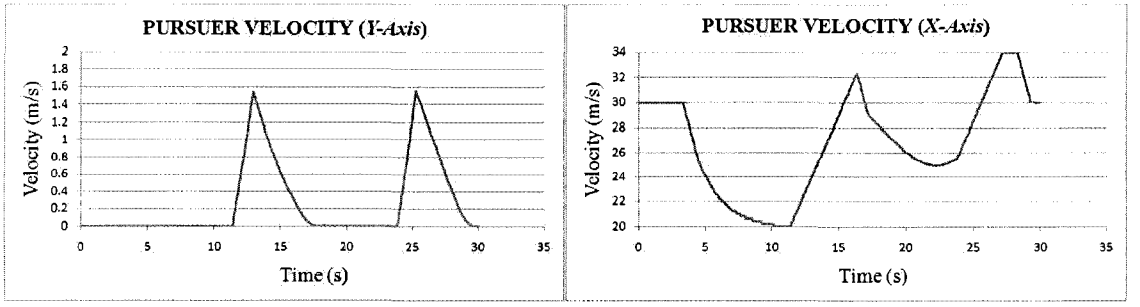

Figure A.20. Lateral and Axial Velocities of *P*.

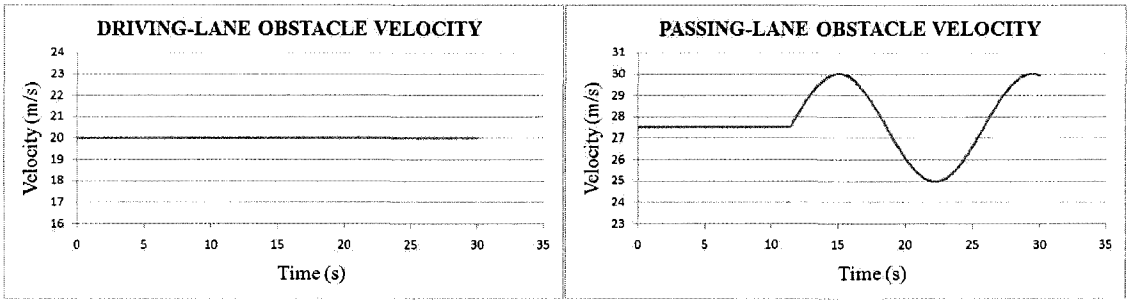

Figure A.21. Velocities of O_D and O_P.

Table A.8. Summary Results for Case 2, Scenario 4.

	Modified RG Technique
Total time taken for overtaking (s)	26
Maximum velocity achieved (m/s)	34
Maximum lateral acceleration (m/s^2)	0.93
Maximum axial acceleration (m/s^2)	2.35

A.2.5 O_D is Accelerating and O_p is Moving with Constant Velocity

The results of the simulations for this scenario are presented in Figures A.22, A.23, and A.24 and Table A.9. The complete manoeuvre took 38.5 s to complete.

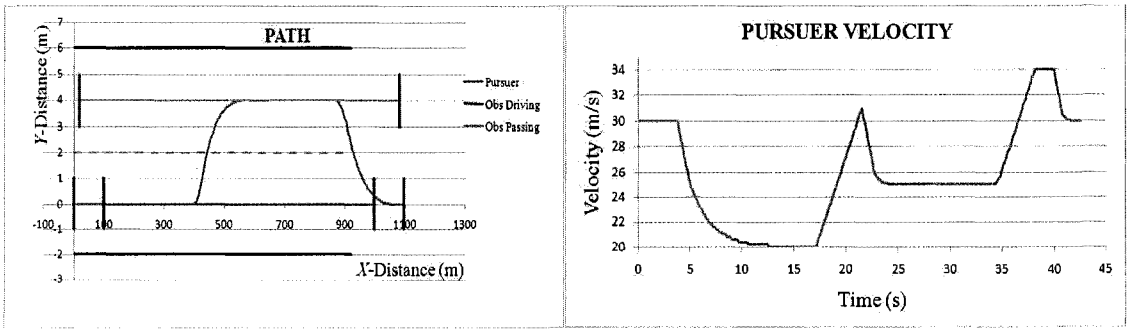

Figure A.22. Path and Velocity Profile of *P*.

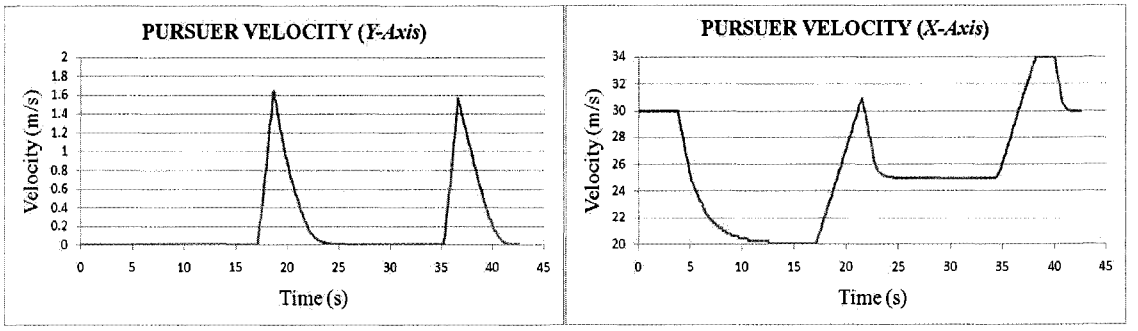

Figure A.23. Lateral and Axial Velocities of *P*.

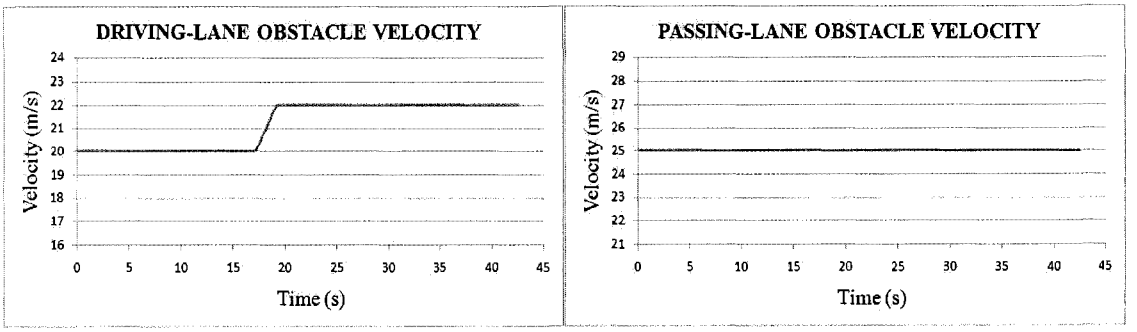

Figure A.24. Velocities of O_D and O_P.

Table A.9. Summary Results for Case 2, Scenario 5.

	Modified RG Technique
Total time taken for overtaking (s)	38.5
Maximum velocity achieved (m/s)	34
Maximum lateral acceleration (m/s^2)	0.89
Maximum axial acceleration (m/s^2)	2.43

A.2.6 Both O_D and O_P are Accelerating

The results of the simulations for this scenario are presented in Figures A.25, A.26, and A.27 and Table A.10. The complete manoeuvre took 31.5 s to complete.

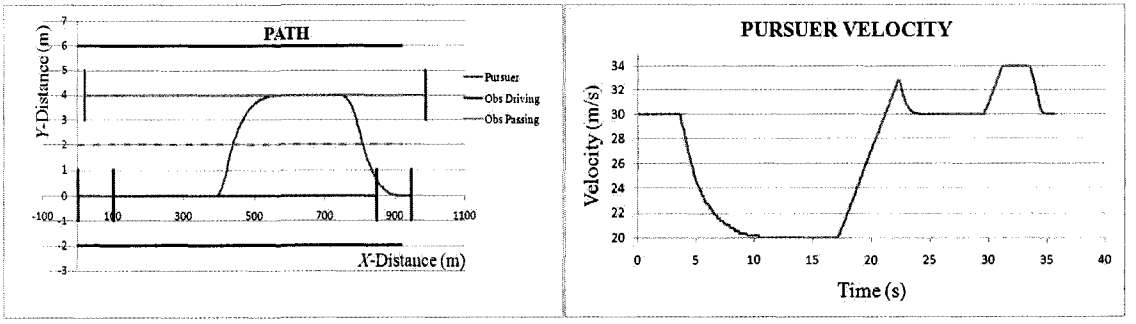

Figure A.25. Path and Velocity Profile of *P*.

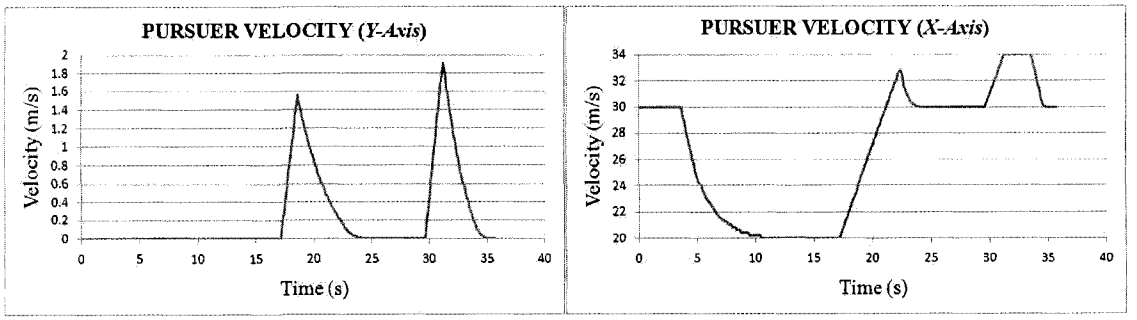

Figure A.26. Lateral and Axial Velocities of *P*.

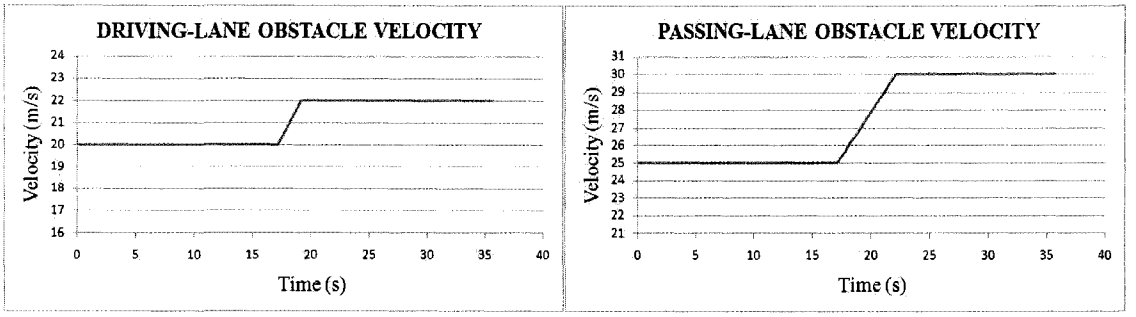

Figure A.27. Velocities of O_D and O_P.

Table A.10. Summary Results for Case 2, Scenario 6.

	Modified RG Technique
Total time taken for overtaking (s)	31.5
Maximum velocity achieved (m/s)	34
Maximum lateral acceleration (m/s^2)	0.91
Maximum axial acceleration (m/s^2)	2.37

A.2.7 O_D is Accelerating and O_P is Decelerating

The results of the simulations for this scenario are presented in Figures A.28, A.29, and A.30 and Table A.11. The complete manoeuvre took 52.8 s to complete.

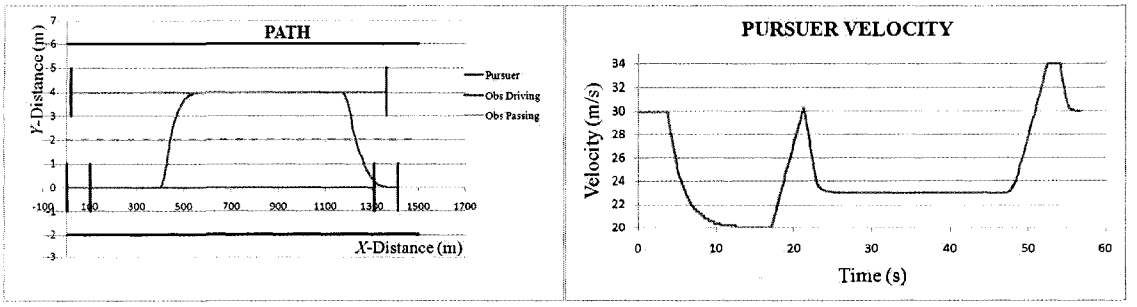

Figure A.28. Path and Velocity Profile of *P*.

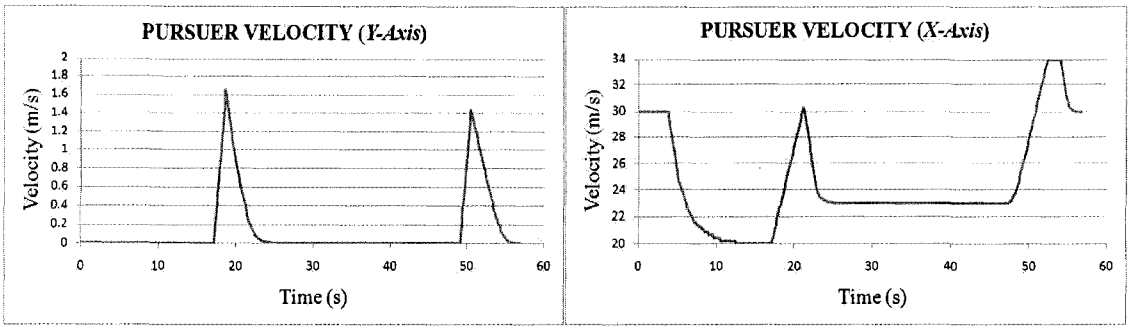

Figure A.29. Lateral and Axial Velocities of *P*.

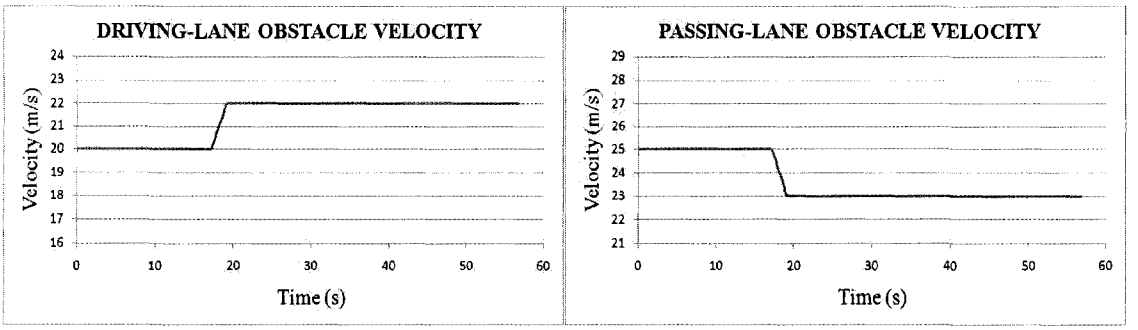

Figure A.30. Velocities of O_D and O_P.

Table A.11. Summary Results for Case 2, Scenario 7.

	Modified RG Technique
Total time taken for overtaking (s)	52.8
Maximum velocity achieved (m/s)	34
Maximum lateral acceleration (m/s^2)	0.91
Maximum axial acceleration (m/s^2)	2.42

A.2.8 O_D is Accelerating and O_P is Moving with Sinusoidal Velocity

The results of the simulations for this case are presented in Figures A.31, A.32, and A.33 and Table A.12. The complete manoeuvre took 30.4 s to complete.

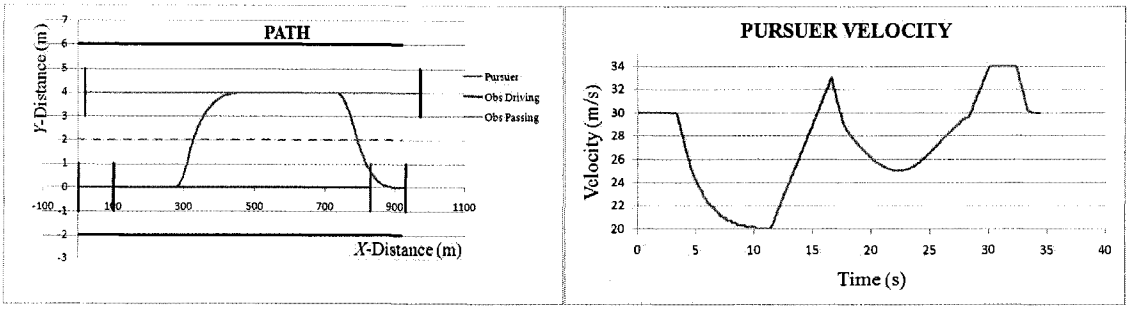

Figure A.31. Path and Velocity Profile of *P*.

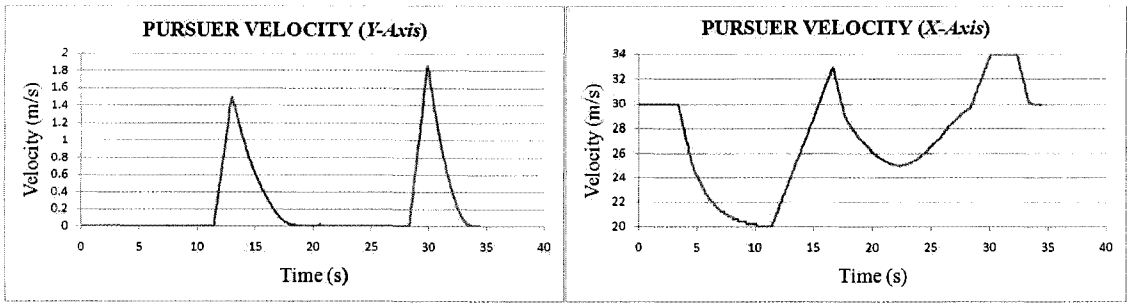

Figure A.32. Lateral and Axial Velocities of *P*.

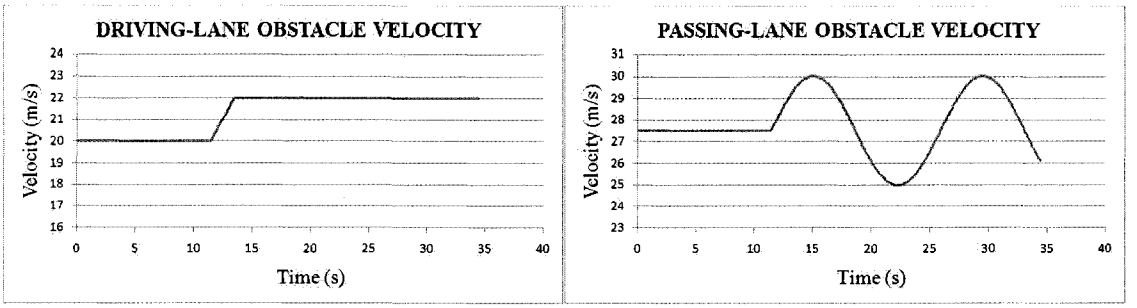

Figure A.33. Velocities of O_D and O_P.

Table A.12. Summary Results for Case 2, Scenario 8.

	Modified RG Technique
Total time taken for overtaking (s)	30.4
Maximum velocity achieved (m/s)	34
Maximum lateral acceleration (m/s^2)	0.93
Maximum axial acceleration (m/s^2)	2.42

A.2.9 O_D is Decelerating and O_p is Moving with Constant Velocity

The results of the simulations for this scenario are presented in Figures A.34, A.35, and A.36 and Table A.13. The complete manoeuvre took 29.6 s to complete.

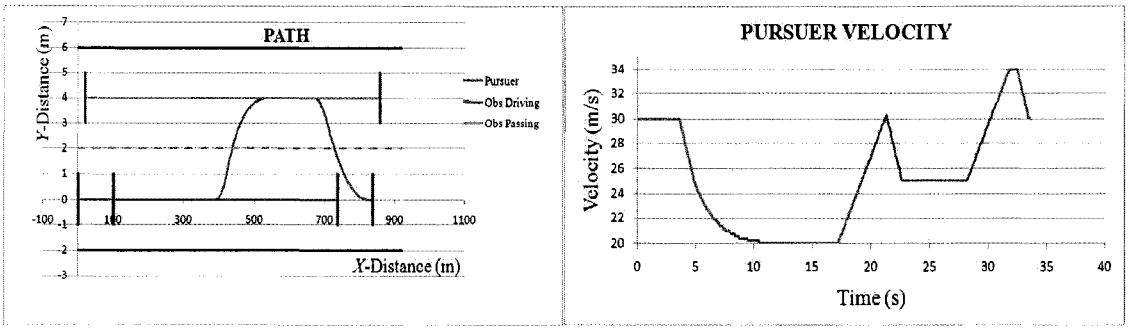

Figure A.34. Path and Velocity Profile of *P*.

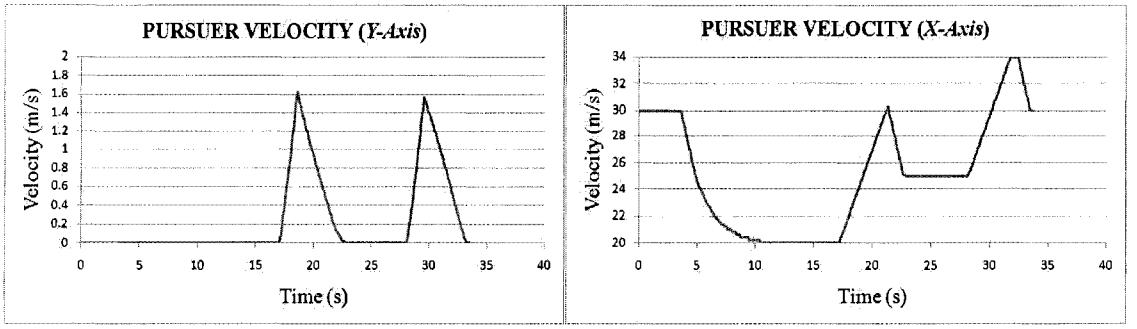

Figure A.35. Lateral and Axial Velocities of *P*.

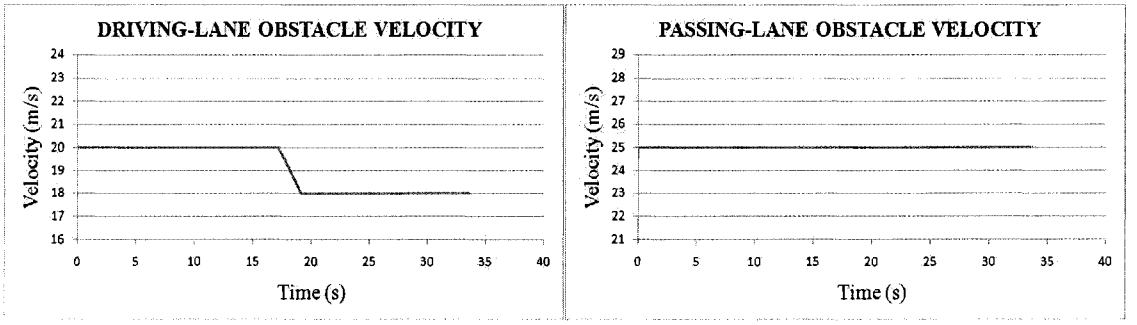

Figure A.36. Velocities of O_D and O_P.

Table A.13. Summary Results for Case 2, Scenario 9.

	Modified RG Technique
Total time taken for overtaking (s)	29.6
Maximum velocity achieved (m/s)	34
Maximum lateral acceleration (m/s^2)	0.88
Maximum axial acceleration (m/s^2)	2.35

A.2.10 O_D is Decelerating and O_P is Accelerating

The results of the simulations for this scenario are presented in Figures A.37, A.38, and A.39 and Table A.14. The complete manoeuvre took 26.2 s to complete.

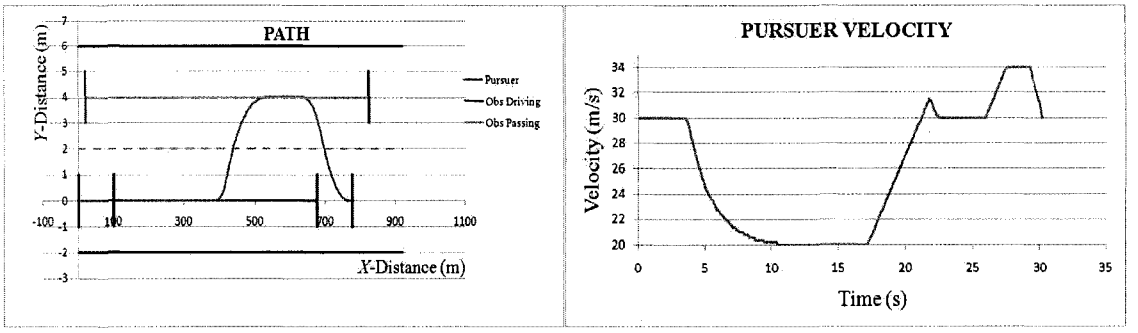

Figure A.37. Path and Velocity Profile of *P*.

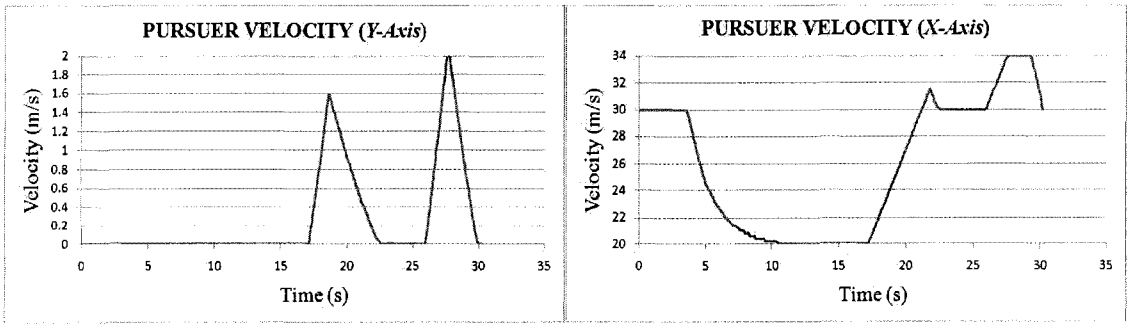

Figure A.38. Lateral and Axial Velocities of *P*.

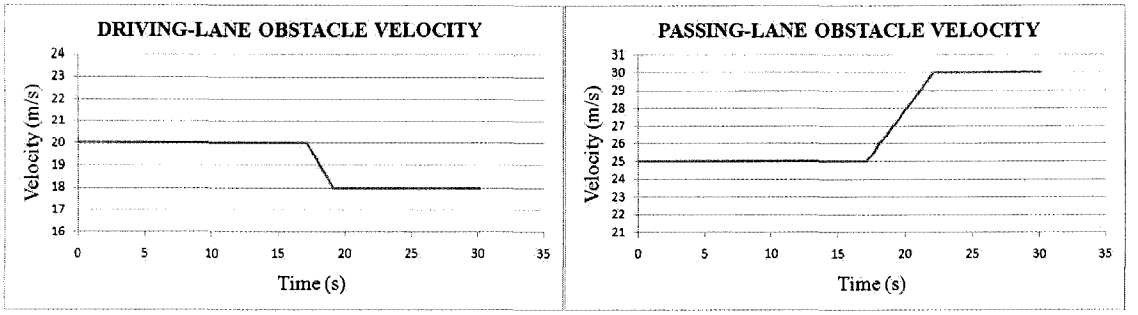

Figure A.39. Velocities of O_D and O_P.

Table A.14. Summary Results for Case 2, Scenario 10.

	Modified RG Technique
Total time taken for overtaking (s)	26.2
Maximum velocity achieved (m/s)	34
Maximum lateral acceleration (m/s^2)	0.92
Maximum axial acceleration (m/s^2)	2.45

A.2.11 Both O_D and O_P are Decelerating

The results of the simulations for this scenario are presented in Figures A.40, A.41, and A.42 and Table A.15. The complete manoeuvre took 32.5 s to complete.

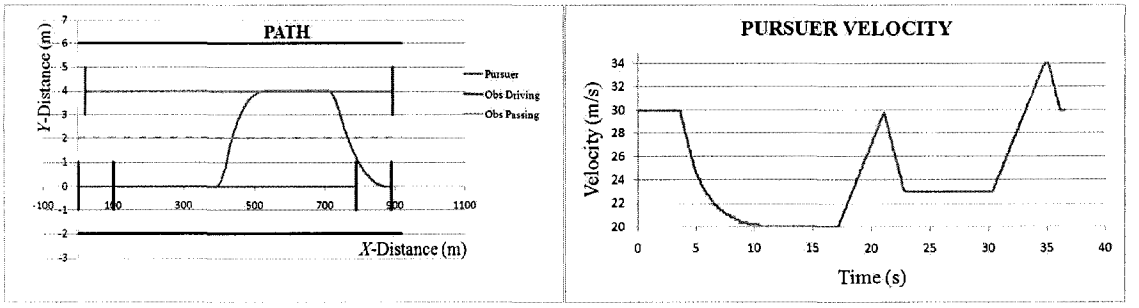

Figure A.40. Path and Velocity Profile of *P*.

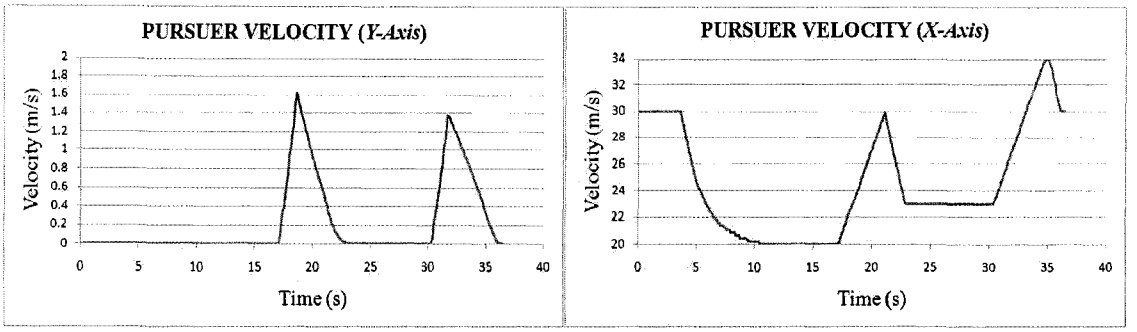

Figure A.41. Lateral and Axial Velocities of *P*.

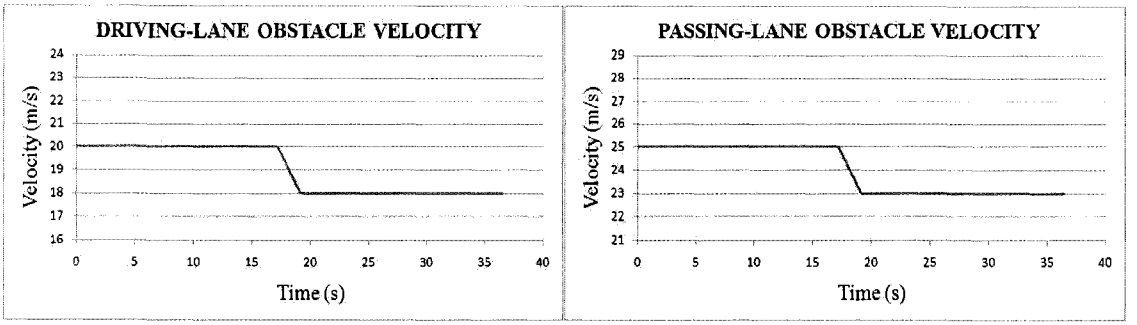

Figure A.42. Velocities of O_D and O_P.

Table A.15. Summary Results for Case 2, Scenario 11.

	Modified RG Technique
Total time taken for overtaking (s)	32.5
Maximum velocity achieved (m/s)	34
Maximum lateral acceleration (m/s^2)	0.90
Maximum axial acceleration (m/s^2)	2.45

A.2.12 O_D is Decelerating and O_P is Moving with Sinusoidal Velocity

The results of the simulations for this scenario are presented in Figures A.43, A.44, and A.45 and Table A.16. The complete manoeuvre took 22.1 s to complete.

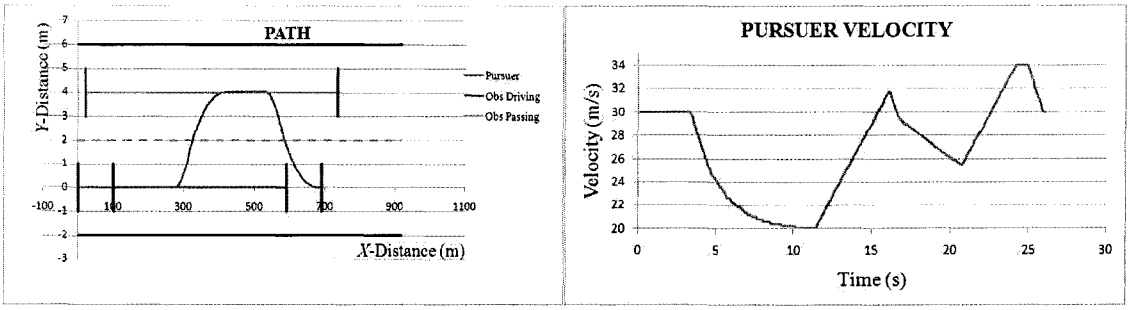

Figure A.43. Path and Velocity Profile of *P*.

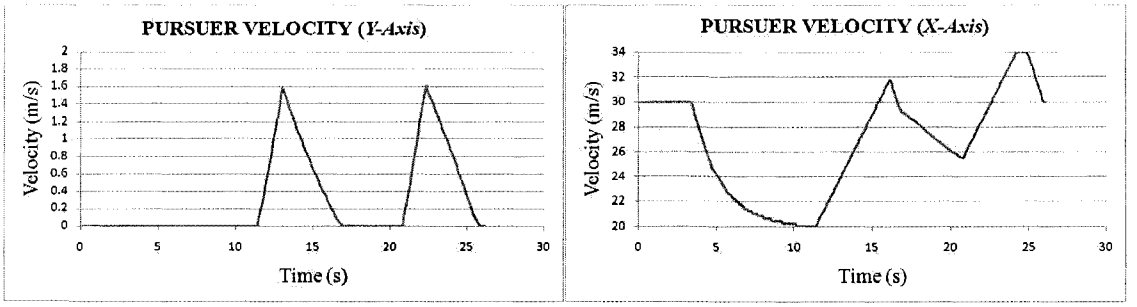

Figure A.44. Lateral and Axial Velocities of *P*.

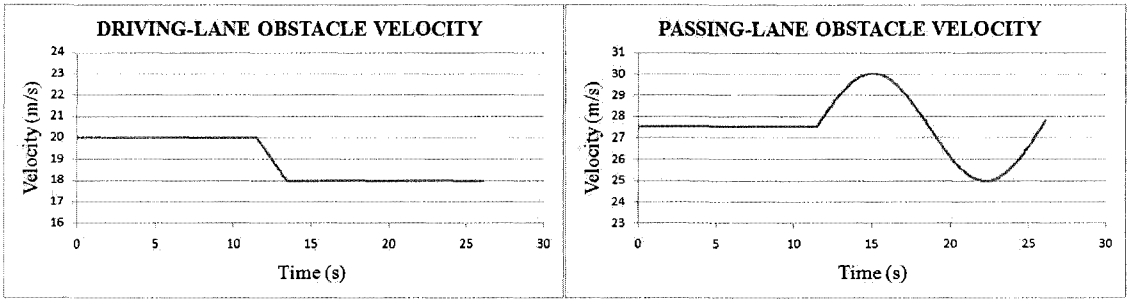

Figure A.45. Velocities of O_D and O_P.

Table A.16. Summary Results for Case 2, Scenario 12.

	Modified RG Technique
Total time taken for overtaking (s)	22.1
Maximum velocity achieved (m/s)	34
Maximum lateral acceleration (m/s^2)	0.82
Maximum axial acceleration (m/s^2)	2.40

A.2.13 O_D is Moving with Sinusoidal Velocity and O_p is Moving with Constant Velocity

The results of the simulations for this scenario are presented in Figures A.46, A.47, and A.48 and Table A.17. The complete manoeuvre took 34.7 s to complete.

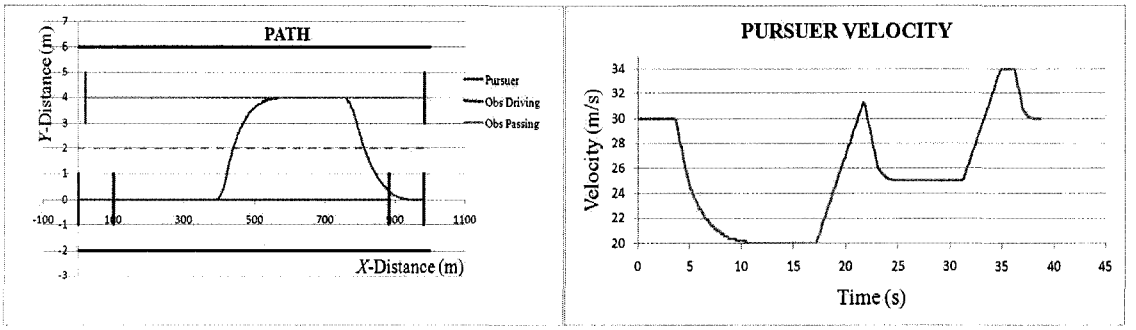

Figure A.46. Path and Velocity Profile of *P*.

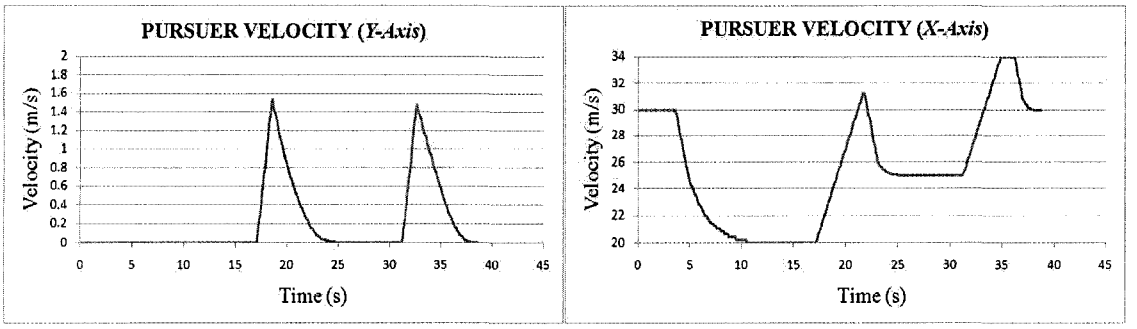

Figure A.47. Lateral and Axial Velocities of *P*.

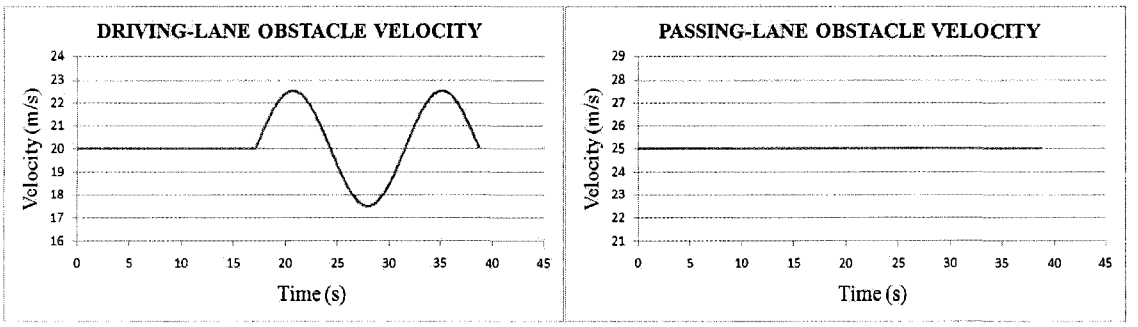

Figure A.48. Velocities of O_D and O_P.

Table A.17. Summary Results for Case 2, Scenario 13.

	Modified RG Technique
Total time taken for overtaking (s)	34.7
Maximum velocity achieved (m/s)	34
Maximum lateral acceleration (m/s^2)	0.90
Maximum axial acceleration (m/s^2)	2.38

A.2.14 O_D is Moving with Sinusoidal Velocity and O_P is Accelerating

The results of the simulations for this scenario are presented in Figures A.49, A.50, and A.51 and Table A.6. The complete manoeuvre took 28.4 s to complete.

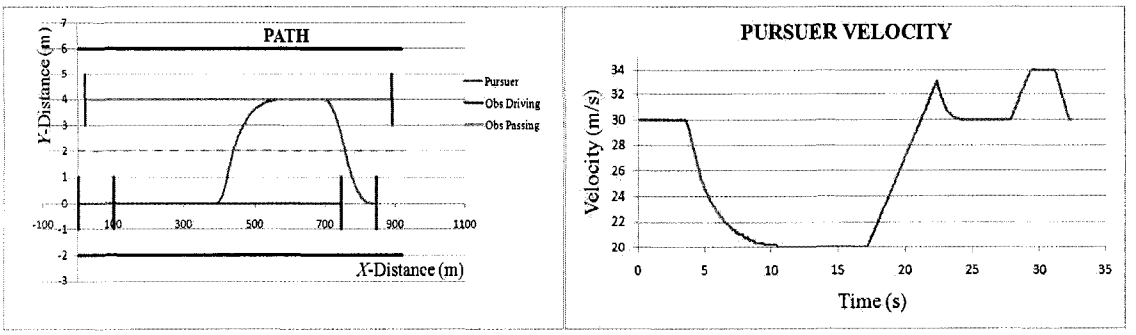

Figure A.49. Path and Velocity Profile of *P*.

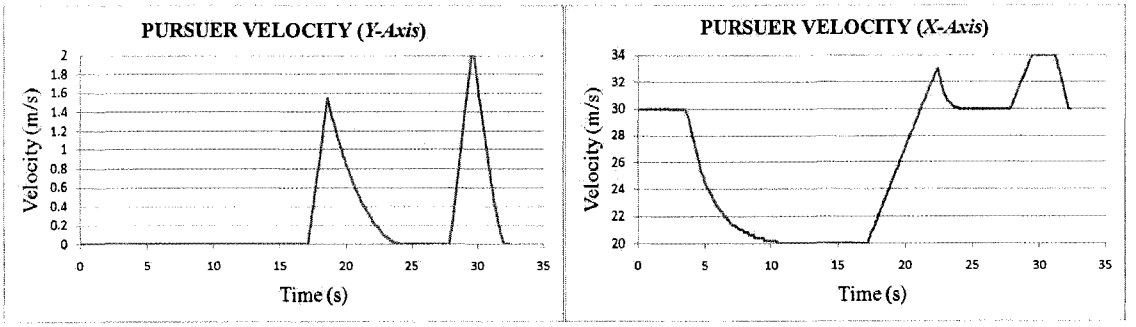

Figure A.50. Lateral and Axial Velocities of *P*.

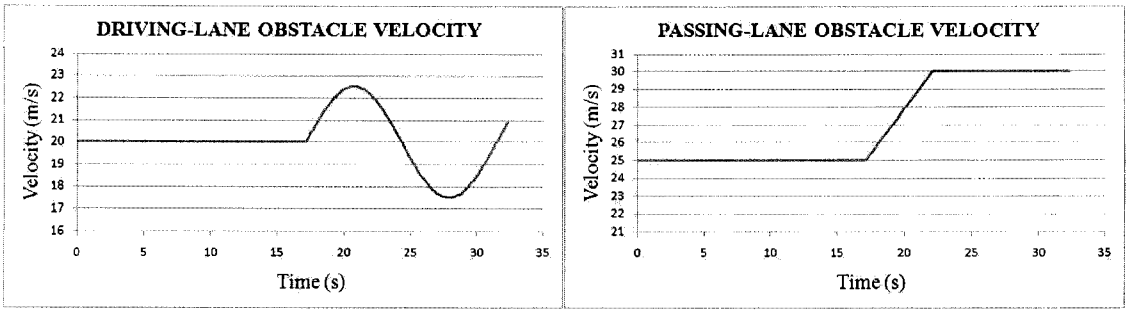

Figure A.51. Velocities of O_D and O_P.

Table A.18. Summary Results for Case 2, Scenario 14.

	Modified RG Technique
Total time taken for overtaking (s)	28.4
Maximum velocity achieved (m/s)	34
Maximum lateral acceleration (m/s^2)	0.92
Maximum axial acceleration (m/s^2)	2.3

A.2.15 O_D is Moving with Sinusoidal Velocity and O_P is Decelerating

The results of the simulations for this scenario are presented in Figures A.52, A.53, and A.54 and Table A.19. The complete manoeuvre took 42.6 s to complete.

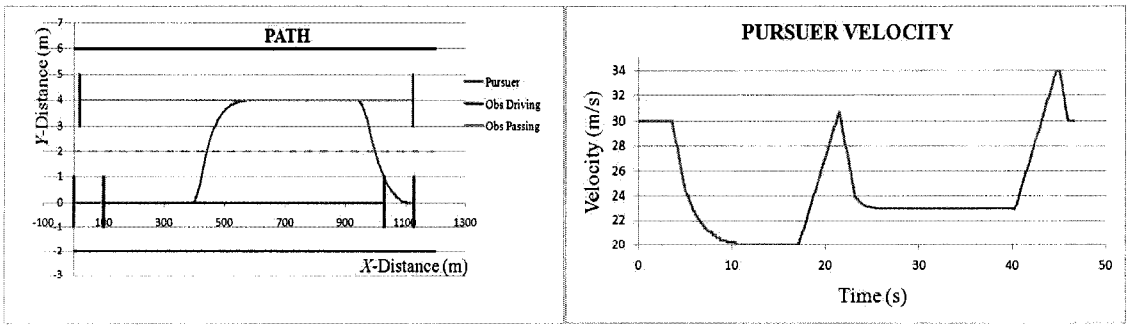

Figure A.52. Path and Velocity Profile of *P*.

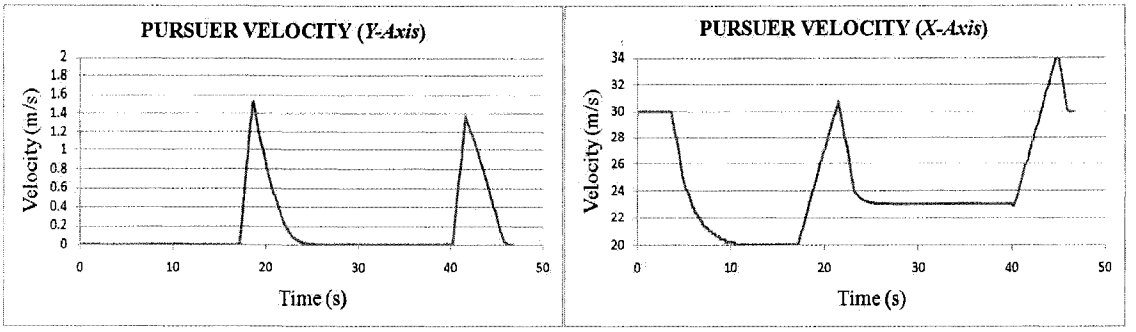

Figure A.53. Lateral and Axial Velocities of *P*.

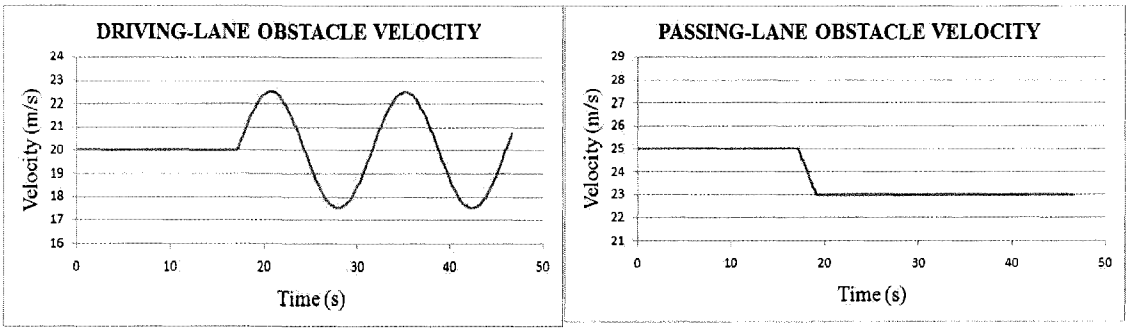

Figure A.54. Velocities of O_D and O_P.

Table A.19. Summary Results for Case 2, Scenario 15.

	Modified RG Technique
Total time taken for overtaking (s)	42.6
Maximum velocity achieved (m/s)	34
Maximum lateral acceleration (m/s^2)	0.86
Maximum axial acceleration (m/s^2)	2.35

A.2.16 Both O_D and O_P are Moving with Sinusoidal Velocity

The results of the simulations for this scenario are presented in Figures A.55, A.56, and A.57 and Table A.20. For this case, the complete manoeuvre took 26.8 s to complete.

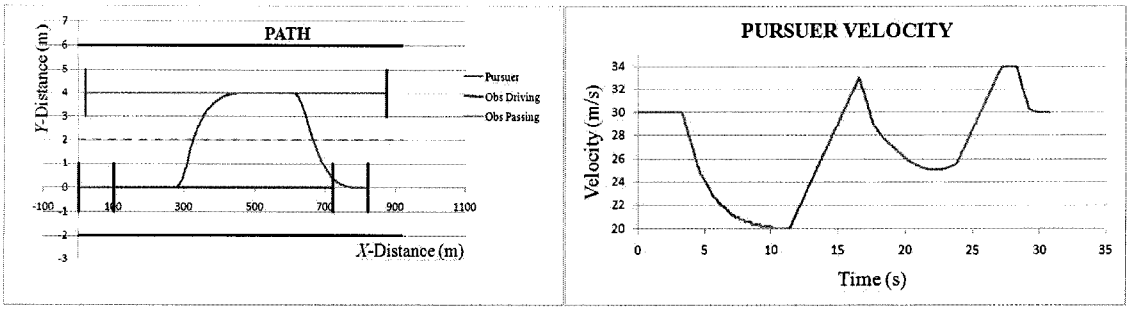

Figure A.55. Path and Velocity Profile of *P*.

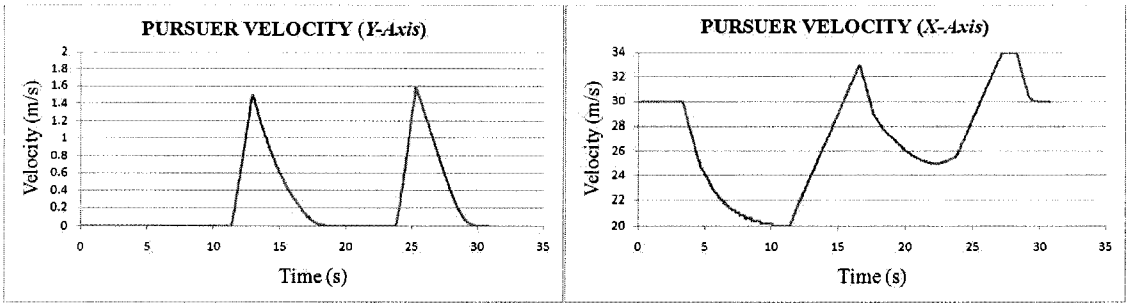

Figure A.56. Lateral and Axial Velocities of *P*.

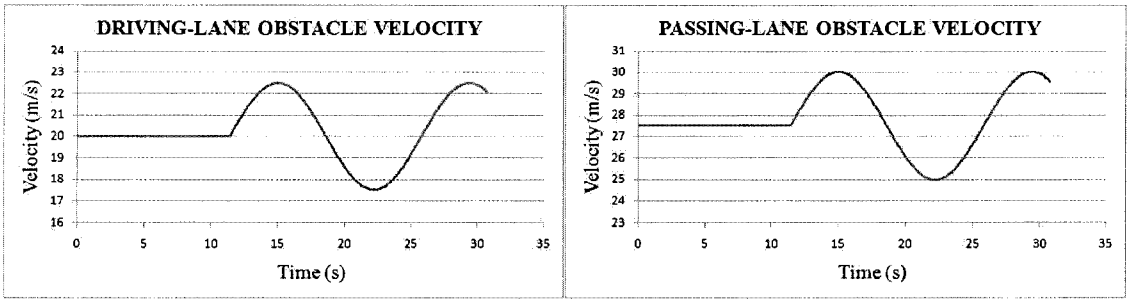

Figure A.57. Velocities of O_D and O_P.

Table A.20. Summary Results for Case 2, Scenario 16.

	Modified RG Technique
Total time taken for overtaking (s)	26.8
Maximum velocity achieved (m/s)	34
Maximum lateral acceleration (m/s^2)	0.88
Maximum axial acceleration (m/s^2)	2.35

APPENDIX B: SIMULATION RESULTS: ORIGINAL RG METHOD

All simulations presented in this Appendix were carried out in a VISUAL BASIC environment. The starting velocity of P is taken as 30 m/s and the starting velocity of O_D is taken as 20 m/s. The starting velocity of O_P is taken 25 m/s except when it is moving with sinusoidal velocity; in that case, it is taken as 27.5 m/s. The simulations are divided into two main Cases: (i) no O_P present and (ii) O_P present, which does not allow P to immediately overtake O_D.

B.1 Case 1: Overtaking in the Absence of An Obstacle Vehicle in the Passing Lane

In this Case, P is required to overtake a slower moving O_D with no O_P present. Once the closing distance between the vehicles is 2 s, P starts its overtaking manoeuvre receiving guidance

commands from the original RG law. The results of simulations for this Case are presented here for four variations of velocity of O_D, (*i*) constant, (*ii*) accelerating, (*iii*) decelerating, and (*iv*) sinusoidal. The velocity profiles of O_D for all the four scenarios are shown in Figure B.1. The results of each scenario are presented via a set of two figures and one table. The first figure in each set shows *P*'s path and velocity profile and the second figure shows the velocity profiles of *P* in both the lateral and axial directions. The table shows the summary results.

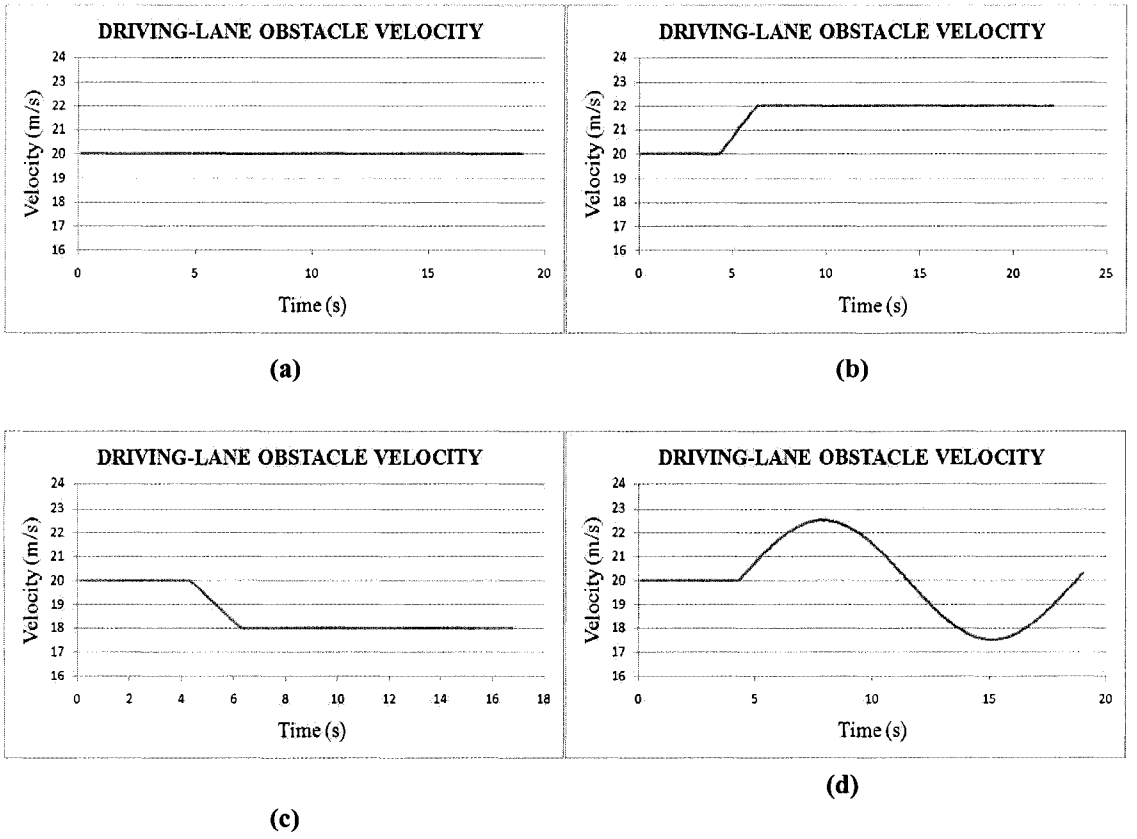

Figure B.1: (a) Constant, (b) Accelerating, (c) Decelerating, and (d) Sinusoidal Velocity Profiles.

B.1.1 O_D is Moving with Constant Velocity

The results of the simulations for this scenario are presented in Figures B.2 and B.3 and Table B.1. The velocity of O_D is shown in Figure B.1 (a). The complete manoeuvre took 15 s to complete.

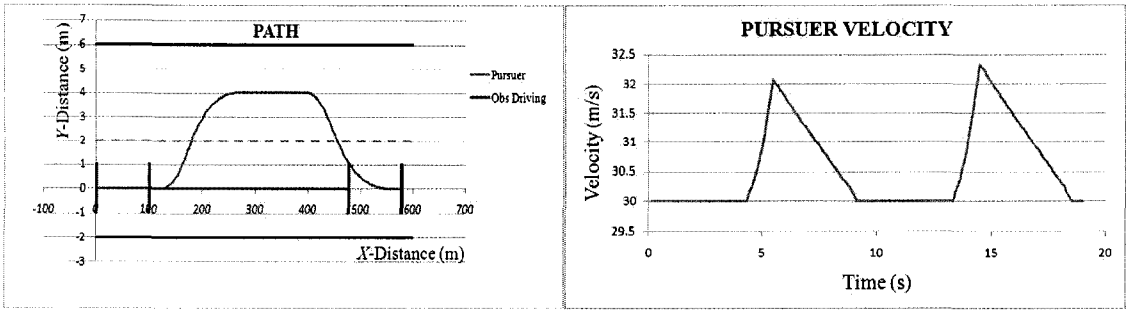

Figure B.2. Path and Velocity Profile of *P*.

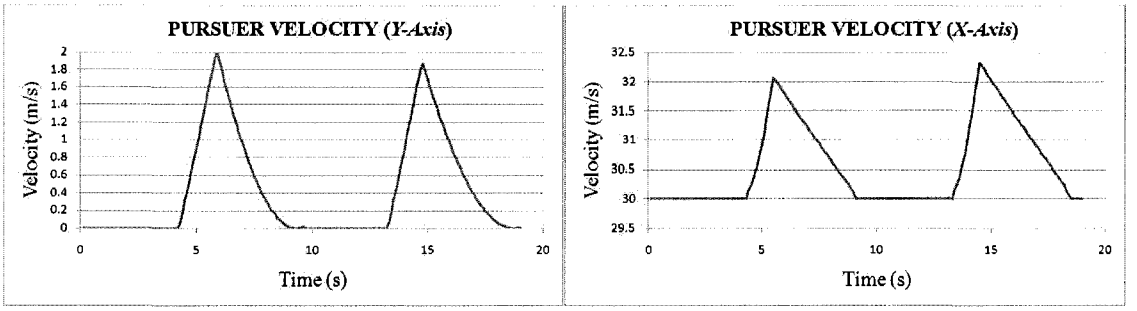

Figure B.3. Lateral and Axial Velocities of *P*.

Table B.1. Summary Results for Case 1, Scenario 1.

	Original RG Technique
Total time taken for overtaking (s)	15
Maximum velocity achieved (m/s)	32.3
Maximum lateral acceleration (m/s^2)	1.0
Maximum axial acceleration (m/s^2)	1.7

B.1.2 O_D is Accelerating

The results of the simulations for this scenario are presented in Figures B.4 and B.5 and Table B.2. The velocity of O_D is shown in Figure B.1 (b). The complete manoeuvre took 18 s to complete.

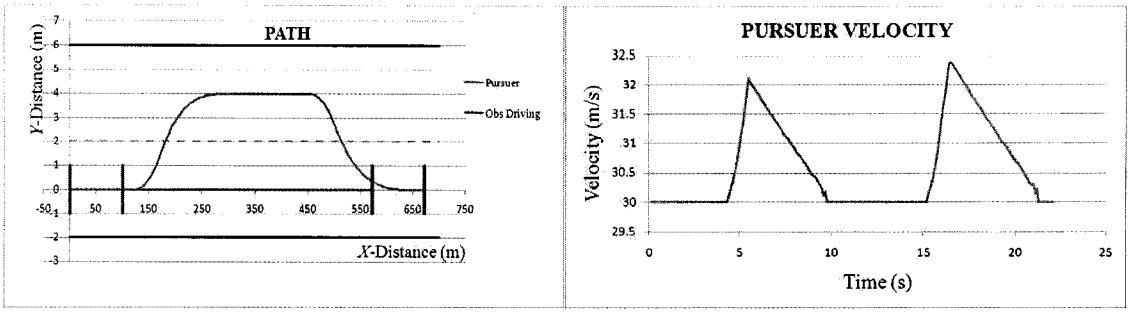

Figure B.4. Path and Velocity Profile of *P*.

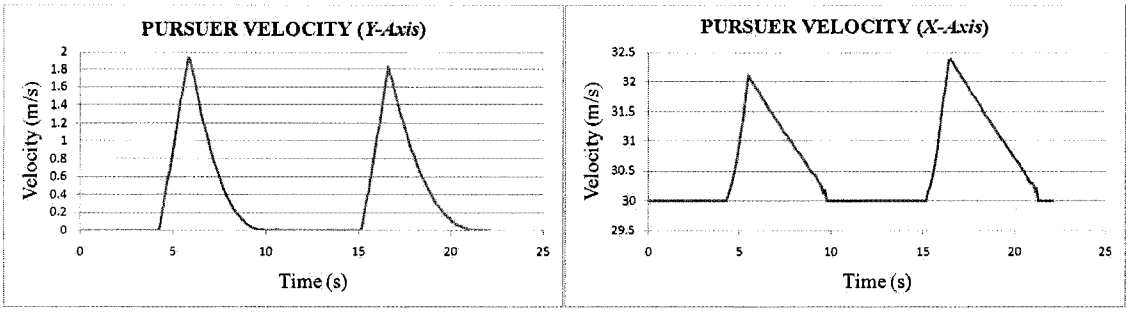

Figure B.5. Lateral and Axial Velocities of *P*.

Table B.2. Summary Results for Case 1, Scenario 2.

	Original RG Technique
Total time taken for overtaking (s)	18
Maximum velocity achieved (m/s)	32.4
Maximum lateral acceleration (m/s^2)	0.9
Maximum axial acceleration (m/s^2)	1.7

B.1.3 O_D is Decelerating

The results of the simulations for this scenario are presented in Figures B.6 and B.7 and Table B.3. The velocity of O_D is shown in Figure B.1 (c). The complete manoeuvre took 12.7 s to complete.

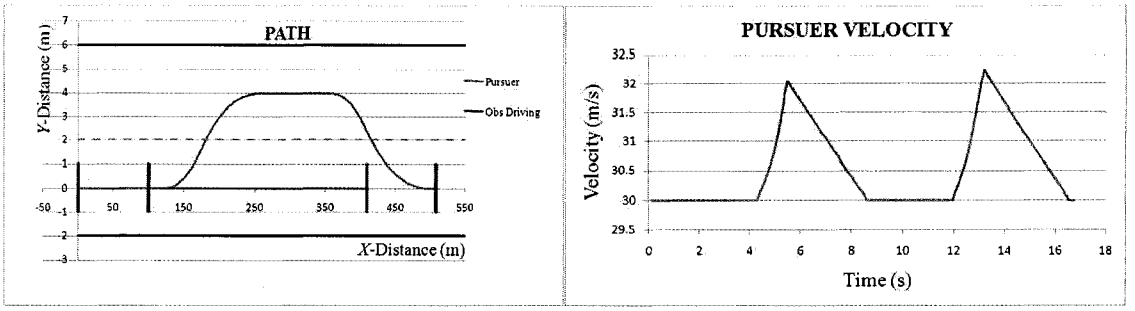

Figure B.6. Path and Velocity Profile of *P*.

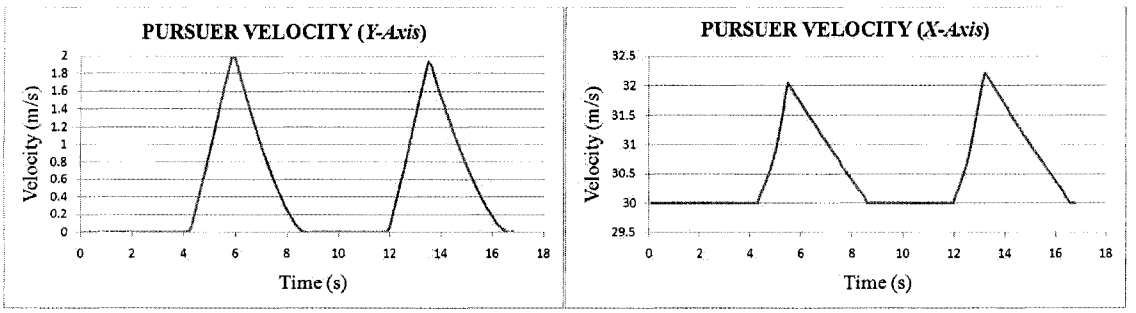

Figure B.7. Lateral and Axial Velocities of *P*.

Table B.3. Summary Results for Case 1, Scenario 3.

	Original RG Technique
Total time taken for overtaking (s)	12.7
Maximum velocity achieved (m/s)	32.2
Maximum lateral acceleration (m/s^2)	1.05
Maximum axial acceleration (m/s^2)	1.69

B.1.4 O_D is Moving with Sinusoidal Velocity

The results of the simulations for this scenario are presented in Figures B.8 and B.9 and Table B.4. The velocity of O_D is shown in Figure B.1 (d). The complete manoeuvre took 14.9 s to complete.

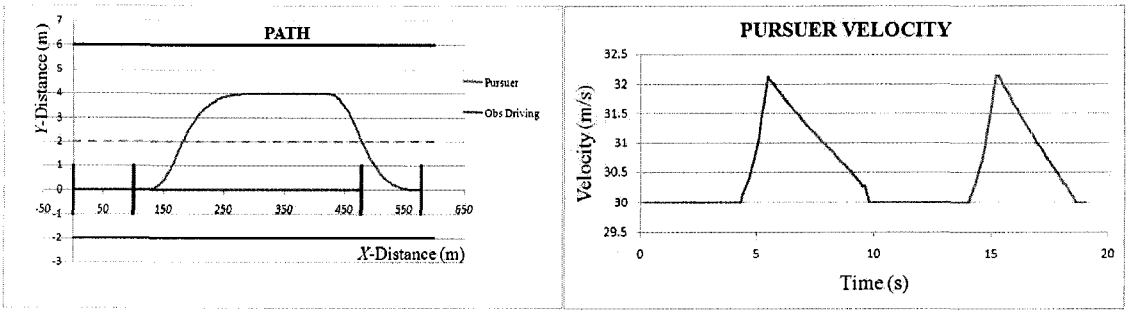

Figure B.8. Path and Velocity Profile of *P*.

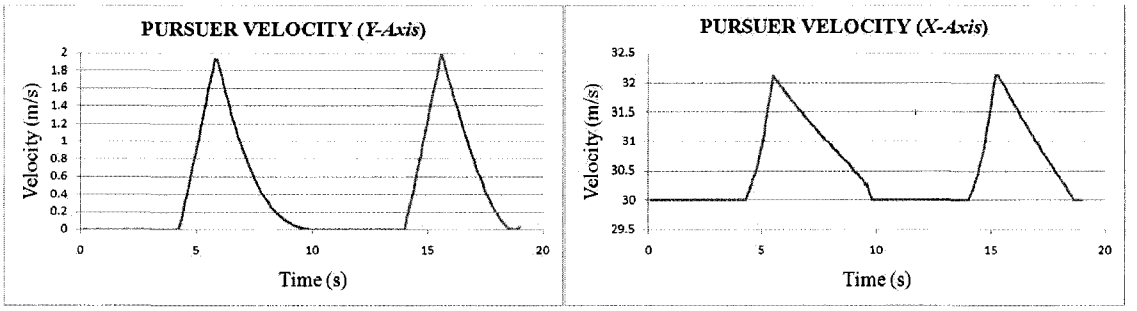

Figure B.9. Lateral and Axial Velocities of *P*.

Table B.4. Summary Results for Case 1, Scenario 4.

	Original RG Technique
Total time taken for overtaking (s)	14.9
Maximum velocity achieved (m/s)	32.1
Maximum lateral acceleration (m/s^2)	1.05
Maximum axial acceleration (m/s^2)	1.8

B.2 Case 2: Overtaking in the Presence of An Obstacle Vehicle in the Passing Lane

In this Case, *P* is required to overtake a slower moving O_D when an O_P is present, which does not allow *P* to immediately overtake O_D. For this Case, the results of simulations are presented here for four variations of velocities of both O_D and O_P: (*i*) constant, (*ii*), accelerating, (*iii*)

decelerating, and (*iv*) sinusoidal. The results of each scenario are presented via a set of three figures and one table. The first figure in each set shows *P*'s path and velocity profile, the second figure shows the velocity profiles of *P* in both the lateral and axial directions and the third figure shows the velocity profiles of both O_D and O_P. The table shows the summary results.

B.2.1 Both O_D and O_P are Moving with Constant Velocity

The results of the simulations for this scenario are presented in Figures B.10, B.11, and B.12 and Table B.5. The complete manoeuvre took 35 s to complete.

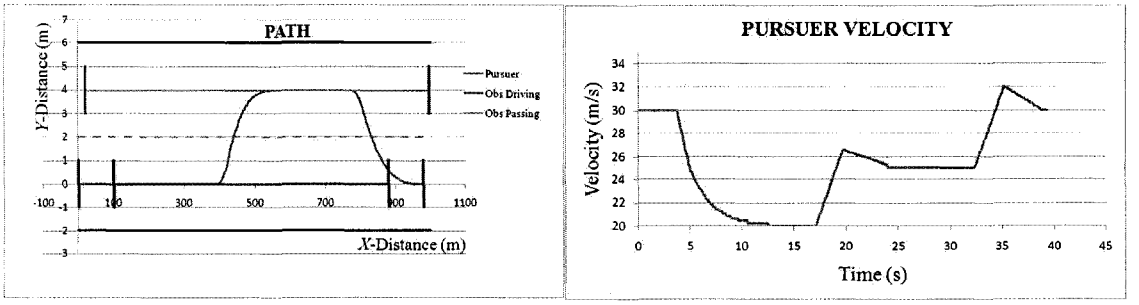

Figure B.10. Path and Velocity Profile of *P*.

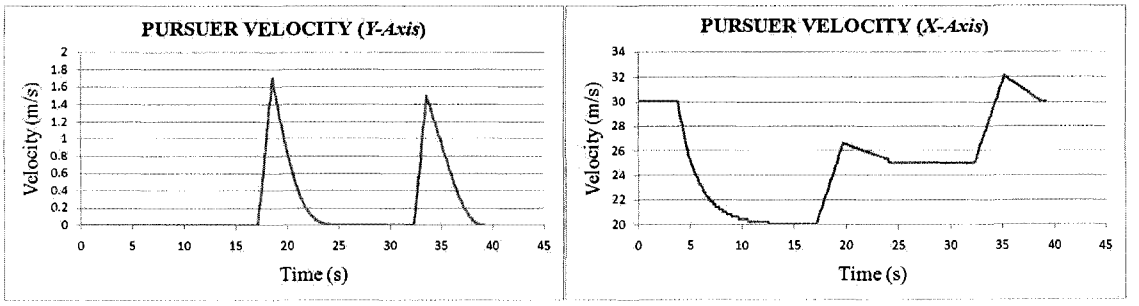

Figure B.11. Lateral and Axial Velocities of *P*.

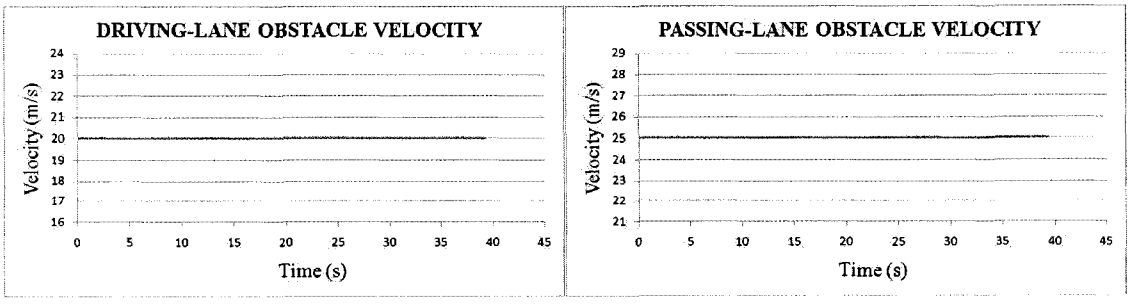

Figure B.12. Velocities of O_D and O_P.

Table B.5. Summary Results for Case 2, Scenario 1.

	Original RG Technique
Total time taken for overtaking (s)	35
Maximum velocity achieved (m/s)	32
Maximum lateral acceleration (m/s^2)	0.95
Maximum axial acceleration (m/s^2)	2.4

B.2.2 O_D is Moving with Constant Velocity and O_P is Accelerating

The results of the simulations for this scenario are presented in Figures B.13, B.14, and B.15 and Table B.6. The complete manoeuvre took 28.6 s to complete.

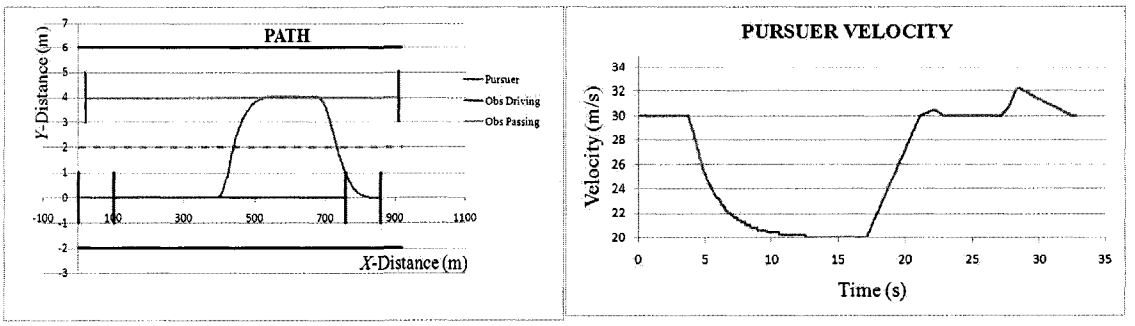

Figure B.13. Path and Velocity Profile of *P*.

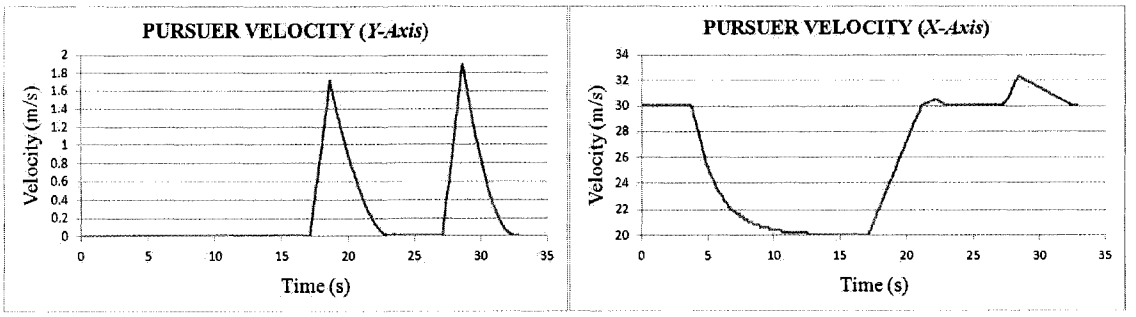

Figure B.14. Lateral and Axial Velocities of *P*.

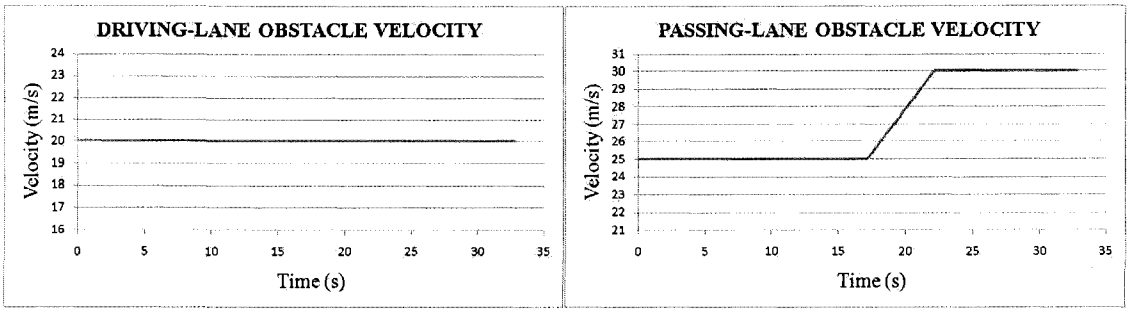

Figure B.15. Velocities of O_D and O_P.

Table B.6. Summary Results for Case 2, Scenario 2.

	Original RG Technique
Total time taken for overtaking (s)	28.6
Maximum velocity achieved (m/s)	32.2
Maximum lateral acceleration (m/s^2)	1.0
Maximum axial acceleration (m/s^2)	2.25

B.2.3 O_D is Moving with Constant Velocity and O_P is Decelerating

The results of the simulations for this scenario are presented in Figures B.16, B.17, and B.18 and Table B.7. The complete manoeuvre took 42.5 s to complete.

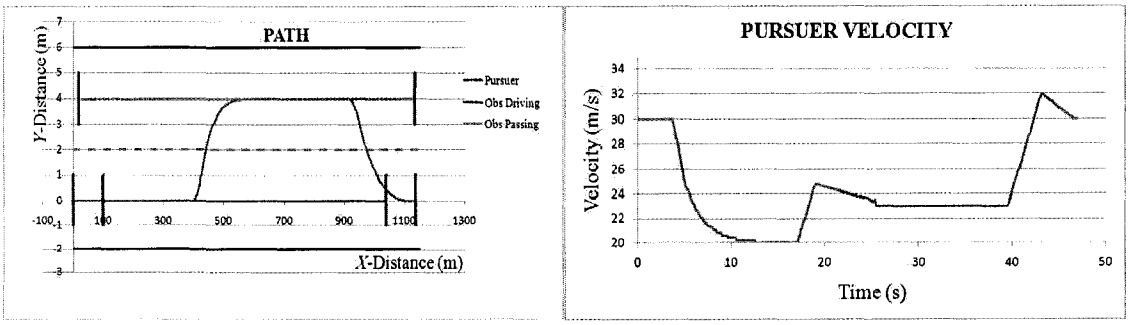

Figure B.16. Path and Velocity Profile of *P*.

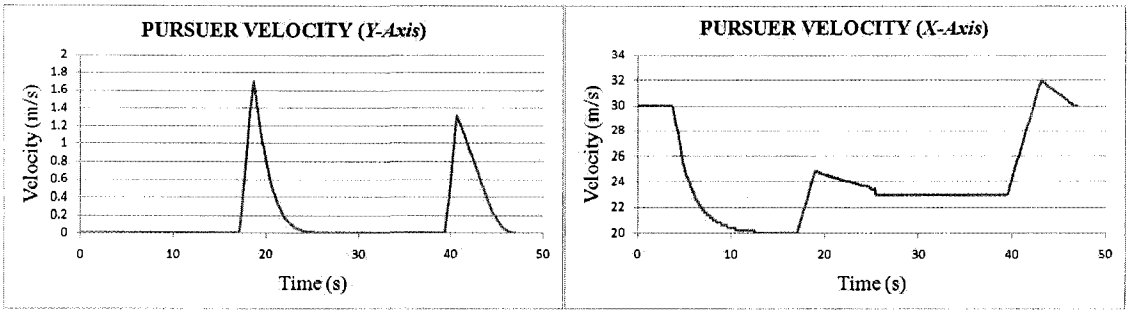

Figure B.17. Lateral and Axial Velocities of *P*.

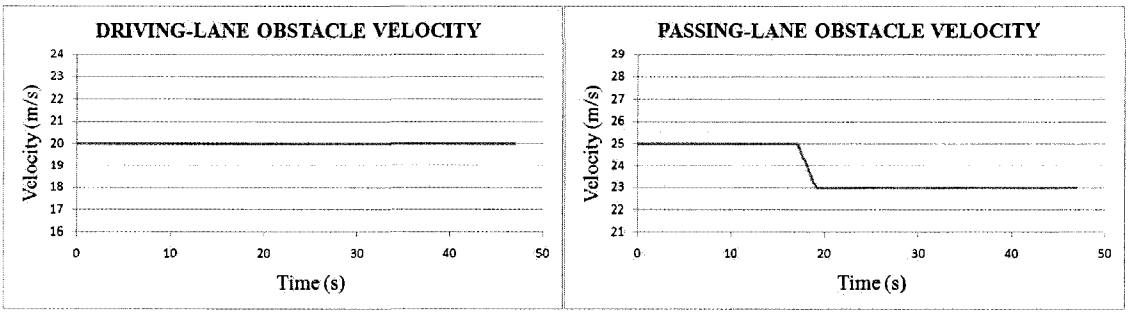

Figure B.18. Velocities of O_D and O_P.

Table B.7. Summary Results for Case 2, Scenario 3.

	Original RG Technique
Total time taken for overtaking (s)	42.5
Maximum velocity achieved (m/s)	32
Maximum lateral acceleration (m/s^2)	0.85
Maximum axial acceleration (m/s^2)	2.24

B.2.4 O_D is Moving with Constant Velocity and O_P is Moving with Sinusoidal Velocity

The results of the simulations for this scenario are presented in Figures B.19, B.20, and B.21 and Table B.8. The complete manoeuvre took 26.2 s to complete.

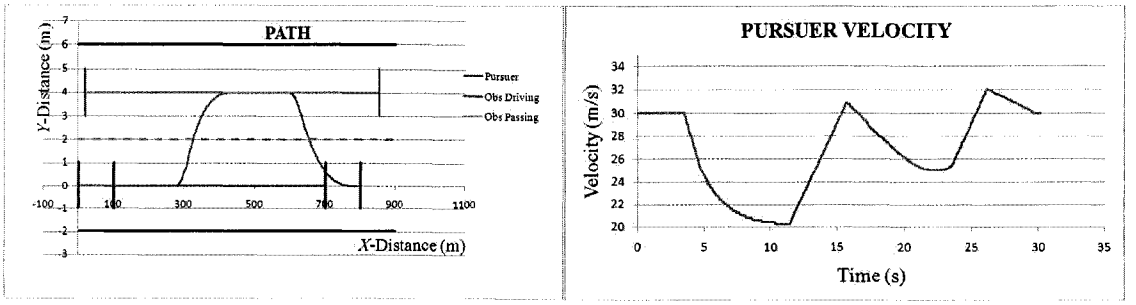

Figure B.19. Path and Velocity Profile of *P*.

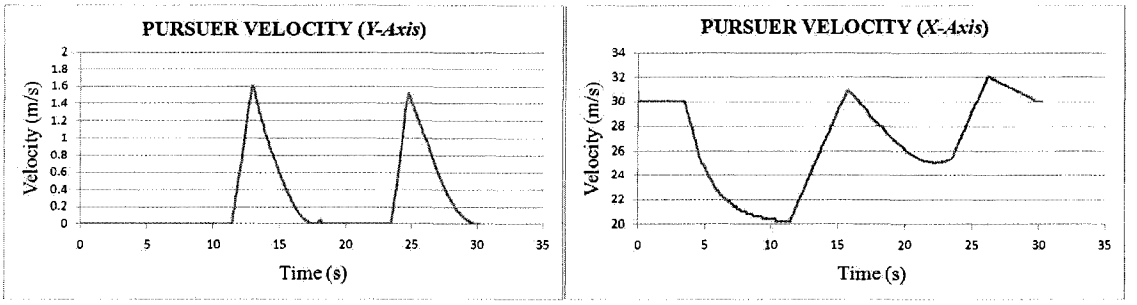

Figure B.20. Lateral and Axial Velocities of *P*.

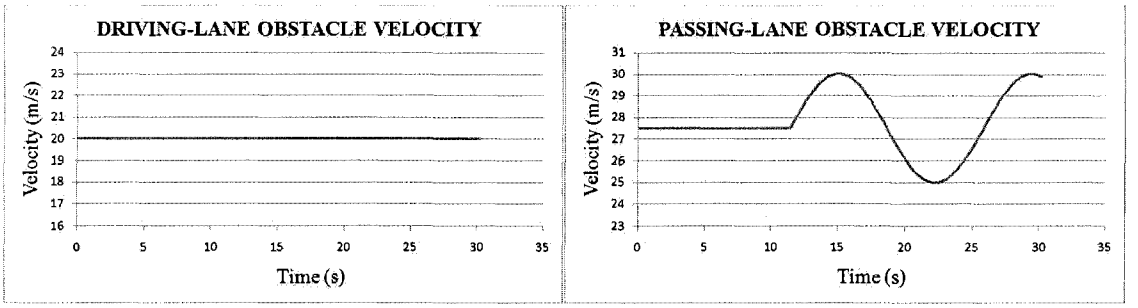

Figure B.21. Velocities of O_D and O_P.

Table B.8. Summary Results for Case 2, Scenario 4.

	Original RG Technique
Total time taken for overtaking (s)	26.2
Maximum velocity achieved (m/s)	32
Maximum lateral acceleration (m/s^2)	0.94
Maximum axial acceleration (m/s^2)	2.25

B.2.5 O_D is Accelerating and O_p is Moving with Constant Velocity

The results of the simulations for this scenario are presented in Figures B.22, B.23, and B.24 and Table B.9. The complete manoeuvre took 44.7 s to complete.

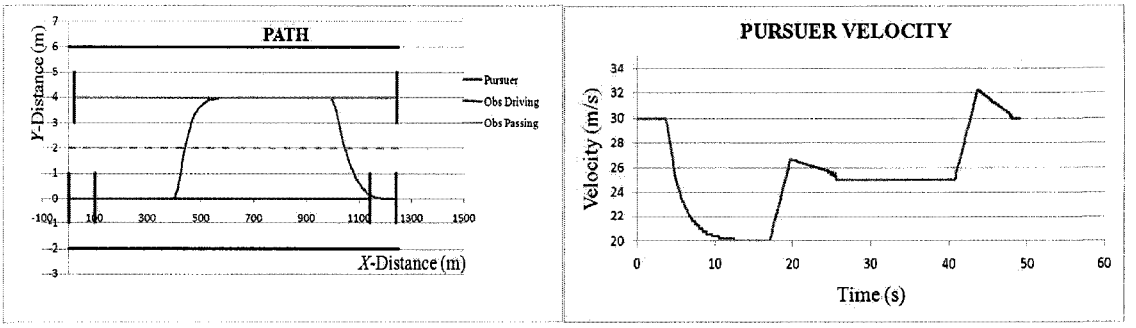

Figure B.22. Path and Velocity Profile of *P*.

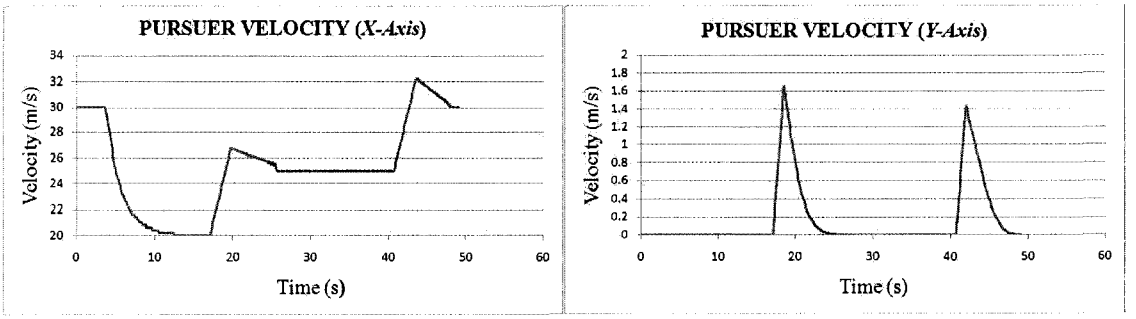

Figure B.23. Lateral and Axial Velocities of *P*.

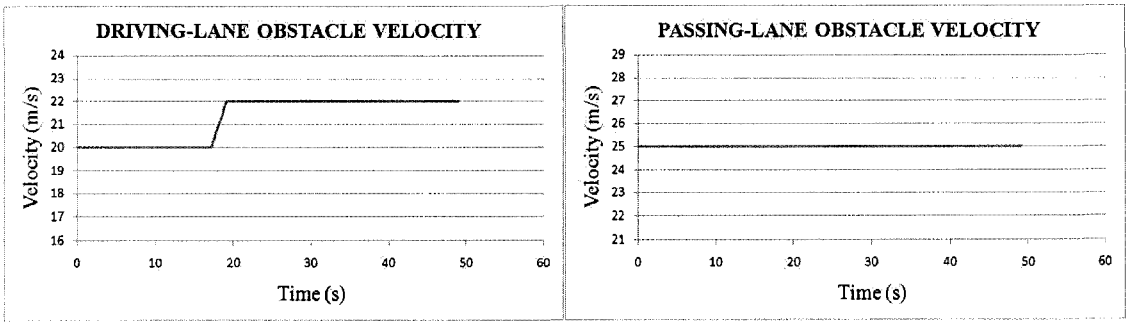

Figure B.24. Velocities of O_D and O_P.

Table B.9. Summary Results for Case 2, Scenario 5.

	Original RG Technique
Total time taken for overtaking (s)	44.7
Maximum velocity achieved (m/s)	32.1
Maximum lateral acceleration (m/s^2)	0.85
Maximum axial acceleration (m/s^2)	2.26

B.2.6 Both O_D and O_P are Accelerating

The results of the simulations for this scenario are presented in Figures B.25, B.26, and B.27 and Table B.10. The complete manoeuvre took 31.7 s to complete.

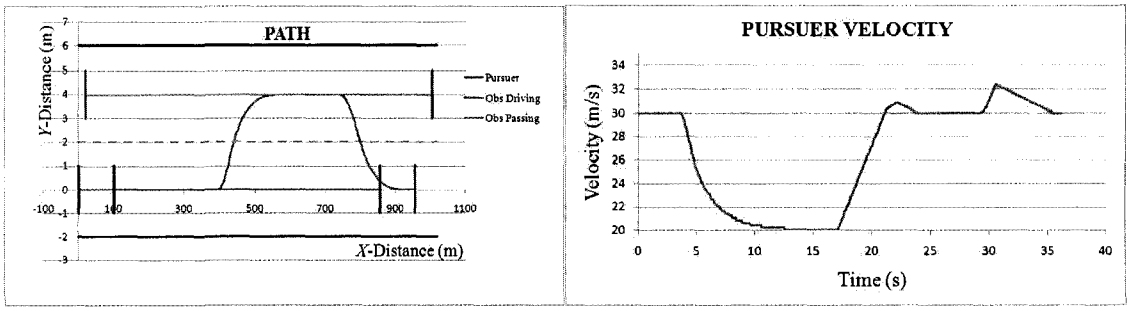

Figure B.25. Path and Velocity Profile of *P*.

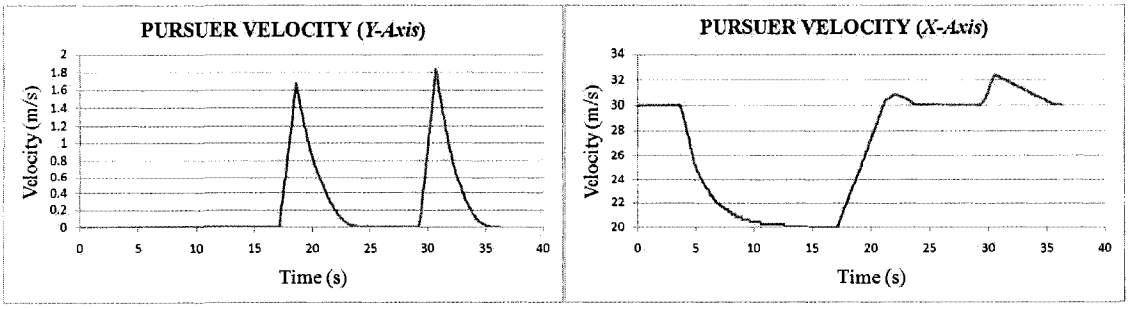

Figure B.26. Lateral and Axial Velocities of *P*.

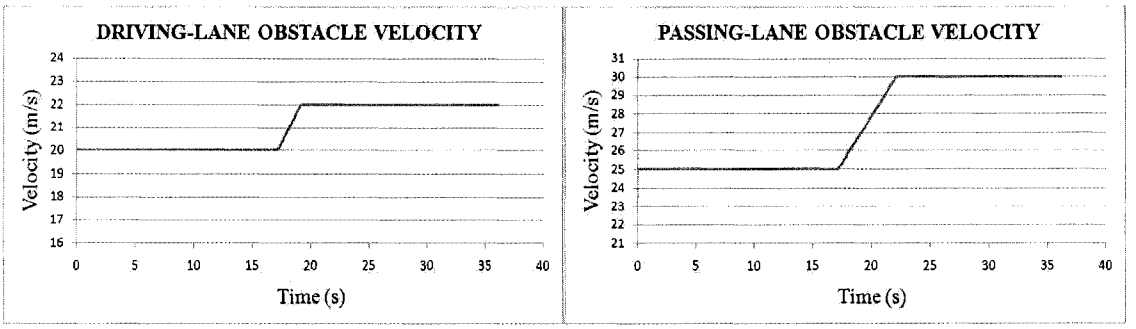

Figure B.27. Velocities of O_D and O_P.

Table B.10. Summary Results for Case 2, Scenario 6.

	Original RG Technique
Total time taken for overtaking (s)	31.7
Maximum velocity achieved (m/s)	32.3
Maximum lateral acceleration (m/s^2)	0.9
Maximum axial acceleration (m/s^2)	2.37

B.2.7 O_D is Accelerating and O_P is Decelerating

The results of the simulations for this scenario are presented in Figures B.28, B.29, and B.30 and Table B.11. The complete manoeuvre took 82 s to complete.

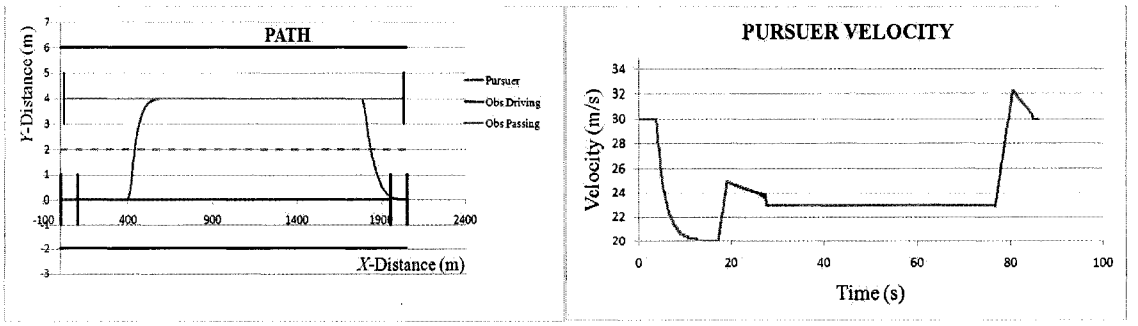

Figure B.28. Path and Velocity Profile of *P*.

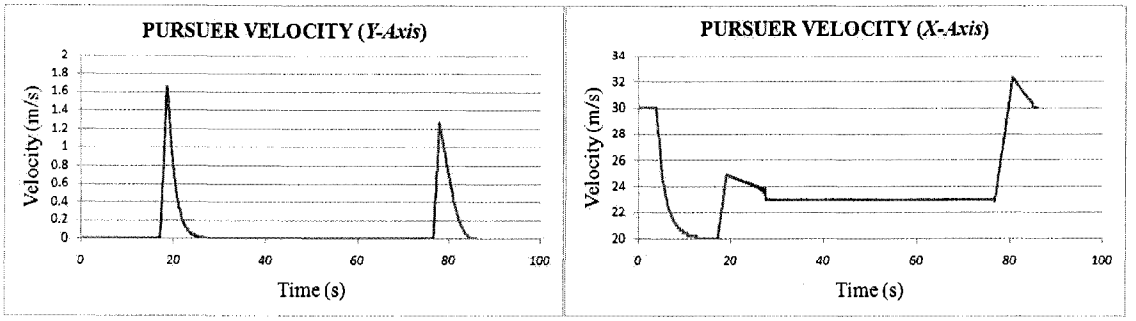

Figure B.29. Lateral and Axial Velocities of *P*.

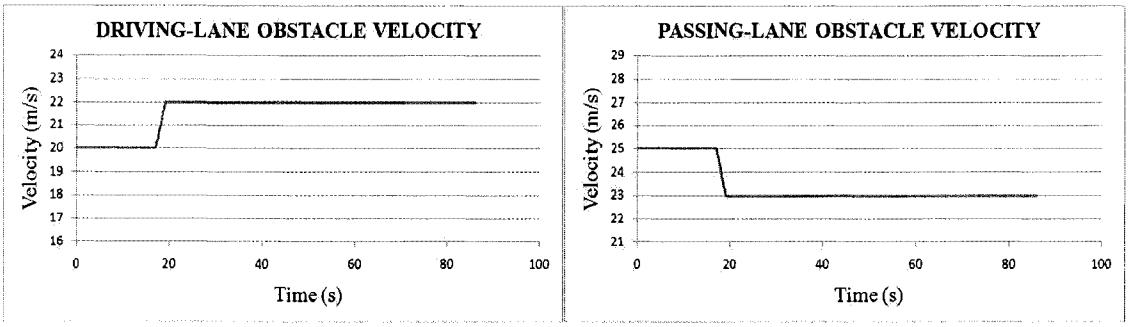

Figure B.30. Velocities of O_D and O_P.

Table B.11. Summary Results for Case 2, Scenario 7.

	Original RG Technique
Total time taken for overtaking (s)	82
Maximum velocity achieved (m/s)	32.3
Maximum lateral acceleration (m/s^2)	0.8
Maximum axial acceleration (m/s^2)	2.2

B.2.8 O_D is Accelerating and O_P is Moving with Sinusoidal Velocity

The results of the simulations for this scenario are presented in Figures B.31, B.32, and B.33 and Table B.12. The complete manoeuvre took 31 s to complete.

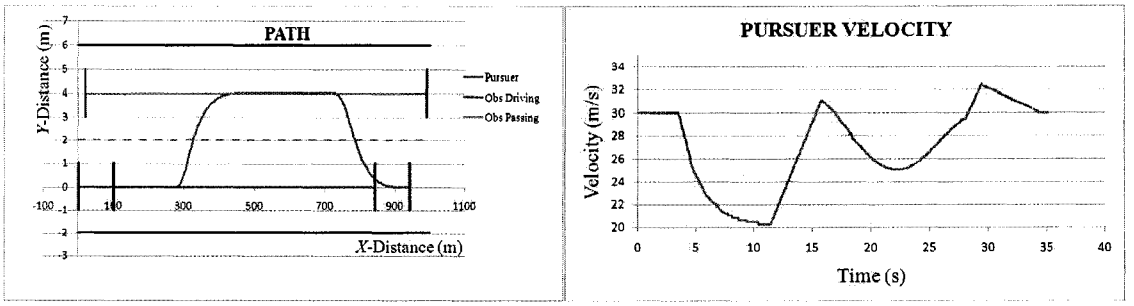

Figure B.31. Path and Velocity Profile of *P*.

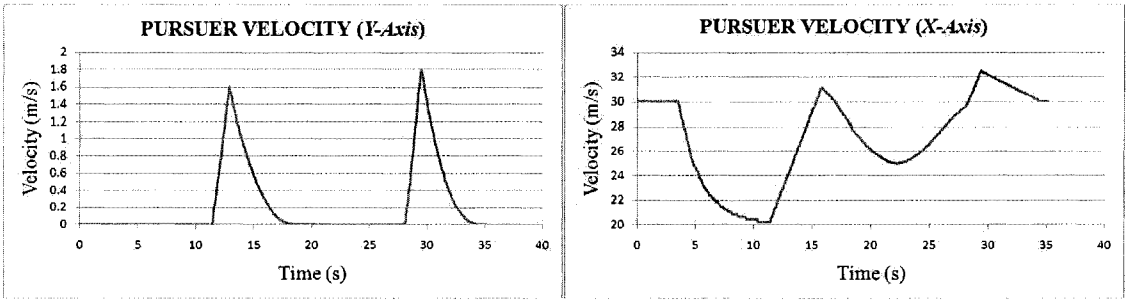

Figure B.32. Lateral and Axial Velocities of *P*.

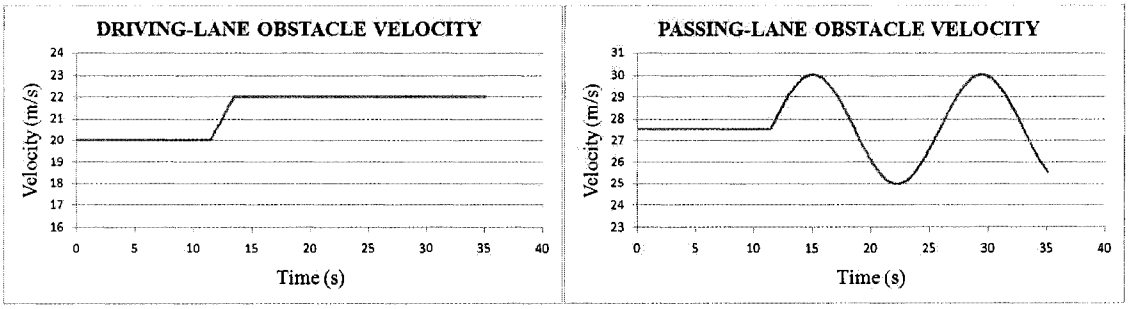

Figure B.33. Velocities of O_D and O_P.

Table B.12. Summary Results for Case 2, Scenario 8.

	Original RG Technique
Total time taken for overtaking (s)	31
Maximum velocity achieved (m/s)	32.5
Maximum lateral acceleration (m/s^2)	1.0
Maximum axial acceleration (m/s^2)	2.4

B.2.9 O_D is Decelerating and O_p is Moving with Constant Velocity

The results of the simulations for this scenario are presented in Figures B.34, B.35, and B.36 and Table B.13. The complete manoeuvre took 30.2 s to complete.

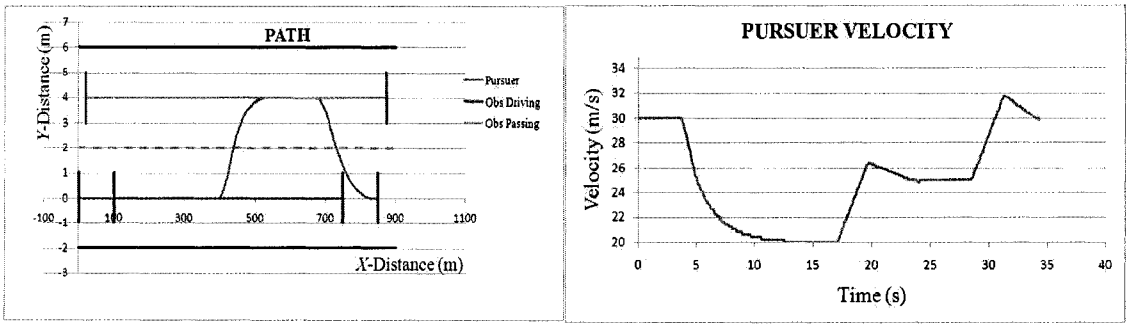

Figure B.34. Path and Velocity Profile of *P*.

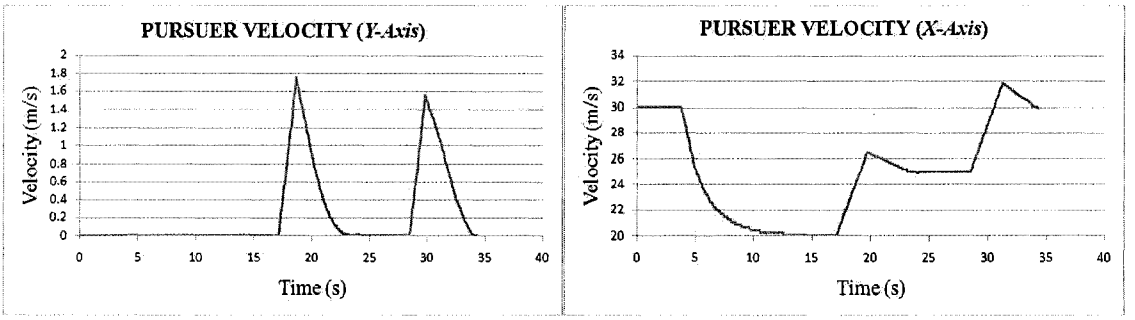

Figure B.35. Lateral and Axial Velocities of *P*.

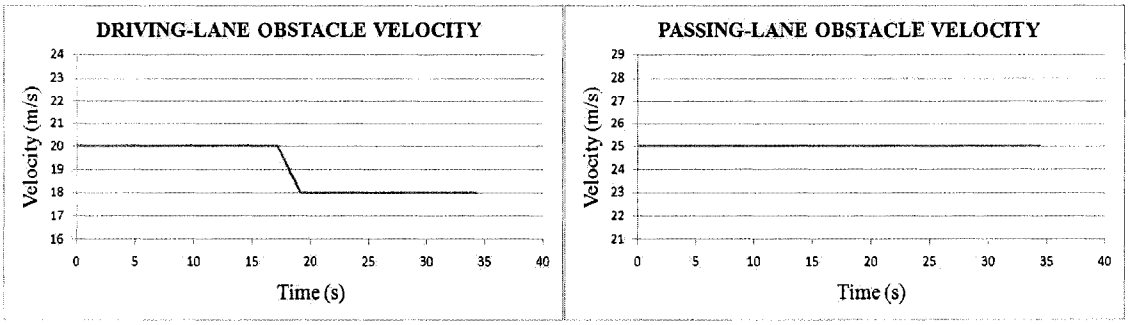

Figure B.36. Velocities of O_D and O_P.

Table B.13. Summary Results for Case 2, Scenario 9.

	Original RG Technique
Total time taken for overtaking (s)	30.2
Maximum velocity achieved (m/s)	31.8
Maximum lateral acceleration (m/s^2)	0.85
Maximum axial acceleration (m/s^2)	2.125

B.2.10 O_D is Decelerating and O_P is Accelerating

The results of the simulations for this scenario are presented in Figures B.37, B.38, and B.39 and Table B.14. The complete manoeuvre took 26.2 s to complete.

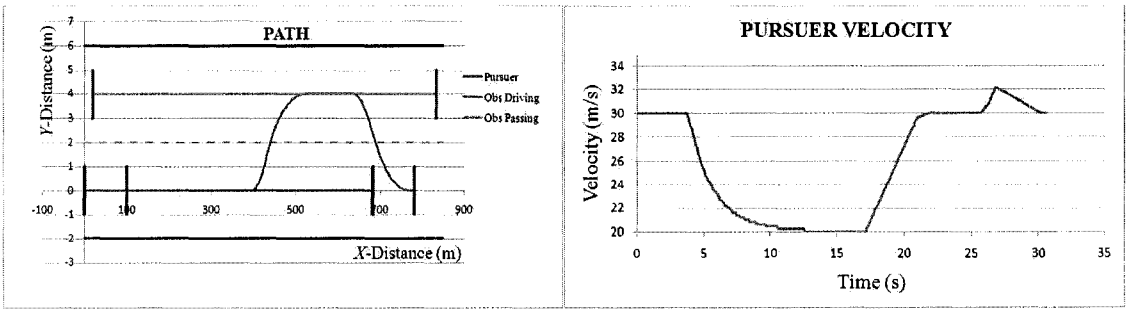

Figure B.37. Path and Velocity Profile of *P*.

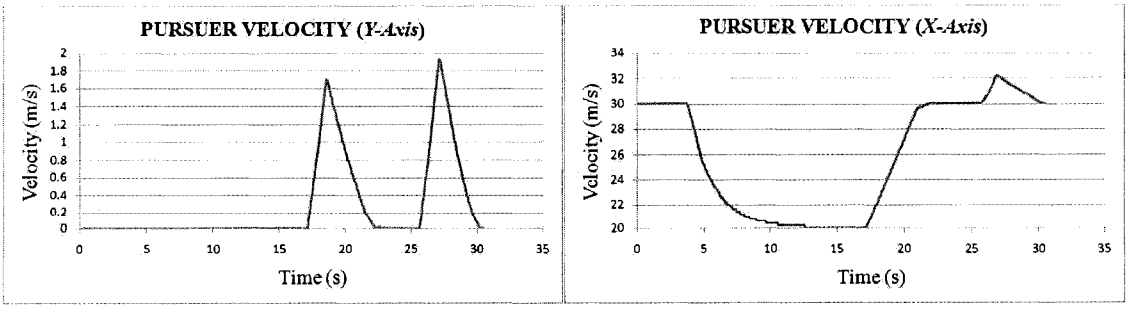

Figure B.38. Lateral and Axial Velocities of *P*.

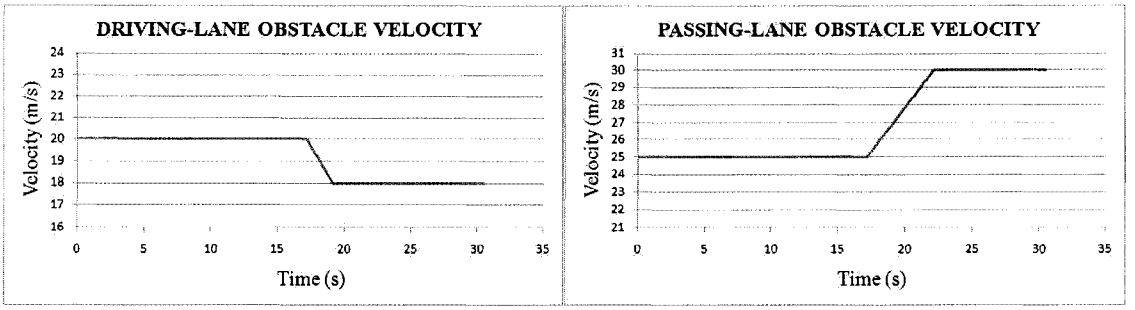

Figure B.39. Velocities of O_D and O_P.

Table B.14. Summary Results for Case 2, Scenario 10.

	Original RG Technique
Total time taken for overtaking (s)	26.2
Maximum velocity achieved (m/s)	32.2
Maximum lateral acceleration (m/s^2)	0.95
Maximum axial acceleration (m/s^2)	2.5

B.2.11 Both O_D and O_P are Decelerating

The results of the simulations for this scenario are presented in Figures B.40, B.41, and B.42 and Table B.15. The complete manoeuvre took 33.9 s to complete.

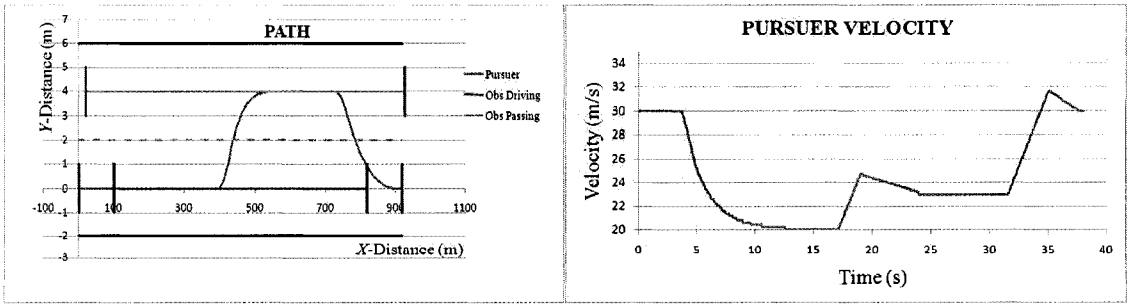

Figure B.40. Path and Velocity Profile of *P*.

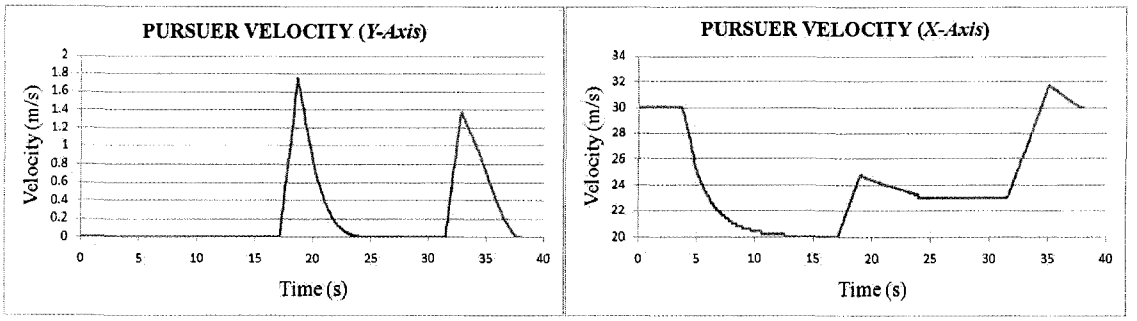

Figure B.41. Lateral and Axial Velocities of *P*.

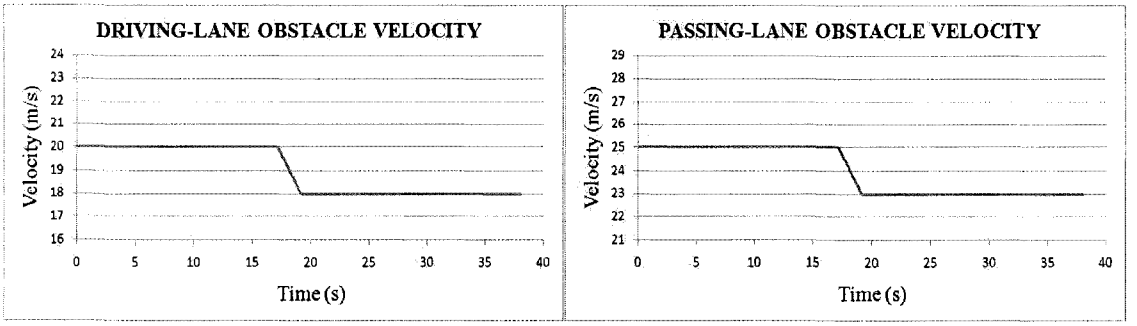

Figure B.42. Velocities of O_D and O_P.

Table B.15. Summary Results for Case 2, Scenario 11.

	Original RG Technique
Total time taken for overtaking (s)	33.9
Maximum velocity achieved (m/s)	31.7
Maximum lateral acceleration (m/s^2)	0.95
Maximum axial acceleration (m/s^2)	2.51

B.2.12 O_D is Decelerating and O_P is Moving with Sinusoidal Velocity

The results of the simulations for this scenario are presented in Figures B.43, B.44, and B.45 and Table B.16. The complete manoeuvre took 22.2 s to complete.

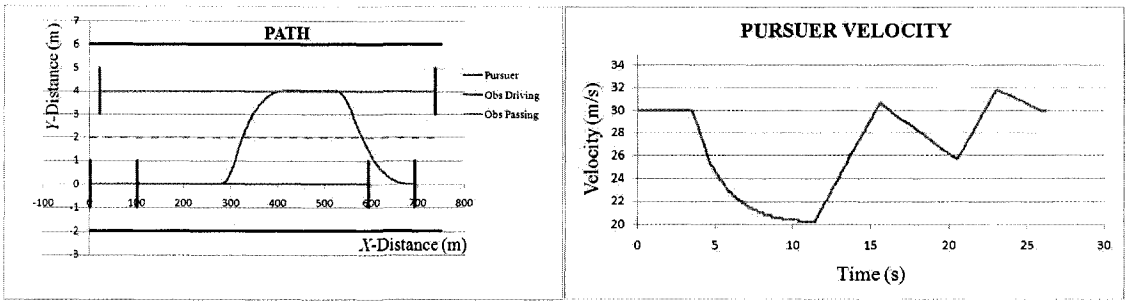

Figure B.43. Path and Velocity Profile of *P*.

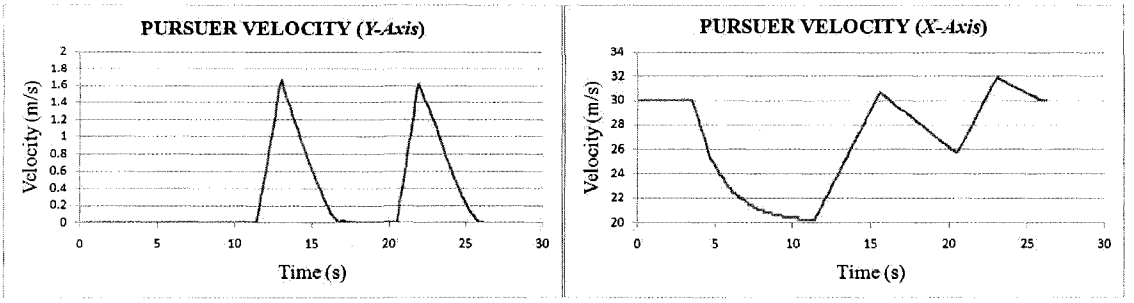

Figure B.44. Lateral and Axial Velocities of *P*.

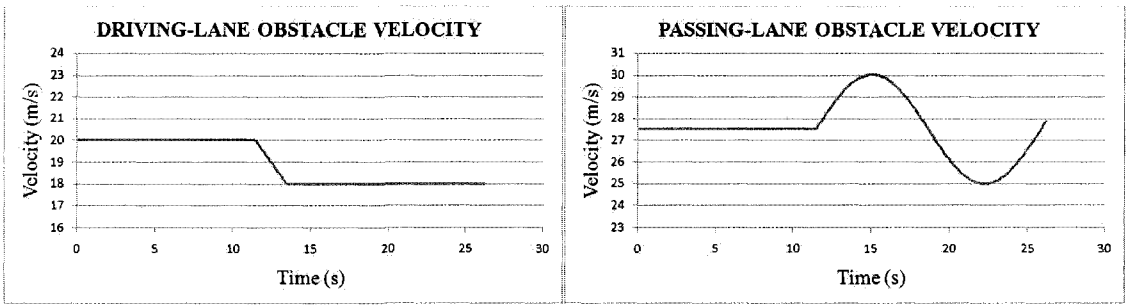

Figure B.45. Velocities of O_D and O_P.

Table B.16. Summary Results for Case 2, Scenario 12.

	Original RG Technique
Total time taken for overtaking (s)	22.2
Maximum velocity achieved (m/s)	31.8
Maximum lateral acceleration (m/s^2)	0.85
Maximum axial acceleration (m/s^2)	2.45

B.2.13 O_D is Moving with Sinusoidal Velocity and O_p is Moving with Constant Velocity

The results of the simulations for this scenario are presented in Figures B.46, B.47, and B.48 and Table B.17. The complete manoeuvre took 35.8 s to complete.

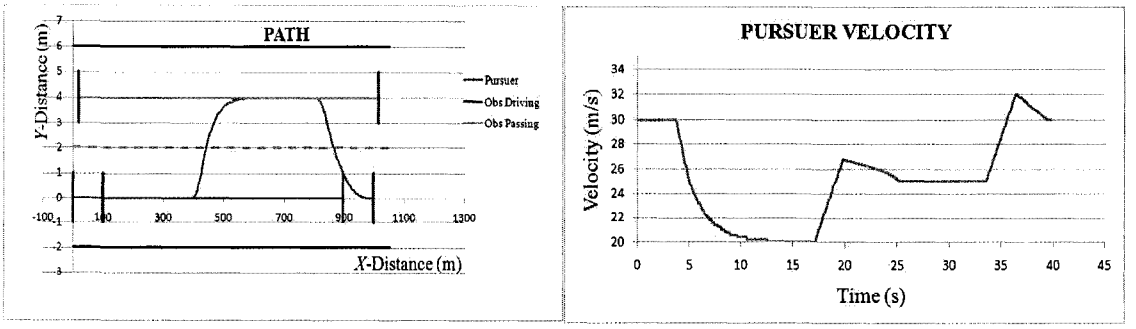

Figure B.46. Path and Velocity Profile of *P*.

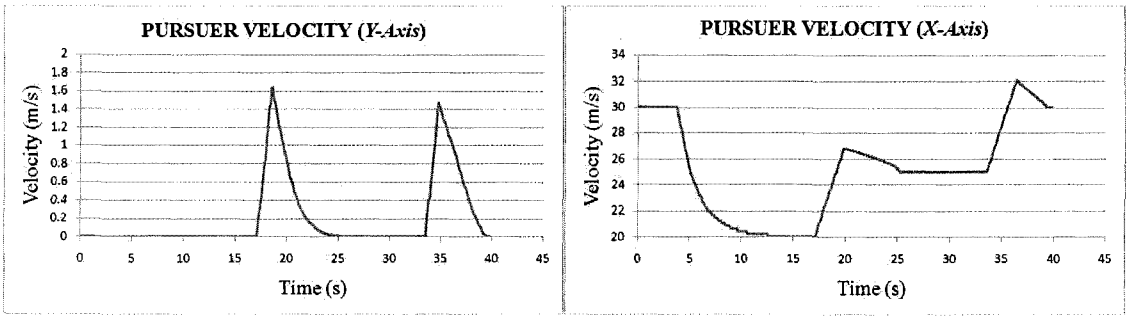

Figure B.47. Lateral and Axial Velocities of *P*.

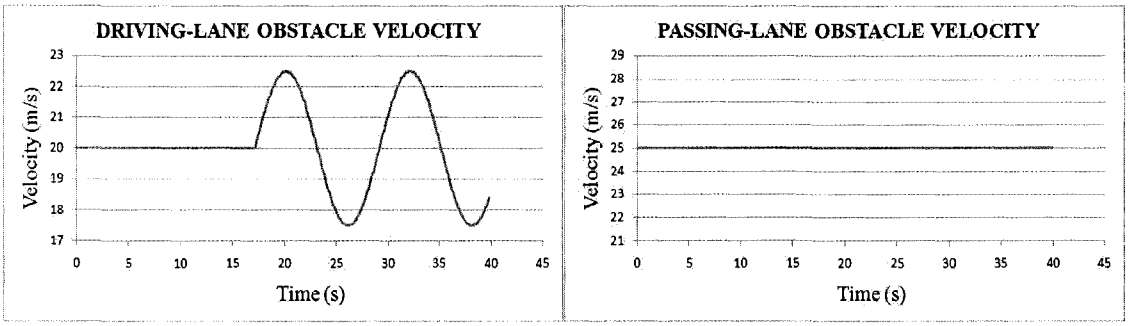

Figure B.48. Velocities of O_D and O_P.

Table B.17. Summary Results for Case 2, Scenario 13.

	Original RG Technique
Total time taken for overtaking (s)	35.8
Maximum velocity achieved (m/s)	32
Maximum lateral acceleration (m/s^2)	0.91
Maximum axial acceleration (m/s^2)	2.33

B.2.14 O_D is Moving with Sinusoidal Velocity and O_P is Accelerating

The results of the simulations for this scenario are presented in Figures B.49, B.50, and B.51 and Table B.6. The complete manoeuvre took 28.7 s to complete.

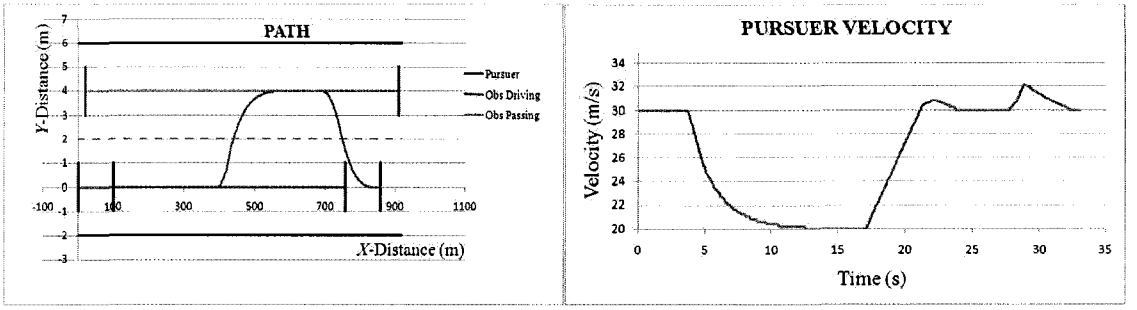

Figure B.49. Path and Velocity Profile of *P*.

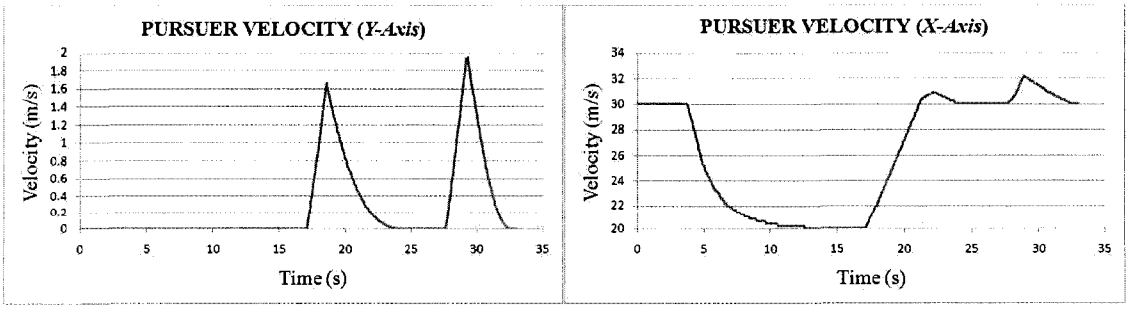

Figure B.50. Lateral and Axial Velocities of *P*.

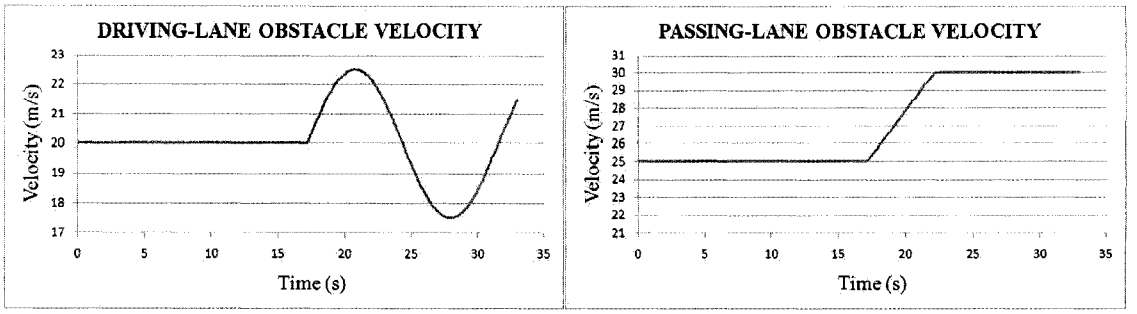

Figure B.51. Velocities of O_D and O_P.

Table B.18. Summary Results for Case 2, Scenario 14.

	Original RG Technique
Total time taken for overtaking (s)	28.7
Maximum velocity achieved (m/s)	32
Maximum lateral acceleration (m/s^2)	1.02
Maximum axial acceleration (m/s^2)	2.28

B.2.15 O_D is Moving with Sinusoidal Velocity and O_P is Decelerating

The results of the simulations for this scenario are presented in Figures B.52, B.53, and B.54 and Table B.19. The complete manoeuvre took 44.6 s to complete.

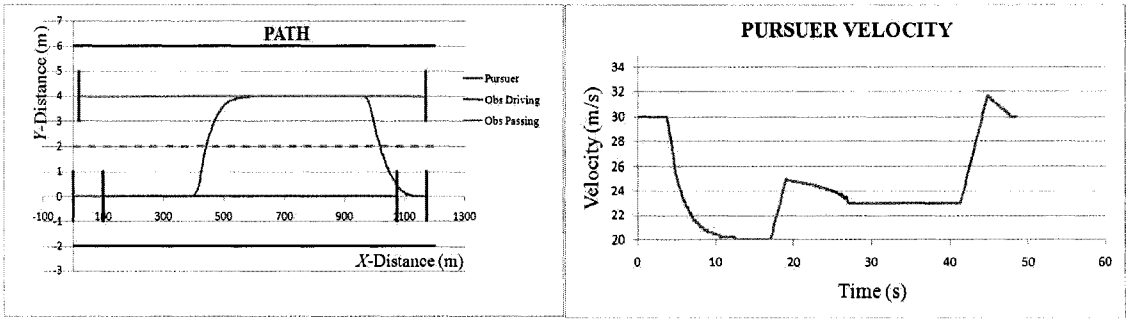

Figure B.52. Path and Velocity Profile of *P*.

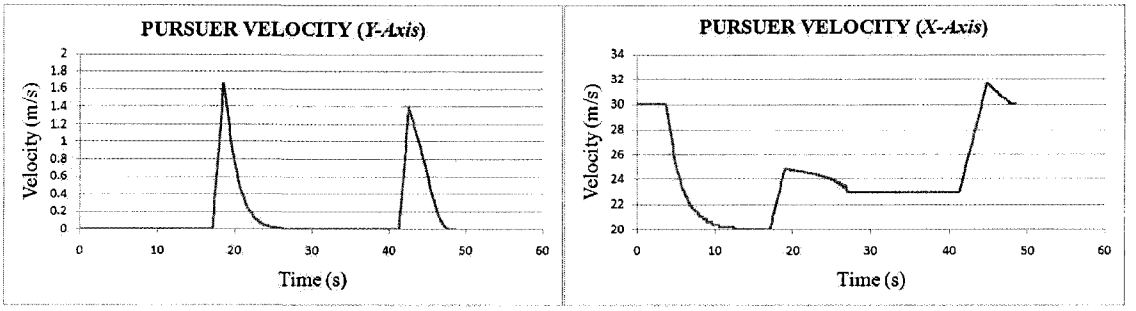

Figure B.53. Lateral and Axial Velocities of *P*.

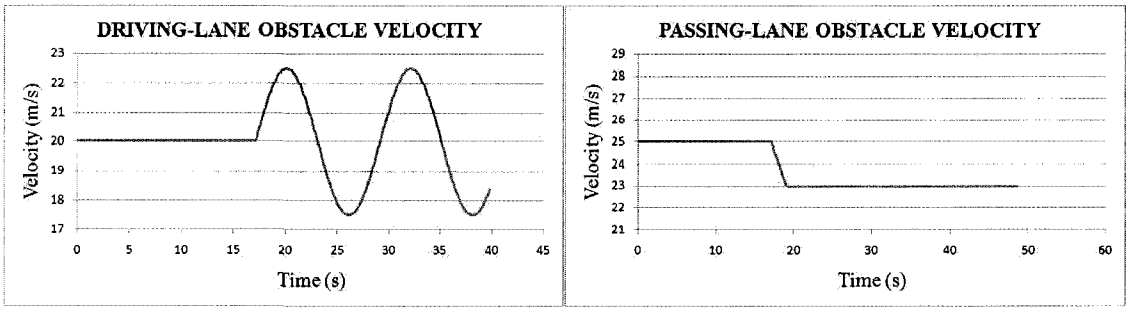

Figure B.54. Velocities of O_D and O_P.

Table B.19. Summary Results for Case 2, Scenario 15.

	Original RG Technique
Total time taken for overtaking (s)	44.6
Maximum velocity achieved (m/s)	31.9
Maximum lateral acceleration (m/s^2)	0.85
Maximum axial acceleration (m/s^2)	2.15

B.2.16 Both O_D and O_P are Moving with Sinusoidal Velocity

The results of the simulations for this scenario are presented in Figures B.55, B.56, and B.57 and Table B.20. The complete manoeuvre took 27.1 s to complete.

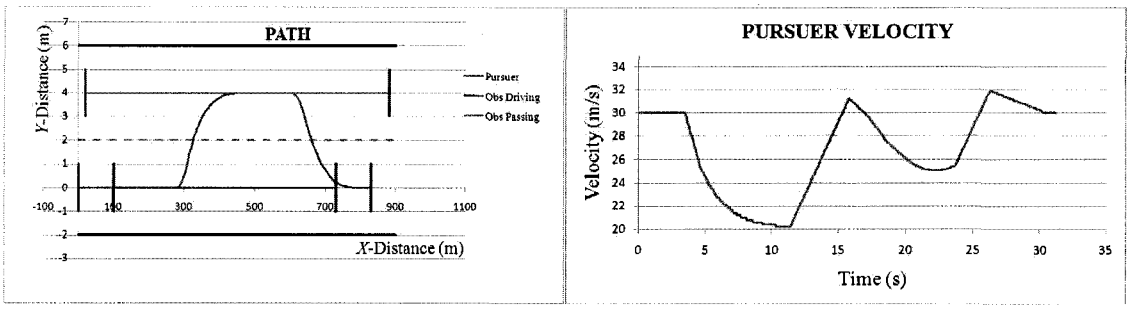

Figure B.55. Path and Velocity Profile of *P*.

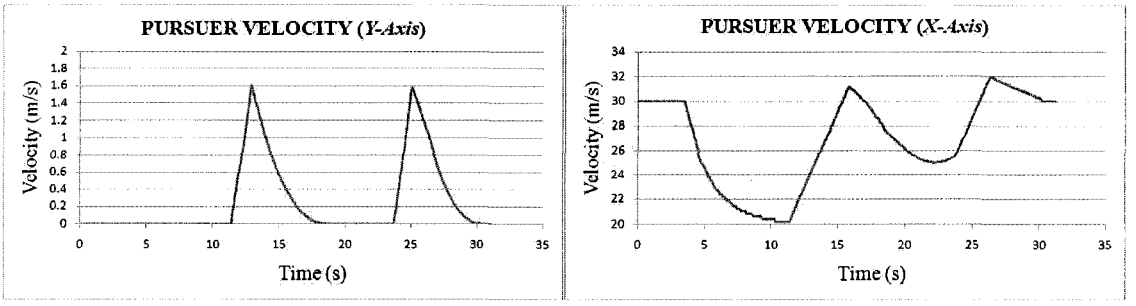

Figure B.56. Lateral and Axial Velocities of *P*.

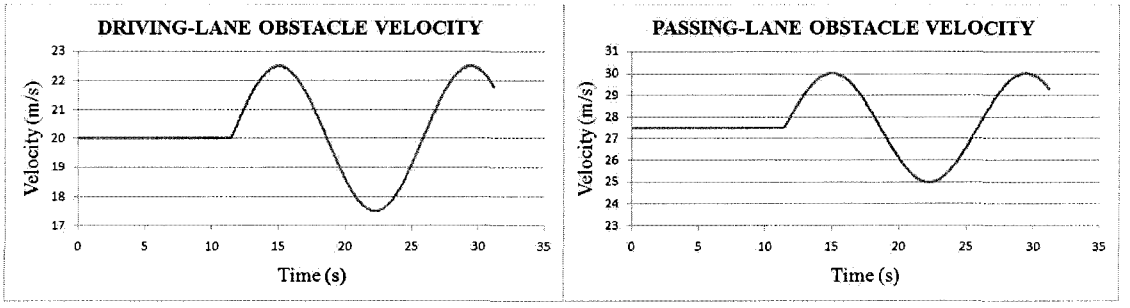

Figure B.57. Velocities of O_D and O_P.

Table B.20. Summary Results for Case 2, Scenario 16.

	Original RG Technique
Total time taken for overtaking (s)	27.1
Maximum velocity achieved (m/s)	32
Maximum lateral acceleration (m/s^2)	0.8
Maximum axial acceleration (m/s^2)	2.25